4-(PHENYLTHIO)BUTANOIC ACID, A NOVEL HISTONE DEACETYLASE INHIBITOR, STIMULATES RENAL PROGENITOR CELL PROLIFERATION

by

Eric David de Groh

BA in Biology, West Virginia University, 1998

MS in Medical Sciences, University of South Florida, 2005

Submitted to the Graduate Faculty of

the School of Medicine in partial fulfillment

of the requirements for the degree of

Doctor of Philosophy

University of Pittsburgh

2010

UNIVERSITY OF PITTSBURGH

SCHOOL OF MEDICINE

This dissertation was presented

by

Eric David de Groh

It was defended on

November 12, 2010

and approved by

Jeffrey L. Brodsky, PhD, Professor, Biological Sciences

Lance A. Davidson, PhD, Assistant Professor, Bioengineering

Beth L. Roman, PhD, Assistant Professor, Biological Sciences

Thomas E. Smithgall, PhD, Professor, Microbiology and Molecular Genetics

Dissertation Advisor: Neil A. Hukriede, PhD, Associate Professor, Developmental Biology

4-(PHENYLTHIO)BUTANOIC ACID, A NOVEL HISTONE DEACETYLASE INHIBITOR, STIMULATES RENAL PROGENITOR CELL PROLIFERATION

Eric David de Groh, MS

University of Pittsburgh, 2010

A chemical screen of approximately 2000 small molecules in zebrafish embryos identified a compound that generated pericardial edema, suggesting aberrant renal development. Treatment with this compound, 4-(phenylthio)butanoic acid (PTBA), increased the size of the pronephric kidney in zebrafish. Earlier in development, PTBA expanded the expression of renal progenitor cell markers, including *lhx1a*, *pax2a*, and *pax8*. Blocking DNA synthesis with hydroxyurea and aphidicolin before PTBA treatment decreased its efficacy, suggesting that PTBA-mediated renal progenitor expansion is proliferation dependent. Structure-activity analysis revealed that PTBA was an analog of the known histone deacetylase inhibitors (HDACis) 4-phenylbutanoic acid (PBA) and trichostatin A (TSA). Like PTBA, PBA and TSA both demonstrated the ability to expand *lhx1a* expression in treated embryos. PTBA was subsequently confirmed to function as an HDACi both *in vitro* and *in vivo*. HDACis are hypothesized to stimulate retinoic acid (RA) signaling by decreasing the concentration of RA necessary to activate RA receptors (RARs) on target genes. Indeed, treatment with PTBA affected the expression of the RA-responsive genes, *cyp26a1* and *cmlc2,* in a manner consistent with increased RA signaling. Furthermore, blocking the RA pathway with a dominant-negative RARα construct decreased PTBA efficiency. Therefore, PTBA appears to stimulate renal progenitor cell proliferation by activating the RA-signaling pathway. HDACis have been shown to improve renal recovery following acute kidney injury. Since PTBA increases renal progenitor cell proliferation, it may exert similar effects on

the multipotent cells involved in regeneration. In an effort to improve PTBA efficacy for pharmacological applications, analogs were generated by modifying the key structural elements of the general HDACi pharmacophore. These were tested along with a panel of known HDACis for their ability to increase *lhx1a* expression in treated embryos. Several compounds were characterized that function at nanomolar concentrations and do not cause toxicity in kidney cell culture. These second generation PTBA analogs are excellent candidates for development as potential renal therapeutics.

TABLE OF CONTENTS

LIST OF TABLES

LIST OF FIGURES

ACKNOWLEDGEMENTS

I thank…

My mentor, Neil Hukriede, for his guidance during my graduate career

All past and present lab members, particularly Rachel Jackson, Lisa Antoszewski, and Chiara Cianciolo Cosentino, who contributed directly to this work

All those that have helped me along the way, including: Bruce Blumberg, Jeff Brodsky, Takuto Chiba, Weixiang Dai, Lance Davidson, Billy Day, Mark de Caestecker, Lori Emert-Sedlak, Agnes Fogo, Ray Harris, Vasiliy Korotchenko, Emily Noël, Elke Ober, Beth Roman, Tom Smithgall, Michael Tsang, and Andreas Vogt

Mom, Dad, Mark, and Brooke for always believing in me, and my wife, Erin, for her continued love, support, and understanding

1.0 INTRODUCTION

1.1 PHYSIOLOGICAL ROLES OF THE KIDNEY

In his classic work *From Fish to Philosopher*, esteemed renal physiologist Homer W. Smith argues that our kidneys provide the means for our physiological freedom:

> *Our bones, muscles, glands, even our brains, are called upon to do only one kind of physiological work, but our kidneys are called upon to perform an innumerable variety of operations. Bones can break, muscles can atrophy, glands can loaf, even the brain can go to sleep, and endanger our survival; but should the kidneys fail in their task neither bone, muscle, gland nor brain could carry on.*[1] *(p. 4)*

This statement underscores the importance of our kidneys in permitting the complex biochemical processes that govern our daily lives. Indeed, renal failure not only compromises musculoskeletal, endocrine, and neurologic function, as mentioned by Dr. Smith, but also affects most other organ systems.[2] The widespread pathology that arises reflects the critical physiological responsibilities of our kidneys. These include excreting metabolic wastes, maintaining water and electrolyte balance, performing gluconeogenesis, and secreting hormones regulating blood pressure, calcium uptake, and erythrocyte production.[3]

1.2 THE NEPHRON

The nephron serves as the functional unit of the kidney.[4] In adult vertebrates, each nephron consists of a renal tubule and an encapsulated capillary tuft, known as a glomerulus.[5] Blood filtration begins at the fenestrated glomerular basement membrane, which excludes macromolecules from entering the capsular space based on their size and charge.[6] The filtrate then enters the renal tubule which reabsorbs virtually all of the water and electrolytes, concentrating wastes for excretion in the urine.[7] A healthy adult human kidney typically contains between 800,000 and 1,200,000 nephrons, with variation arising from age, sex, ethnicity, and birth weight.[5,8] However, other vertebrates, including mice, amphibians, and fish, manage to maintain normal renal function with a fraction of the nephrons that humans require.[5,9] Furthermore, simple kidneys containing only a few nephrons sustain all vertebrates during the early phases of development.

1.3 STAGES OF VERTEBRATE KIDNEY DEVELOPMENT

The vertebrate kidney passes through up to three developmental stages of increasing complexity: the pronephros, mesonephros, and metanephros (**Figure 1**).[10]

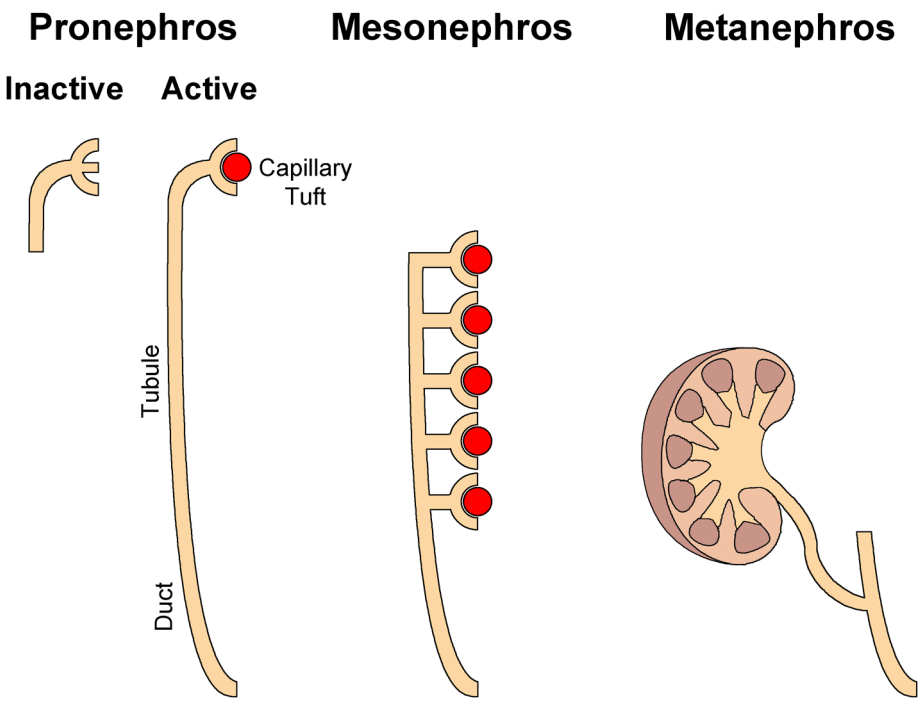

Figure 1. Stages of vertebrate kidney development.

1.3.1 The pronephros

The composition of the first kidney, the pronephros, varies between active and rudimentary forms depending on the requirements of the developing organism. Vertebrates living in freshwater must constantly excrete the excess water entering their bodies and consequently must also reabsorb electrolytes to prevent ion depletion.[11] Therefore, during the development of fish, amphibians, and certain reptiles, the pronephros must serve as a functional embryonic kidney.[5] Active pronephroi typically contain a pair of bilateral nephrons.[5] Each consists of an anterior capillary tuft emptying into a tubule which connects to the urinary opening via a pronephric (nephric) duct.[5] Importantly, the functioning pronephroi of fish and amphibians contain cell types typical of more complex kidneys, making them excellent model systems.[12,13]

Other vertebrates, including mammals and birds, enjoy protection from the osmotic demands of the external environment because they develop within an egg or uterus.[14] Combined with the assistance of an allantois or placenta to remove wastes, these conditions preclude the need for renal function during early development.[14] Therefore, their pronephroi primarily consist of vestigial structures, including short regions of tubule and duct, which almost certainly lack excretory capability.[10,15] However, proper formation of the pronephros, whether active or inactive, is necessary to induce the development of more complex kidneys.[10] Mauch and coworkers demonstrated this concept by observing that excision of chick pronephroi prevents the formation of the subsequent kidney form, the mesonephros.[16]

1.3.2 The mesonephros

The mesonephros functions as the adult kidney in fish and amphibians, and the embryonic kidney in other vertebrates.[5] Mesonephric development begins with the formation of condensates known as renal vesicles from the mesenchymal tissue surrounding the nephric duct or tubule.[10] Renal vesicles then proceed through two morphological stages, the comma- and S-shaped body, before becoming mesonephric nephrons.[4] In mammals and birds, extension of the nephric duct toward the urinary opening induces nephron formation in an anterior to posterior pattern.[14,17] Mesonephric nephrons in fish and amphibians arise in a similar manner, even though their nephric ducts already connect to the urinary opening.[9,18]

In fish and amphibians, where the mesonephros represents the terminal adult kidney, hundreds or thousands of well-formed nephrons typically develop.[5,9] Conversely, in other vertebrates, where the mesonephros serves only as a transitory organ, nephron numbers rarely exceed 60.[5] Furthermore, many of the posterior nephrons exhibit primitive morphology and fail

to connect to the nephric duct.[14] For example, of the approximately 18 nephrons of the mouse mesonephros, only 4 to 6 anterior nephrons actually fuse with the nephric duct.[5] In almost all vertebrates, formation of the mesonephros triggers the degeneration of the now-obsolete pronephros.[5] However, in some fish, the pronephros becomes repurposed as a lymphoid organ, known as the head kidney, and persists into adulthood.[5] Similarly, the mesonephros will eventually adopt several new roles after ceding its renal responsibilities to its successor, the metanephros.

1.3.3 The metanephros

The terminal and most complex kidney, the metanephros, provides renal function to adult mammals, birds, and reptiles.[19] Metanephric development begins with the establishment of a blastema of cells, known as the metanephric mesenchyme (MM), expressing the transcription factors Wt1 and Pax2.[20,21] Subsequently, the MM secretes glial-cell-line derived neurotrophic factor to induce outgrowth of the ureteric bud (UB) from the posterior nephric duct.[22] As the UB invades the MM, signals from the MM trigger repeated branching morphogenesis events, creating the collecting ducts of the metanephros.[4] At the same time, the UB branches reciprocate by inducing condensation of the MM into renal vesicles.[4] These will develop into metanephric nephrons by proceeding through the comma- and S-shaped body stages in a similar manner to mesonephric nephrogenesis. Reciprocal induction between the MM and UB continues until terminated by an unknown factor, thought to originate from differentiating MM.[23]

As the metanephros becomes active, the mesonephros begins to degenerate and ceases its renal function.[5] However, some portions of the mesonephros will become incorporated into the developing reproductive tract. In females, the nephric duct completely degenerates, but in males,

testosterone induces the duct to become the epididymis, vas deferens, and seminal vesicles.[24] In both sexes, some mesonephric cells migrate to the adjacent primordium and contribute to the formation of the adrenal glands and gonads.[4]

Fully-formed metanephroi contain anywhere from thousands of nephrons (mice) to about a million nephrons (human), depending on organism size and renal requirements.[5] Importantly, the completion of the metanephros represents the end of new nephron development, also known as neonephrogenesis.[5,25] Therefore, as the metanephros grows in a maturing organism, the existing nephrons respond by increasing in cell density and length, but not number. [26]

1.4 ORIGIN OF THE PRONEPHROS

Although the pronephros forms the foundation for subsequent kidney development, this foundation depends on inductive events occurring long before the first nephron appears. The pronephros arises from the intermediate mesoderm (IM), located within the embryonic trunk between the paraxial and lateral-plate mesoderm.[10] As embryos emerge from gastrulation, the presumptive IM undergoes specification to a kidney fate, creating a population of renal progenitor cells.[27] The process of specification signifies that renal progenitor cells will differentiate into kidney in the absence of further inductive events.[28] However, as the definition suggests, specified renal progenitor cells retain some developmental plasticity. As James and Schultheiss demonstrated in chick, transplanting specified IM to the lateral plate (LP) transforms many grafted cells to an LP fate.[27]

Following specification, signals from nearby tissues define the boundaries of the emerging IM and trigger expression of the first IM-specific markers: *Pax2*, *Lhx1*, and *Osr1*.[16,29-

[31] Later in development, during early somitogenesis, renal progenitor cells become irreversibly committed (or determined) to a kidney fate.[27,28,32] At this point, IM transplanted to another embryonic environment continues to express IM-specific markers and fails to integrate into the host tissue.[27,32] However, committed renal progenitor cells will continue to respond to a variety of molecular signals that will prepare the nascent kidney field for pronephric morphogenesis.

1.5 MOLECULAR CONTROL OF PRONEPHRIC DEVELOPMENT

Formation of the pronephros requires input from multiple signaling pathways acting in concert (**Figure 2**).[15,33,34] A comprehensive review of all molecular mediators involved in this process sits beyond the scope of my work. Instead, I will discuss only the elements directly related to understanding of the experimental data. These include the Pax and Lhx proteins, transcription factors serving as early markers of renal progenitor cells, and the retinoic acid pathway.

1.5.1 Pax pathway

The paired-box (Pax) family of transcription factors directs the organogenesis of many tissues, including the central nervous system, pancreas, thyroid, and kidney.[35] Each of the nine *Pax* genes encodes their namesake DNA-binding domain, along with a homeodomain and/or an uncharacterized octapeptide motif.[36] The unique combinations of these domains further categorize the family into four well-defined groups.[36] Of these, only two members of group II, *Pax2* and *Pax8*, exhibit any expression in the developing kidney.[20,37] The other group II member, *Pax5*, coexpresses with *Pax2* and *Pax8* in the central nervous system, but not elsewhere.[38]

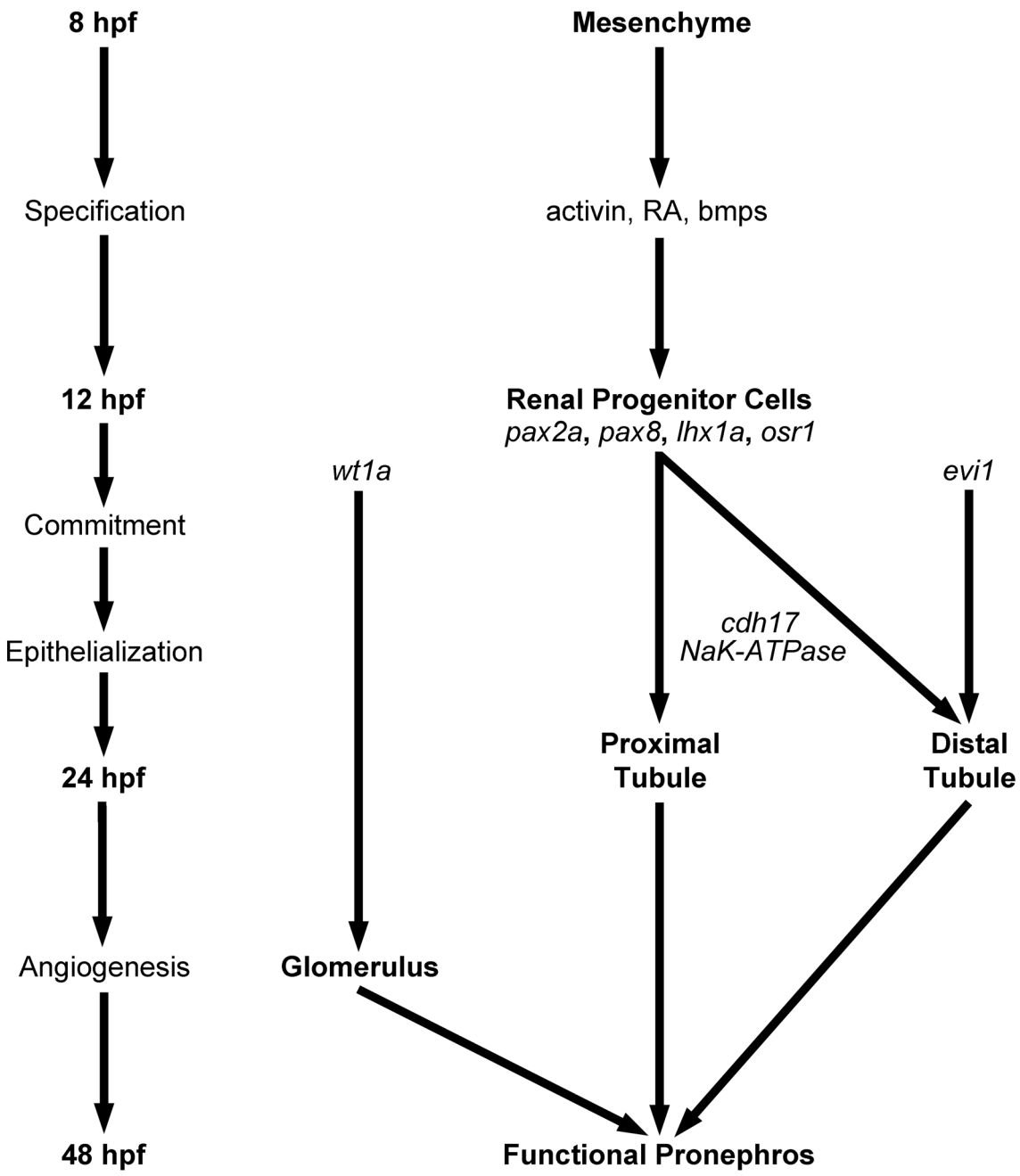

Figure 2. Summary of developmental and molecular events forming the active pronephros.

Knockout studies revealed that mice carrying homozygous-null alleles of *Pax2* fail to generate either mesonephric tubules or metanephroi.[39] Although they still form nephric ducts, these extend only partway toward the urinary opening before beginning to degenerate.[39] Therefore, the lack of inductive signals resulting from a failure of duct extension explains the phenotype. Although not explicitly investigated by the authors, this also suggests that the loss of *Pax2* interferes with pronephric development. In stark contrast, the kidneys of *Pax8*-deficient mice appear completely normal.[40] The lack of phenotype probably reflects the ability of *Pax2* to compensate for the loss of *Pax8*.[41] *Pax2* expression spans much of the developing mouse kidney and includes the more-restricted pattern of *Pax8*.[40] Furthermore, evidence suggests functional redundancy between *Pax2* and *Pax5*, providing additional support for a compensatory response among group II members.[42] Importantly, mice homozygous-null for both *Pax2* and *Pax8* fail to form even the rudimentary nephric ducts observed in *Pax2*-deficient mice.[29,39] The more severe phenotype exhibited by the double knockouts suggests that *Pax8*, like *Pax2*, also contributes to the development of the pronephros.

Experiments utilizing zebrafish, *Xenopus*, and chick offer additional insights into the function of these genes. In particular, the zebrafish *pax2a* mutant, *no isthmus*, provides a convenient platform for examining the regulatory relationships maintained by *Pax2* during pronephric development.[43] Homozygous expression of hypomorphic or null alleles of *no isthmus* prevents the formation of pronephric tubules and ducts, but spares the glomeruli.[43-45] This occurs because *pax2a* specifies renal progenitor cells to the tubule and duct lineages, while *wt1a* drives cells to a glomerular fate.[46]

Overexpression of *Pax2* in chick embryos causes the formation of ectopic pronephric tubules and ducts.[29] Similarly, *pax8* overexpression in *Xenopus* embryos generates ectopic

tubules and, in addition, increases tubule size.[41] These results again emphasize the important individual contributions of both *Pax2* and *Pax8* to proper pronephric development. However, the relationship between the two genes appears to vary among vertebrates. In mice, *Pax2* and *Pax8* work together to initiate pronephric development by inducing renal progenitor cells to undergo a mesenchymal to epithelial transition.[29] Moreover, this process occurs independently of any cross-regulation.[29] In contrast, expression of *pax8* during development of the zebrafish pronephros requires the presence of functional pax2a protein.[47] The differing regulatory strategies of mice and zebrafish may reflect the evolutionary differences between rudimentary and active pronephroi.

1.5.2 Lhx pathway

The LIM homeobox protein (Lhx) family of nuclear transcription factors consists of over a dozen members that regulate the development of many tissue types.[48] They are characterized by two unique zinc fingers, the LIM domains, located N-terminally to a DNA-binding homeodomain.[49] These LIM domains direct interactions with protein cofactors, resulting in the formation of active transcriptional complexes on target genes as specified by the homeodomain.[48] The initial characterization of *Lhx1* revealed that it was expressed in the developing kidneys of both *Xenopus* and mice.[50-52] When Shawlot and Behringer later generated homozygous-null *Lhx1* mice, they observed that the rare stillborn neonates (4 out of about 1000) all lacked heads, gonads, and kidneys.[53] A subsequent study using the same *Lhx1*-null line examined the effects of the mutation on formation of the pronephros.[31] Loss of *Lhx1* expression caused IM disorganization and restricted the expression of *Pax2* in the emerging nephric duct to a short anterior region.[31] However, the establishment of the IM remained unaffected, suggesting *Lhx1*

plays a role in IM differentiation, but not specification.[31] Experiments in *Xenopus* kidney explants support this hypothesis. Treatment of *Xenopus* animal cap explants with both activin and retinoic acid (ARA) induces pronephric specification and subsequent tubulogenesis.[54] Chan and coworkers demonstrated that overexpressing *lhx1* in explants treated with either activin or retinoic acid was not sufficient to induce pronephric differentiation.[55] However, expression of a dominant-negative form of lhx1 in ARA-treated explants prevented tubule formation.[55] These results suggest that *lhx1* is essential for pronephric tubulogenesis, but may not be primarily involved in kidney field specification.[55]

Overexpression of *lhx1* in *Xenopus* embryos causes the formation of both enlarged, as well as ectopic pronephric tubules.[41] Moreover, *lhx1* synergizes with either *pax2* or *pax8* to further increase pronephric size.[41] Therefore, overexpression of these renal progenitor markers increases the pool of cells that will eventually be committed to the kidney fate. However, mice homozygous-null for *Pax2* and *Pax8* demonstrate no expression of *Lhx1* in the developing nephric duct.[29] This suggests that *Lhx1* may act primarily as a competence factor that maintains the renal progenitor population following specification.[29]

Dkk1, a Wnt signaling inhibitor, has emerged as a potential downstream effector of Lhx1. Conditional knockouts of *Lhx1* in the kidneys of transgenic mice greatly reduced *Dkk1* expression.[56] Furthermore, the phenotypes of *Lhx1*- and *Dkk1*-null mice appear very similar, although kidney phenotypes were not reported for the Dkk1 mutants.[53,56,57] Significantly, the conserved non-coding elements in the *Dkk1* locus contain conserved *Lhx1*-binding sites.[58] However, the observation that *Dkk1* overexpression in transgenic zebrafish embryos inhibits differentiation of the pronephric tubule complicates this relationship.[59] Perhaps, Lhx1 regulates

Dkk1 transcript levels in order to delimit the size of the pronephros as it undergoes differentiation.

Little is known regarding the molecular factors that control the expression of *Lhx1*. Indeed, this represents part of the impetus for performing this dissertation work. However, several groups have hypothesized that *Lhx1* regulation, as well as other aspects of pronephric development, require input from the retinoic acid pathway.

1.5.3 Retinoic acid pathway

Retinoic acid (RA) signaling influences many aspects of vertebrate development, including cell survival, proliferation, specification, differentiation, and organogenesis.[60] RA functions as a morphogen, a locally-produced signaling molecule acting at a distance to pattern tissue fields in a concentration-dependent manner.[61] The RA concentration gradient is refined by the local expression of Raldh enzymes, which synthesize RA, and Cyp enzymes, which catalyze its degradation.[61] RA alters gene expression by binding retinoic acid receptor (RAR)/retinoic X receptor (RXR) heterodimers located on the retinoic acid response elements (RAREs) of target genes.[61] Receptor activation by RA alleviates transcriptional inhibition mediated by a corepressor complex containing histone deacetylases (HDACs) and other factors.[62]

Experimental manipulation of RA levels in embryos reveals that the pathway performs important functions during pronephric development. In *Xenopus*, stimulating signaling with exogenous RA increases the expression of *pax8* and *lhx1* in the pronephric field.[63] Furthermore, RA-dependent kidney field expansions have also been reported for *Lhx1* in chick and *wt1a* in zebrafish.[64,65] In fact, a retinoic acid response element shown to bind RAR/RXR dimers *in vitro* was recently characterized in the zebrafish *wt1a* enhancer.[66] Treating *Xenopus* embryos with RA

also positively regulates the expression of the *Irx* genes, which likely function as competence factors during pronephric development.[67] Conversely, blocking the RA pathway decreases expression of *pax2*, *pax8*, and *lhx1* in the *Xenopus* pronephric field and eliminates *wt1a* expression.[63]

The ability of RA to affect the expression of renal progenitor markers suggests that the pathway may be involved in specification of the pronephric field. Indeed, treating *Xenopus* animal pole explants with both activin, a mesodermal inducer, and RA functions synergistically to induce *lhx1* expression.[52] Furthermore, treating mouse embryoid bodies, *in vitro* models of early embryogenesis,[68] with RA stimulates the expression of *Pax2* and *Wt1* more than 20-fold.[69] These data, taken together, support the idea that RA serves as an important factor in renal progenitor cell specification.

Two hypotheses have emerged to explain the effects of RA signaling on formation of the pronephric field. The first, supported by Cartry and coworkers, suggests that RA exerts a direct effect on renal progenitor cells.[63] They observed that cycloheximde treatment, which inhibits protein synthesis, failed to prevent an RA-dependent increase in *lhx1* expression during *Xenopus* pronephric development.[63] Therefore, they concluded that RA did not require protein mediators to regulate *lhx1*.[63] However, no RAREs have been reported in the *Xenopus lhx1* promoter to date. Alternatively, RA could exert an indirect effect. This hypothesis, proposed by Preger-Been Noon and coworkers, is based on their observation that expression of the homeobox gene, *Hoxb4*, increased following RA treatment in chick embryos.[64] RA directly regulates *Hoxb4* expression,[70] and overexpression of *Hoxb4* expands the expression of both *Pax8* and *Lhx1* in the chick pronephric field.[64] Work by Taira and coworkers supports this hypothesis.[71] They observed that RA treatment induces the expression of *hoxb4* in the *Xenopus* pronephric field prior to the

appearance of *lhx1*.[71] In addition, the expression domains of *hoxb4* and *lhx1* overlap, greatly improving the likelihood of interactions.[71] Regardless of the true mechanism, both hypotheses emphasize the importance of RA in patterning the pronephric fields of several vertebrate models, including zebrafish.

1.6 APPLICATIONS OF THE ZEBRAFISH MODEL

The zebrafish (*Danio rerio*), a small freshwater vertebrate native to India, first emerged as an experimental model in the 1950's.[72] The initial studies by Kenichi Hisaoka investigated the effects of small molecules, including carcinogens and barbiturates, on zebrafish development.[73-76] Despite these efforts, zebrafish publications rarely appeared over the next several decades, primarily due to a lack of genetic and molecular tools. In the 1980's, pioneering work by George Streisinger provided several useful techniques, laying the foundation for the current popularity of the zebrafish model.[77,78]

Zebrafish gained acceptance over the years as researchers came to appreciate the advantages they offer over other vertebrate models. Depending on age, adult zebrafish typically measure between 2 to 5 cm, their small size limiting housing requirements and husbandry costs.[79,80] Breeding pairs regularly produce hundreds of embryos per mating, providing the necessary numbers for even high-throughput applications.[81] Conveniently, fertilization occurs *ex utero*, greatly simplifying embryo collection and manipulation.[72] Embryos develop rapidly, initiating organogenesis by 24 hours post-fertilization (hpf) and forming most organs by 48 hpf.[81,82] The optical transparency of zebrafish embryos allows the observation of these processes

without the need for dissection or sacrifice.[83] In addition, at only a few millimeters in length, embryos fit easily into microwell plates, facilitating screening and automation.[72]

Zebrafish also exhibit qualities common to all widely-used vertebrate model systems. Their generation time of two to four months rivals that of mice and *Xenopus tropicalis*, making them comparably useful for genetic analyses.[80,84,85] Furthermore, all vertebrate embryos develop under the control of a highly-conserved program of patterning events.[79] Consequently, zebrafish exhibit the same general body plan as mammals, consisting of many homologous organs and cell types.[86] Importantly, the molecular and genetic tools currently used in zebrafish mirror those available in the mouse model. These include methods for transgenesis, mRNA overexpression, morpholino knockdown, and nuclease-based gene targeting.[72,80,87-89]

However, the zebrafish model also presents a unique set of challenges that should be considered when assessing its experimental utility. Unlike inbred mouse strains, it is likely that independent laboratory stocks of the most commonly-used zebrafish strains are not isogenic.[90] Indeed, even in so-called "inbred" zebrafish lines, polymorphisms have been reported in 7% to 11% of the tested loci.[91] This variation could greatly complicate zebrafish techniques relying on genetic mapping, such as positional cloning.[90,91] Furthermore, an ancient genomic event resulted in the duplication of approximately 30% of zebrafish genes in comparison to their mammalian orthologs.[92,93] For some applications, particularly knockdown or mutational analysis, the presence of extra gene loci may present a significant challenge. In addition, the availability of immortalized zebrafish cells for *in vitro* experimentation remains limited, as few stable lines have been established.[94,95] Finally, since antibodies are rarely raised against zebrafish proteins, finding antibodies that exhibit reactivity in zebrafish extracts can be difficult.

However, despite these limitations, the use of zebrafish in research has exploded over the past two decades; performing a PubMed search using the keyword "zebrafish" returns 18 articles from 1989, 531 articles from 1999, and 1686 articles from 2009.[96] The applications of the zebrafish model span a number of disciplines, each benefitting differently from its use. Studies of infection and immunity take advantage of the well-developed immune system of the zebrafish, which functions much like its mammalian counterpart.[97,98] Toxicologists use the rapid embryonic development of zebrafish to assess chemicals for lethality or teratogenicity in a matter of days, rather than weeks.[79] In addition, the small volumes needed to treat the embryos minimize the generation of hazardous waste, especially in high-throughput experiments.[79] Researchers investigating human genetic disorders employ a number of relevant zebrafish models, generated from a long history of random and targeted mutagenesis studies.[99-101] Zebrafish also demonstrate their value in the areas of kidney development and drug discovery, both of which constitute important parts of this dissertation.

1.6.1 Modeling kidney development

The early inductive events involved in patterning all three forms of the adult kidney likely have much in common.[102] Indeed, both pronephric and metanephric kidneys require input from factors such as *Pax2* and *Lhx1* to initiate development.[34,103] Therefore, the program of morphogenesis and epithelialization generating the two nephrons of the zebrafish pronephros probably reflects aspects of nephrogenesis in all vertebrates.[102] In zebrafish, this process occurs in four general steps.[12,104] Around 12 hpf, inductive signals affecting the IM specify some mesenchymal cells to a nephric fate, forming the first renal progenitor cells.[12,104] By 24 hpf, additional signals trigger the renal progenitor cells to undergo a mesenchymal to epithelial transition, forming the nephric

tubules and ducts.[12,104] Subsequent patterning of the glomerular capsule and anterior tubules, which takes place between 30 and 40 hpf, prepares the emerging nephron for operation.[12,104] Finally, invasion of the glomerular capsule by a capillary tuft completes the process of nephrogenesis and allows renal filtration to begin by 48 hpf.[12,104]

At this point, the zebrafish pronephros contains cells characteristic of metanephric nephrons. In the glomerulus, a fenestrated endothelium lines one side of the basement membrane, while extended podocyte foot processes protect the other.[12] In the tubule and duct, polarized epithelia have formed which exhibit apical brush borders, well-defined cell junctions, and ion-transport proteins.[104] Furthermore, recent studies have determined that zebrafish pronephric nephrons express segment-specific genes in a pattern consistent with that of mammalian metanephric nephrons.[105] Thus, in only two days of development, zebrafish provide a relevant model of both mammalian nephrogenesis and renal function.

In addition, several techniques available in the zebrafish model emphasize its value for studies of kidney development and function. Transgenic reporter lines for genes such as *lhx1a* and *pax2a* allow the real-time observation of renal progenitor cells in live embryos.[106,107] Kidney function can be easily assessed by injecting a 10 kD fluorescent dextran into the zebrafish circulatory system and monitoring its passage into the tubular lumen.[108] Alternatively, injecting a 500 kD dextran, which should be retained in a healthy kidney, tests the integrity of the filtration barrier for glomerular leakage.[109] Furthermore, researchers have developed many models of renal dysfunction in zebrafish. Damaging the pronephric tubules or glomerulus with nephrotoxic chemicals, for example, generates models of acute renal failure and minimal change disease, respectively.[110-112] Genetic analysis has also contributed a wide selection of valuable mutants, including models of polycystic kidney disease, ciliopathies, and proteinuria. [77,82-84]

1.6.2 Drug discovery

Of all the vertebrates, zebrafish are probably the best suited for high-throughput drug discovery using forward chemical genetics.[83] This approach involves screening small-molecule libraries to identify compounds capable of generating a desired phenotype.[113] Forward screens in zebrafish offer several advantages over classical reverse chemical screens, which seek compounds binding a specific target of interest *in vitro*.[113] Zebrafish cells appear in their normal context of cell-cell and cell-matrix interactions, unlike those maintained in culture.[114] Furthermore, performing whole-organism screens allows the examination of complex processes, such as organogenesis, that are not easily reproduced *in vitro*.[113] Screening in zebrafish also simultaneously provides animal testing data.[114] Therefore, compounds generating phenotypes likely possess favorable properties for future pharmacological development.[114]

Zebrafish embryos absorb small molecules directly from their culture environment, removing the need for labor-intensive microinjections.[115] However, since compounds must penetrate cell membranes to enter the embryo, typically only hydrophobic compounds exhibit biological activity.[116] Zebrafish embryos also develop normally in up to 1% dimethyl sulfoxide (DMSO), which frequently serves as a vehicle to improve compound solubility.[114,117] Therefore, it is often possible to test several compound concentrations from a single DMSO stock.[114] The ability to array zebrafish embryos in microwell plates permits screening in small volumes, minimizing compound costs.[97] This also facilitates automation, which has been successfully applied to observe the effects of small molecule libraries on zebrafish behavior.[118,119] Moreover, the emergence of sophisticated algorithms capable of detecting reporter fluorescence in transgenic lines offers a powerful tool for future high-throughput chemical screens.[120-122]

Zebrafish have been successfully used to identify interesting compounds in over a dozen published small molecule screens.[72,114] Compounds have been characterized that modulate aspects of zebrafish development and physiology, including heart rate,[120] hematopoiesis,[123] central nervous system morphogenesis,[124,125] ear development,[125] or even behavior.[118,119] Furthermore, zebrafish screens have revealed small molecules capable of influencing the bone morphogenetic protein (BMP),[126] fibroblast growth factor (FGF),[127] prostaglandin,[128] and RA signaling pathways.[116] Importantly, a study by Cao and coworkers demonstrated that screening small molecule libraries in zebrafish is a viable approach in examining aberrant kidney development.[129] They observed that treatment with histone deacetylase inhibitors (HDACis) suppressed cyst formation and axis curvature in zebrafish models of polycystic kidney disease.[129] Therefore, using zebrafish to screen for small molecules interfering with kidney development may also promote the identification of compounds affecting renal progenitor cells.

2.0 IDENTIFICATION AND CHARACTERIZATION OF PTBA

2.1 HYPOTHESIS

In 2004, the Hukriede lab performed an unbiased chemical library screen on zebrafish embryos, seeking small molecules capable of generating edemic phenotypes. Since edema may reflect renal dysfunction[130], they hoped to identify compounds capable of interfering with normal pronephric development. Determining the mechanisms of such compounds would provide insight into the molecular events guiding the specification of renal progenitor cells. Of the almost 2000 compounds tested, only four caused embryos to develop edema by the 72 hpf endpoint. One of these, 4-(phenylthio)butanoic acid (PTBA), demonstrated the ability to increase the expression of renal progenitor cell markers. After joining the lab in 2006, I began working to further characterize the effects of PTBA on the kidney field. I hypothesized that PTBA increased the number of renal progenitor cells, resulting in aberrant pronephric development.

2.2 RESULTS

2.2.1 PTBA causes edema in zebrafish larvae

Rachel Jackson performed the initial chemical screen using a library of small molecules with diverse structures. She observed that 61 compounds (3%) were lethal and identified four compounds (NSC115787, NSC134664, NSC357777, and NSC35400) that generated pericardial edema in treated zebrafish larvae at 72 hpf (**Figure 3**).

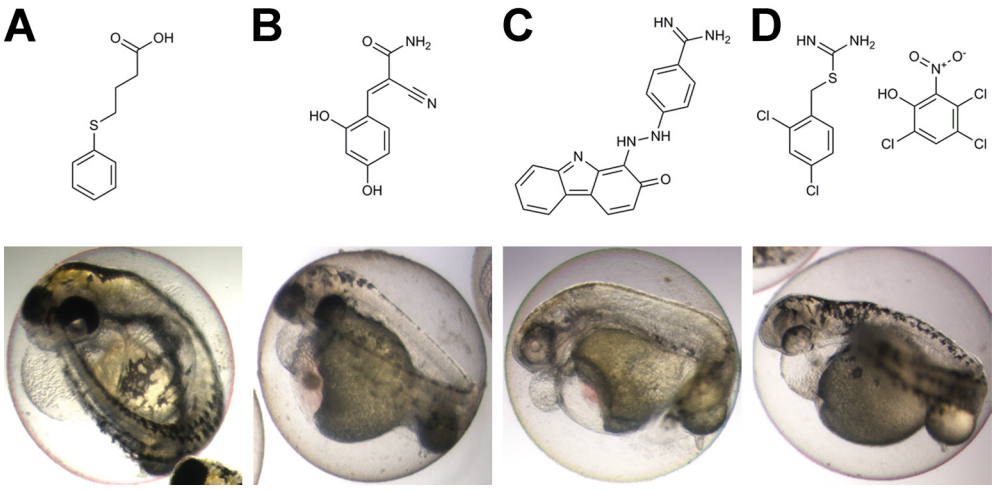

Figure 3. Four compounds causing pericardial edema in the initial phenotypic screen. (A through D) Top panels: chemical structures of NSC115787 (A), NSC134664 (B), NSC357777 (C), or NSC35400 (D). Bottom panels: edemic phenotypes in 72 hpf larvae treated with the corresponding compounds at 10 μM. Data generated by Rachel Jackson.

In situ hybridization performed by Rachel and Guangzu Gao determined that treatment with NSC134664, NSC357777, or NSC35400 (a disconnected structure) did not affect the size of the kidney field (data not shown). However, Rachel observed that treatment with various

concentrations of 4-(phenylthio)butanoic acid (PTBA, NSC115787) appeared to expand the expression of some renal markers during pronephric development (data not shown). To ensure experimental reproducibility, Dr. Weixiang Dai of the Department of Pharmaceutical Sciences synthesized and purified PTBA for use in all subsequent studies.

2.2.2 PTBA expands the kidney field

To determine the concentration of PTBA that maximized efficacy, while minimizing toxicity, I performed concentration-response experiments. Treatment with 3 μM PTBA caused 92% (n = 88) of the embryos to develop an edemic phenotype by 72 hpf without causing significant death (**Figure 4**). Therefore, I chose 3 μM PTBA as my working concentration. All embryos treated with 10 μM PTBA (n = 90), the concentration used in the initial screen, died before 72 hpf (**Figure 4**). This discrepancy probably reflects the concentration variability common in small molecule libraries.[131]

The edemic phenotypes elicited by PTBA treatment, coupled with Rachel's preliminary observations, prompted me to examine whether the compound affects renal progenitor cells. To address this, I determined the expression patterns and relative abundance of *lhx1a*, *pax2a*, and *pax8* at the 10-somite stage (14 hpf). This developmental stage occurs just after specification of the first renal progenitor cells.[104] *Lhx1a* expression was expanded in 95% of embryos treated with PTBA (n = 60) as compared with controls (n = 60) (**Figure 5, A and B**). This represented a three-fold increase in relative transcript as determined by quantitative real-time PCR (qPCR; **Figure 5, A and B**). Increased *lhx1a* expression appeared in the bilateral stripes of intermediate mesoderm that give rise to the pronephros (**Figure 5B**, arrowheads), as well as in the axial mesoderm (notochord; **Figure 5B**, asterisk).

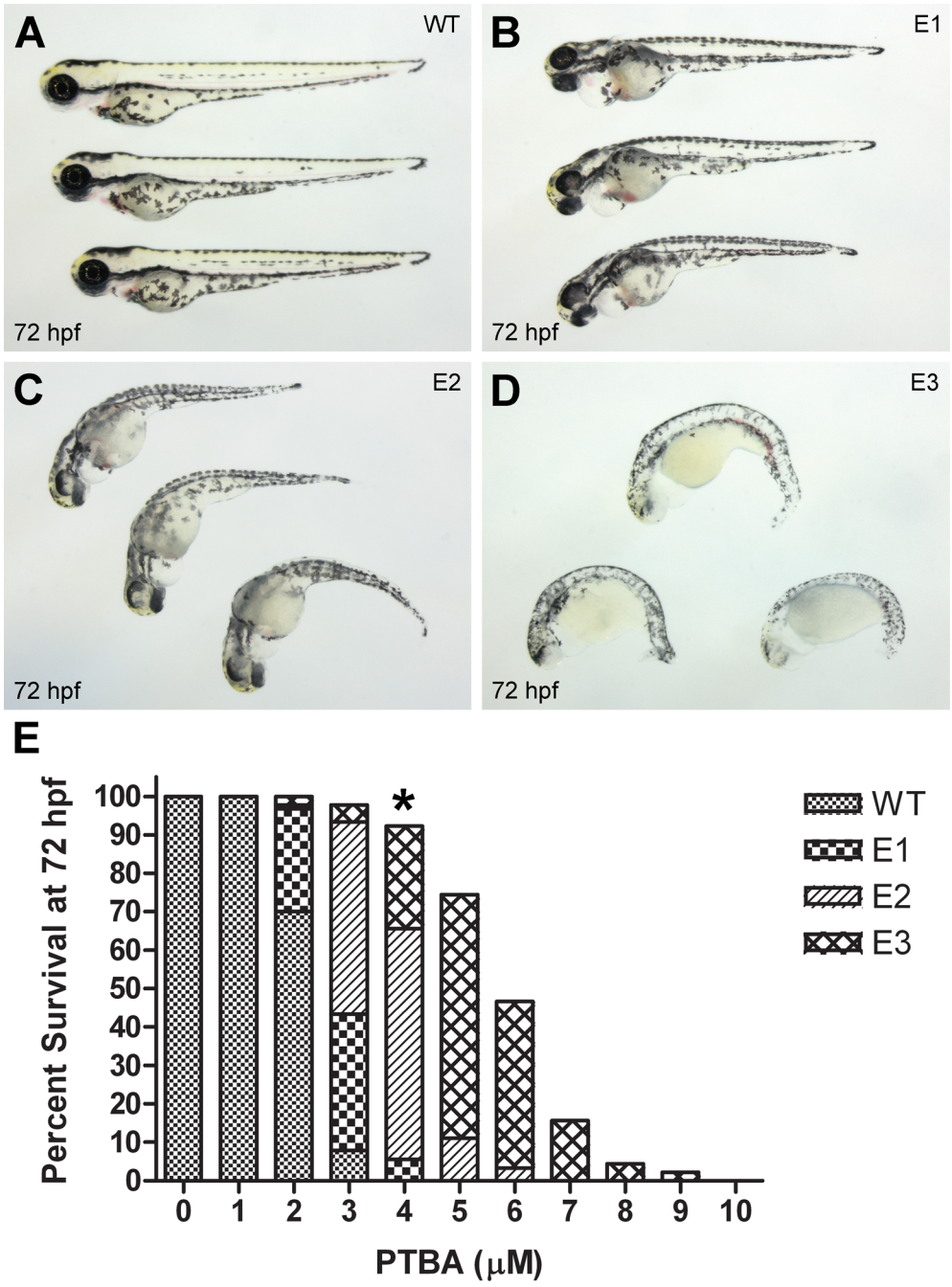

Figure 4. PTBA elicits concentration-dependent effects on larval edema and survival. (A through D) Embryos were treated with 0 to 10 μM PTBA from 2 hpf, and larvae were scored at 72 hpf using a phenotype-based classification system (see Methods). (A) Wild-type (WT). (B) Edemic 1 (E1). (C) Edemic 2 (E2). (D) Edemic 3 (E3). (E) Graph of phenotypes after treatment with 0 to 10 μM PTBA (n = 90 per concentration). Asterisk denotes lowest PTBA concentration that exhibits a significant effect ($p < 0.05$) on survival.

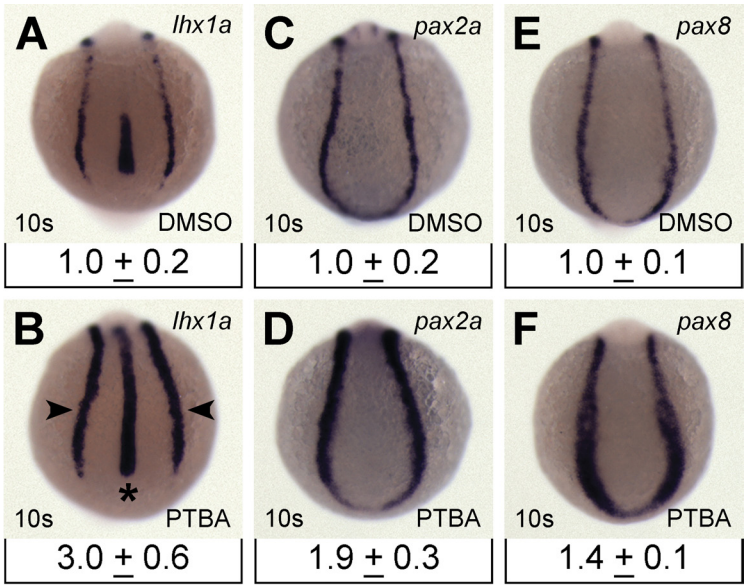

Figure 5. PTBA treatment increases the expression of renal progenitor markers. (A through F) *In situ* hybridization for *lhx1a* (A and B), *pax2a* (C and D), or *pax8* (E and F), in 10-somite embryos treated with 0.5% DMSO (A, C, and E) or 3 μM PTBA (B, D, and F). Arrowheads indicate renal progenitor cells, asterisk indicates notochord. Relative qPCR in the trunk region of 10-somite embryos (n = 4, 60 embryos per group) is displayed under the corresponding *in situ* image. Data are mean expression with 95% confidence interval, determined as described in the Methods section.

The expression domains of *pax2a* and *pax8* were also expanded in 95% and 97% of treated embryos, respectively, (*n* = 60, *pax2a*; *n* = 59, *pax8*) as compared with controls (*n* = 60, *pax2a*; *n* = 59, *pax8*) (**Figure 5, C through F**). This accounted for an almost two-fold increase in *pax2a* expression and a 50% increase in *pax8* expression as determined by qPCR (**Figure 5, C through F**).

Although these studies demonstrated that PTBA treatment resulted in increased gene expression, they did not indicate whether there are more renal progenitor cells or simply higher expression levels per cell. To differentiate between these two possibilities, I treated the *Tg(lhx1a:EGFP)*^{pt303} reporter line[107] with PTBA and counted the number of renal progenitor cells. As compared with control embryos, PTBA-treated embryos showed a 2.4-fold increase in the number of renal progenitor cells (**Figure 6, A through H**).

2.2.3 PTBA is effective during specification

Previously, Rachel had performed a temporal assay to determine the timing of PTBA efficacy. Initiation of PTBA treatments between 2 hpf and 14 hpf (10 somites) resulted in expanded *pax2a* expression at 24 hpf (**Figure 7, A through F**). However, beginning treatment at 16.5 hpf (15 somites) resulted in no kidney field expansion (**Figure 7G**). I later determined that initiating treatments at 15 somites or later did not affect the functional kidney as assayed by a lack of edema in 72 hpf larvae (*n* = 90, data not shown). Thus, the effective temporal treatment window exhibited by PTBA coincides with the period when renal progenitor cells are specified.[46,104]

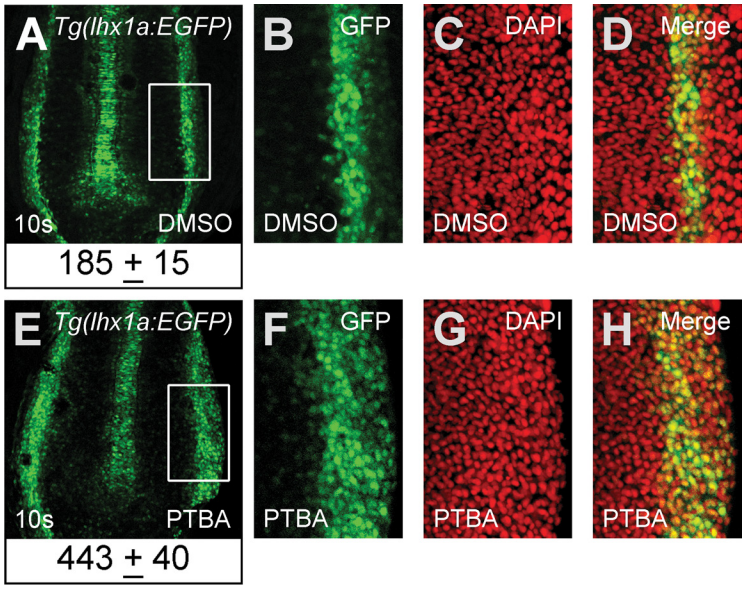

Figure 6. PTBA treatment increases the number of renal progenitor cells. (A through H) Confocal projections of 10-somite *Tg(lhx1a:EGFP)*^{pt303} embryos treated with 0.5% DMSO (n = 18 [A through D]) or 3 μM PTBA (n = 21 [E through H]). Boxed areas (A and E) were counted for GFP- and DAPI-positive nuclei and are shown in B and F (GFP), C and G (DAPI), and D and H (merge). Cell counts are mean number of positive cells plus 95% confidence interval (A and E). Confocal microscopy performed by Lisa Antoszewski.

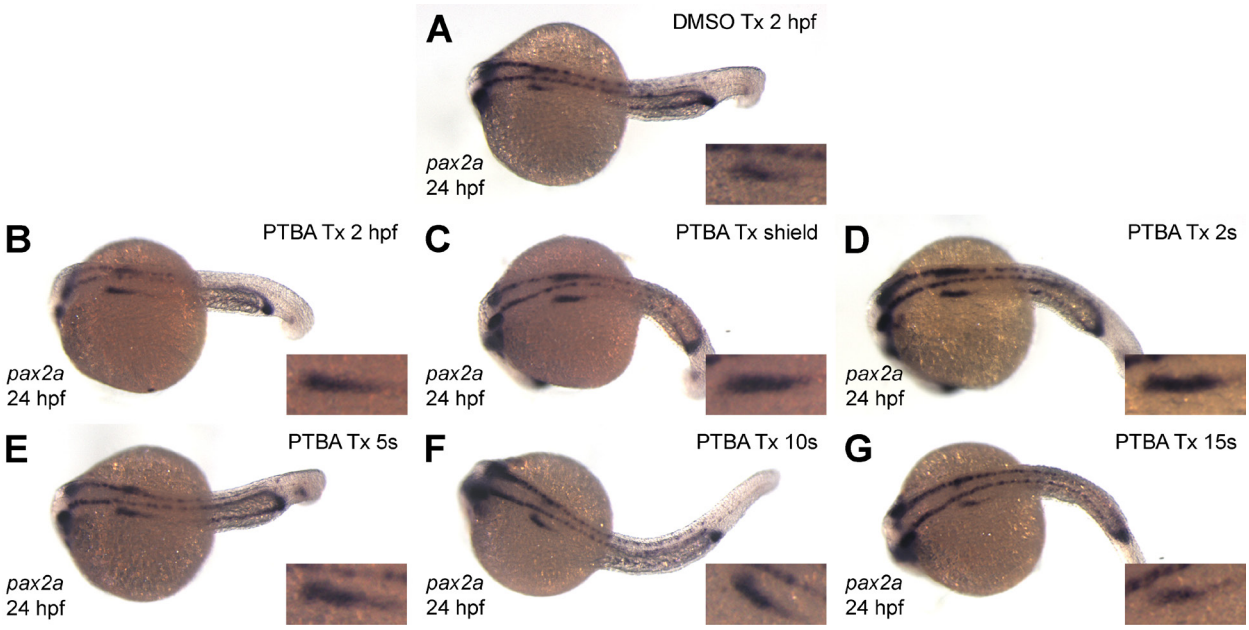

Figure 7. PTBA is effective during renal progenitor cell specification. (A through G) *In situ* hybridization for *pax2a* in 24 hpf embryos treated with 0.5% DMSO from 2 hpf (A, *n* = 132) or 3 μM PTBA from: 2 hpf (B, *n* = 67), shield (C, 6 hpf, *n* = 100), 2 somites (D, 10.7 hpf, *n* = 71), 5 somites (E, 11.7 hpf, *n* = 87), 10 somites (F, 14 hpf, *n* = 89), or 15 somites (G, 16.5 hpf, *n* = 72). Insets are *pax2a* enlargements (lower field). Data generated by Rachel Jackson.

2.2.4 PTBA increases pronephric size

To determine whether PTBA treatment resulted in a transient or persistent expansion of the kidney field, I examined the kidney at 48 hpf using markers of glomerulus and tubule. [65,108,132] As compared with controls (n = 54), 89% of PTBA-treated embryos (n = 56) displayed an expansion of the pan-tubule marker *cdh17* (**Figure 8, A through D**). Cross-sections from the proximal region of the *cdh17* expression domain confirmed the expansion (**Figure 8, E and F**).

I also assessed pronephric expansion at the protein level by examining the expression of NaK-ATPase, another pan-tubule marker (**Figure 9, A and B**). As compared with controls (n = 10), 100% of PTBA-treated embryos (n = 10) exhibit expansion of NaK-ATPase protein expression. Cross-sections taken from the distal region of the NaK-ATPase expression domain show an increase in tubular diameter consistent with that observed with *cdh17*. (**Figure 9, C and D**, compare with **Figure 8, E and F**).

To determine if PTBA exhibits any segment-specific effects on the size of the pronephros, I examined markers of podocytes (*wt1a*), proximal tubule (*slc4a4*), and distal tubule (*slc12a1*). As compared with controls (n = 57, 58, and 56, respectively), PTBA-treated embryos exhibited 74% expansion of *wt1a* (n = 50), 92% expansion of *slc4a4* (n = 60), and 64% expansion of *slc12a1* (n = 59) (**Figure 10**). These results argue that PTBA treatment likely causes expansion of the entire pronephros. Furthermore, while the *wt1a* expression domains in control embryos have migrated to the midline by 48 hpf, the domains of PTBA-treated embryos remain separated (**Figure 10, A and B**). Since *wt1a* is essential for proper glomerular morphogenesis,[133] this misexpression may contribute to a loss of kidney function. This observation could explain the edemic phenotypes associated with PTBA treatment.

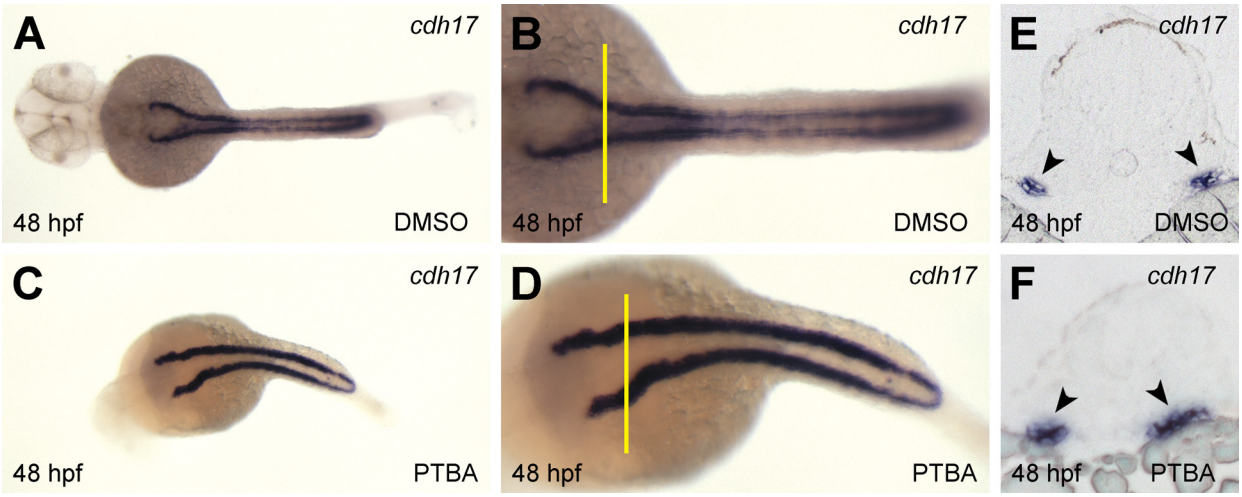

Figure 8. PTBA treatment expands *cdh17* expression. (A through D) *In situ* hybridization for *cdh17* expression in 48 hpf embryos treated with 0.5% DMSO (A [magnified in B]) or 3 μM PTBA (C [magnified in D]). (E and F) Proximal tubule cross-sections (5 μm) taken from *cdh17 in situ* hybridizations of 48 hpf embryos treated with 0.5% DMSO (E) or 3 μM PTBA (F). Cross-sections were taken from the locations indicated in B and D by yellow lines. Sectioning performed by Chiara Cianciolo Cosentino.

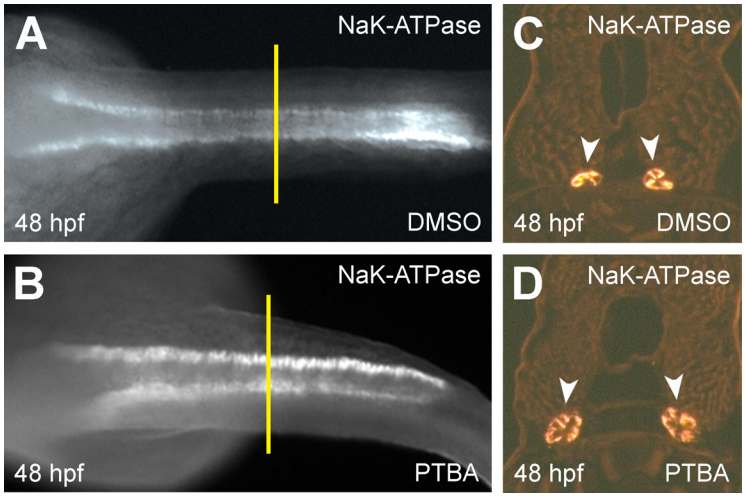

Figure 9. PTBA treatment expands NaK-ATPase expression. (A and B) Whole-mount antibody staining for NaK-ATPase in 48 hpf embryos treated with 0.5% DMSO (A) or 3 μM PTBA (B). (C and D) Distal tubule cross-sections (5 μm) taken from NaK-ATPase antibody-stained 48 hpf embryos treated with 0.5% DMSO (C) or 3 μM PTBA (D). White arrowheads indicate NaK-ATPase protein expression. Cross-sections were taken from the locations indicated in A and B by yellow lines. Sectioning performed by Chiara Cianciolo Cosentino.

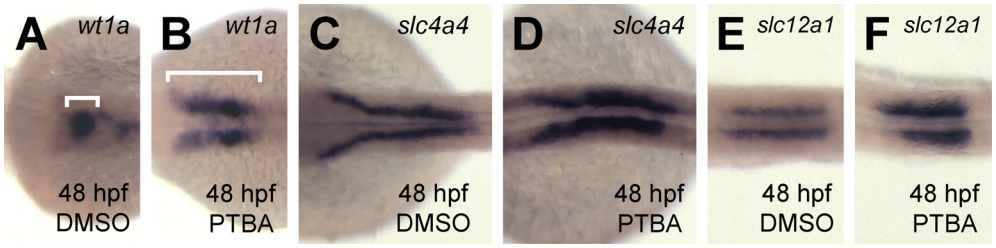

Figure 10. PTBA treatment expands several pronephric regions. (A through F) *In situ* hybridization for the podocyte marker *wt1a* (A and B), the proximal tubule marker *slc4a4* (C and D) and the distal tubule marker *slc12a1* (E and F) in 48 hpf embryos treated with 0.5% DMSO (A, C, and E) or 3 μM PTBA (B, D, and F). Brackets in A and B indicate the expression domain of *wt1a*.

2.2.5 PTBA does not transform neighboring tissues to a kidney fate

The PTBA-mediated increase in kidney field size could result from the transformation of non-renal cells to a renal progenitor fate. To assess this possibility, I examined the effects of PTBA on markers of two mesodermal tissues juxtaposed to renal progenitor cells: *myod1* (somites) and *fli1a* (vasculature). By *in situ* hybridization, I observed that *myod1* expression was slightly decreased in 95% of PTBA-treated embryos (n = 60) at the 10-somite stage, as compared with controls (n = 60) (**Figure 11, A and B**). However, subsequent qPCR analysis did not confirm the significance of this observed decrease (**Figure 11, A and B**). Expression of *fli1a* remained unchanged in 97% of PTBA-treated embryos (n = 60), as compared with controls (n = 59), and as assayed by qPCR (**Figure 11, C and D**).

In addition to increased *lhx1a* expression in renal progenitor cells, I had also observed increased *lhx1a* expression in the notochord (**Figure 5B, asterisk**). To determine whether this expansion reflected an effect on notochord size or a general increase in *lhx1a* expression, I assayed the notochord-specific marker *ntla*. I observed that *ntla* was increased in 88% of PTBA-

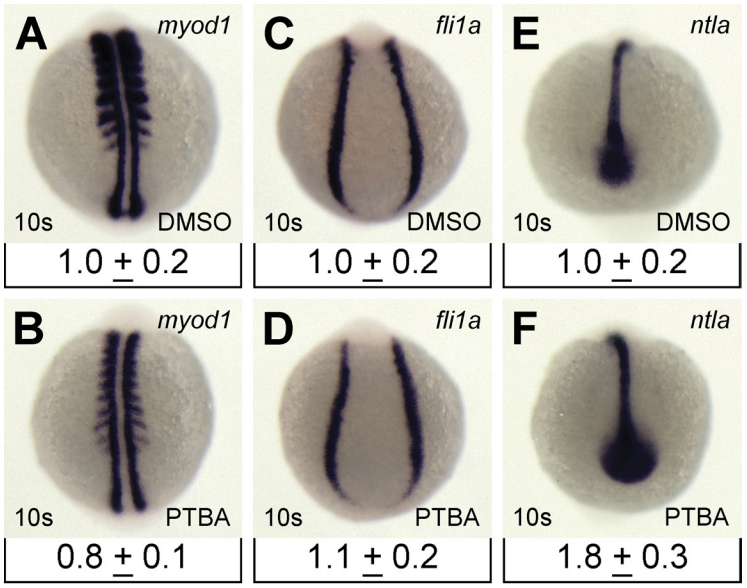

Figure 11. PTBA treatment does not transform nearby tissues to a renal fate. (A through F) *In situ* hybridization for the mesodermal markers *myod1* (A and B), *fli1a* (C and D), and *ntla* (E and F) in 10-somite embryos treated with 0.5% DMSO (A, C, and E) or 3 μM PTBA (B, D, and F). Relative mRNA abundance in the trunk region of 10-somite embryos (n = 4, 60 embryos per group) is displayed under the corresponding *in situ* image. Data are mean expression with 95% confidence interval, determined as described in the Methods section.

treated embryos (n = 60), as compared with controls (n = 59) (**Figure 11, E and F**). This represented an 80% increase in *ntla* expression by qPCR analysis (**Figure 11, E and F**). The minimal effect on juxtaposed tissues coupled with an increase in the size of the notochord suggests that these cell types are not being converted to renal progenitor cells. Therefore, PTBA treatment cannot be definitively linked to a fate-transformation event.

2.2.6 PTBA requires proliferation for efficacy

To examine the alternative possibility that PTBA-mediated renal progenitor cell expansion depends on cell proliferation, I tested the efficacy of PTBA in the presence of hydroxyurea and aphidicolin (HUA). HUA treatment has been previously shown to block cell division without affecting tissue specification.[134] As expected, 97% of PTBA-treated embryos (n = 123) exhibited an expansion of *lhx1a* expression at 10 somites, as compared with controls (n = 136), (**Figure 12, A and B**). HUA treatment alone did not affect *lhx1a* expression (**Figure 12C**). However, treatment with both HUA and PTBA resulted in *lhx1a* expansion in only 13% of 10-somite embryos (n = 104) (**Figure 12D**). Furthermore, although *lhx1a* expression was decreased in the intermediate mesoderm, expression in the axial mesoderm still appeared to be increased in treated embryos (**Figure 12D**). This result suggests that the PTBA-mediated *lhx1a* expansion in the axial region is proliferation independent. Since *lhx1a* expression in the axial mesoderm is gradually restricted to the tailbud during somitogenesis,[107] the effect may reflect transcript perdurance.

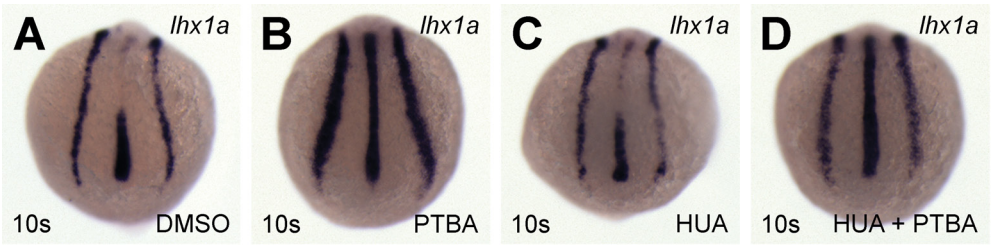

Figure 12. PTBA requires proliferation for efficacy. (A through D) *In situ* hybridization for *lhx1a* expression in 10-somite embryos treated at 5 hpf with 0.5% DMSO (A and B) or HUA (C and D). At 8 hpf, treatment solutions were replaced with 0.5% DMSO (A), 3 μM PTBA (B), HUA (C), or 3 μM PTBA and HUA (D).

2.3 METHODS

2.3.1 Zebrafish husbandry

Zebrafish were maintained under standard conditions[135] and staged as previously described.[136] Embryos were collected from group matings of wild-type AB adults. All animal husbandry adhered to the National Institutes of Health Guide for the Care and Use of Laboratory Animals.

2.3.2 Small molecule screening

The screen was performed in zebrafish embryos using the National Cancer Institute's Developmental Therapeutics Program (NCI/DTP) Diversity Set I.[137] This library contains 1990 compounds selected by pharmacophore modeling to represent the more than 140,000 small molecules maintained in the NCI/DTP Open Repository. Compounds from the NCI/DTP Diversity Set I were diluted to 10 μM in E3 embryo medium (5 mM NaCl, 0.33 mM $CaCl_2$, 0.33 mM $MgSO_4$, and 0.17 mM KCl) in a final DMSO concentration of 0.5% and arrayed in 96-well plates. Beginning at approximately 2 hpf, embryos were transferred to each well in groups of five using a glass pipette. The plates were incubated at 28.5 ^{o}C for 70 hours. Individual wells were then scored for a dominant phenotype, representative of at least four of the five embryos. The primary objective was to identify compounds that caused edema in treated embryos at 72 hpf. Small molecules generating edema were retested once for verification, before obtaining additional compound from the NCI/DTP Open Repository.

2.3.3 Compound sources and treatments

PTBA was synthesized as described below. Hydroxyurea and aphidicolin were obtained from Sigma-Aldrich. Groups of 20 to 30 chorionated 2 hpf embryos were arrayed in individual wells of 12-well plates. E3 medium was removed with a glass pipette and replaced with 1.5 ml treatment solutions containing 0.5% DMSO in E3 with or without compound at the reported concentrations. Treatments for all studies were initiated at 2 hpf, except for the temporal studies (**Figure 7**) and the HUA studies (**Figure 12**). HUA studies were performed as described previously,[138] with the following modifications. HUA in 0.5% DMSO was added at early gastrulation (5 hpf) and PTBA was subsequently added at late gastrulation (8 hpf) to allow for penetration of the proliferation inhibitors. All embryos were incubated at 28.5 ^{o}C until the required developmental stage.

2.3.4 Synthesis of PTBA

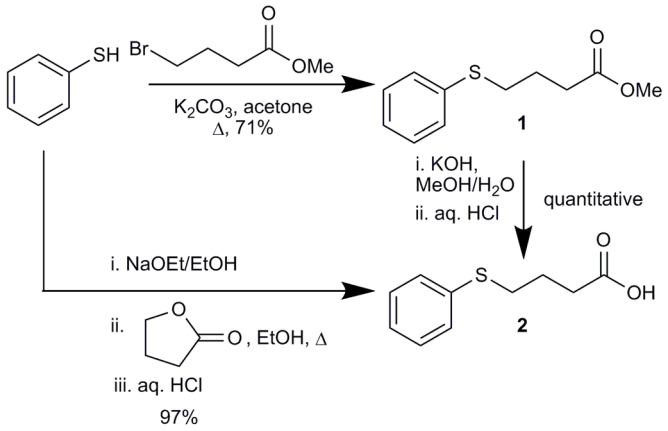

Figure 13. Synthesis scheme for PTBA

Methyl 4-(phenylthio)butanoate (**1**) was prepared from thiophenol, potassium carbonate, and methyl 4-bromobutyrate in refluxing acetone as previously described.[139] 4-(phenylthio)butanoic acid (**2**) was prepared either in quantitative yield by saponification of **1** with aqueous KOH in MeOH overnight at room temperature followed by acidification with aqueous HCl, or in 97% yield from reaction of the sodium salt of thiophenol and γ-butyrolactone in refluxing EtOH and subsequent acidification with aqueous HCl as previously described.[140] All compounds gave ^{1}H and ^{13}C NMR (400/100 MHz and/or 600/150 MHz), mass spectra (GC-EI-MS, LC-ESI-MS, and high-resolution MALDI-TOF-MS), and melting points consistent with the literature and their structures. All spectral and melting point data suggested >99% purity.[139-141]

2.3.5 Concentration-response studies

Following 70 hours of treatment (as described above), edemic phenotypes in 72 hpf larvae were scored using a phenotype-based classification system. Wild type: no visible edema or developmental delay. Edemic 1: pericardial edema evident, may exhibit slight developmental delay, little or no axis curvature, axis length normal. Edemic 2: pericardial edema evident, slight to moderate developmental delay, axis curvature, axis length normal or slightly reduced. Edemic 3: pericardial edema evident, moderate to severe developmental delay, gross axis curvature frequently accompanied by tail kink, axis noticeably shortened. Significant effects ($p < 0.05$) on survival were determined by two-tailed Fisher's exact test in comparison with the 0 μM PTBA treatment group.

2.3.6 *In situ* hybridization and immunocytochemistry

In situ hybridization was performed as previously described with some modifications.[142] Hybridization temperature was 65 ^{o}C. Embryos were blocked in 2% blocking reagent (Roche) with 5% sheep serum in MAB (100 mM maleic acid and 150 mM NaCl [pH 7.5]). Whole-mount immunocytochemistry with 1:25 mouse anti-α6F antibody (Developmental Studies Hybridoma Bank) and 1:100 Cy3 secondary antibody (Jackson ImmunoResearch) was performed as described previously.[108] Embryos were embedded in JB-4 for sectioning per the manufacturer's instructions (Polysciences), sectioned at 5 μm, and mounted with Cytoseal 60 (Richard-Allan Scientific).

2.3.7 Relative qPCR

2.3.7.1 cDNA synthesis

Several of the genes analyzed by qPCR, including *lhx1a* and *pax2a*, show expression in anterior regions of the embryo as well as the IM. To focus more specifically on effects in the IM, I examined cDNA samples taken from the trunks of treated and control embryos. Samples for trunk RNA extraction were prepared by cutting embryos just above the first somite with microscissors and discarding the anterior portion. The trunk portions were homogenized with a plastic microcentrifuge pestle in 500 μL of TRI reagent (Ambion), and RNA was isolated using an RNeasy Micro Kit (QIAGEN) per the manufacturer's instructions. 1 μg RNA was heated to 75 ^{o}C for 5 min and then placed on ice. The following reagents were then added to a final volume of 29 μl: 1X Expand High-Fidelity PCR buffer without $MgCl_2$ (Roche), 3 mM $MgCl_2$, 500 μM dNTPs, 3.3 μM random hexamers, and 30 U Protector RNase Inhibitor (Roche). The

mixture was preincubated to 42 ^{o}C for 5 min. 1 µl of 200 U/µl SuperScript II Reverse Transcriptase (RT) or RNase-free water was added for +RT or –RT reactions, respectively. Reactions were incubated at 42 ^{o}C for 1 hr and then stopped by heating to 95 ^{o}C for 5 min. Reaction products were stored at -20 ^{o}C.

2.3.7.2 Primer sets

Primer sets were designed using NetPrimer and Beacon Designer (ver. 7.51) primer analysis software (PREMIER Biosoft). In each set, one primer was designed to span an exon boundary. In addition, at least one primer was confirmed to exhibit no significant cross-homology when compared against the NCBI zebrafish RefSeq mRNA library by BLAST search. Primer melting temperatures were maintained between 60 and 64 ^{o}C as determined by NetPrimer. Each primer set was observed to generate a single amplicon of expected length following qPCR.

The reference gene primer sets have been previously described[143] with one modification. The *β-actin* (F) sequence was changed to: CGTGCTGTCTTCCCATCCA. This corrects a one-base discrepancy from the reported ENSDART accession number. The other primer sets included: *lhx1a* (F): TTCATACTATGGAGATTATCAAAGCG, *lhx1a* (R): GGTCCTGATGAGGGAACAAAAG, *pax2a* (F): GTCCCTGGAAGCGACTTTTC, *pax2a* (R): TTGACTGGGCTGCGATGG, *pax8* (F): GCTCCGCCGTCACTCCTC, *pax8* (R): TCTCCTGGTCACTGTCATCGTG, *ntla* (F): CGCAGCACTACCACCAATAACTAC, *ntla* (R): GAGCCTGATGGGGTGAGAGTC, *myod1* (F): TTCTGGAACATTACAGTGGAGACTC, *myod1* (R): GTGCGTCAGCATTTGGTGTG, *fli1a* (F): CGGAAAAGGCTCTCCAACAG, *fli1a* (R): TGCTGGTGGGTCCTAATATCTG.

2.3.7.3 qPCR conditions

Relative qPCR was performed as described previously[143] with some modifications. 25 µl reactions were prepared containing the following reagents: 12.5 µl 2X iQ SYBR Green Supermix (Bio-Rad), 5 µl 1 µM primer mix (1 µM each of forward and reverse primer), 5.5 µl RNase-free water, and 2 µl 1:10-diluted template (+RT or –RT product) or 2 µl RNase-free water (no template control). Each assay was performed in triplicate wells using an iQ5 Real-Time PCR Detection System (Bio-Rad). Thermal cycling was performed for 40 cycles, each consisting of 94 ^{o}C for 15 s, then 59 ^{o}C for 1 min. Following amplification, melt curve analysis was performed to assess non-specific amplification. Each primer set yielded a single peak, indicative of specific amplification. Reactions performed using –RT product or no template controls were observed to exhibit little or no amplification in comparison with their +RT counterparts.

2.3.7.4 Reference gene determination

Seven reference gene candidates [*β-actin*, *β2 microglobulin*, *elongation factor 1 alpha*, *hypoxanthine guanine phosphoribosyl transferase 1*, *RNA polymerase subunit D*, *ribosomal protein L13a*, and *succinate dehydrogenase complex subunit A* (*SDHA*)][143] were screened to determine the gene(s) least affected by PTBA treatment. Relative qPCR experiments (n = 3, 180 embryos) were performed using trunk cDNA obtained from 10-somite embryos treated from 2 hpf with either 0.5% DMSO or 3 µM PTBA. The results were analyzed using NormFinder software (ver. 0.953) to determine the most stable reference gene or combination of genes.[144] The combination of *β-actin* and *SDHA* was observed to exhibit the most stability, and was therefore used for normalization of all qPCR data.

2.3.7.5 Data analysis

Relative gene expression was calculated using iQ5 software (ver. 2.0, Bio-Rad) to determine normalized expression levels (ΔΔCt method). For comparison of fold-differences, the expression levels obtained from DMSO-treated controls were set to a value of 1.0. The amplification efficiency of each reaction was calculated using LinRegPCR software (ver. 11.4).[145] The mean efficiencies of each tested primer set fell between 91% and 100%. Mean expression levels (normalized to the control group) and the corrected expression SD were used to generate 95% confidence intervals for each data set.

2.3.8 Cell counting

Tg(lhx1a:EGFP)^{pt303} embryos[107] were treated with 3 μM PTBA and then fixed in 4% paraformaldehyde in PBS for 8 hours at 4 ^{o}C. Embryos were washed in PBS containing 0.1% TWEEN 20 (PBT) and incubated in 1 μg/ml DAPI in PBT for 30 minutes at room temperature. Embryos were flat-mounted on glass slides with Cytoseal 60 and imaged with either a Leica M205 FA epifluorescent microscope or an Olympus FluoView 1000 confocal microscope. Confocal projections contained stacks of six 3 μm images.

A predefined box was positioned at the most posterior region of the notochord and included the most lateral GFP-positive cell in a kidney field. The cells that were positive for both GFP and DAPI within this box were counted manually with the aid of ImageJ. Variances of the control and PTBA-treated groups were compared by *F* test and found to be unequal. Therefore, a two-tailed *t* test with unequal variance was used to determine significance ($\alpha = 0.05$).

3.0 MECHANISM OF PTBA EFFICACY

3.1 HYPOTHESIS

Having established that PTBA stimulates renal progenitor cell proliferation (Chapter 2), I next attempted to determine the mechanism responsible for this effect. Initial structure-activity relationship experiments demonstrated that certain structural motifs within PTBA modify its efficacy. While these results provided important leads for future analog development, they did not reveal any clues to the underlying mechanism. The breakthrough came when subsequent analysis revealed that PTBA is structurally similar to known histone deacetylase inhibitors (HDACis), including 4-phenylbutanoic acid (PBA) and trichostatin A (TSA). HDACis are thought to attenuate retinoic acid receptor-mediated inhibition of target genes, lowering the threshold of retinoic acid (RA) required to activate transcription.[62] Since RA affects pronephric development,[63,65] I hypothesized that PTBA functions as an HDACi and its effects are mediated through the RA pathway.

3.2 RESULTS

3.2.1 PTBA structure-activity studies reveal critical motifs

I performed structure-activity analyses using a series of seven analogs (**Figure 14**). *In situ* hybridization for *lhx1a* was performed on 10-somite embryos treated with each analog at 3 μM. The results were compared with control (no expansion, *n* = 53) (**Figure 14A**) and PTBA-treated embryos (100% expansion, *n* = 52) (**Figure 14B**). I observed that replacement of the phenylthio ether with a phenylsulfonyl linkage stripped the compound of its effects on renal progenitor cells (no expansion, *n* = 54) (**Figure 14C**). Therefore, the oxidation state of the sulfur atom is a critical activity determinant. However, 4-(naphthalen-2-yl thio)butanoic acid, an analog carrying a naphthalene ring in place of the phenyl moiety of PTBA, still expands *lhx1a* expression to some extent (33% expansion, *n* = 39) (**Figure 14D**). Thus, modifications of the ring structure are tolerated and suggest a site for future analog development.

Two analogs containing substitutions of the butanoic acid backbone, 2-amino-PTBA and 3-(phenylthio)benzoic acid had no effect on *lhx1a* expression (no expansion, *n* = 64 and *n* = 53, respectively) (**Figure 14, E and F**), suggesting a requirement for a flexible hydrocarbon backbone for biological activity. I also examined 4-phenoxybutanoic acid and 5-phenylpentanoic acid, which contain oxygen and carbon substitutions for the sulfur atom, respectively. 4-Phenoxybutanoic acid exhibited reduced activity compared with the parent compound (13% expansion, *n* = 56) (**Figure 14G**), while 5-phenylpentanoic acid was inactive (no expansion, *n* = 55) (**Figure 14H**). These results suggest that compound efficacy is improved when an atom with a nonbonding electron pair(s) occupies this position. Finally, the esterified analog methyl-4-(phenylthio)butanoate exhibited equal potency to PTBA (100% expansion, *n* = 41) (**Figure 14I**).

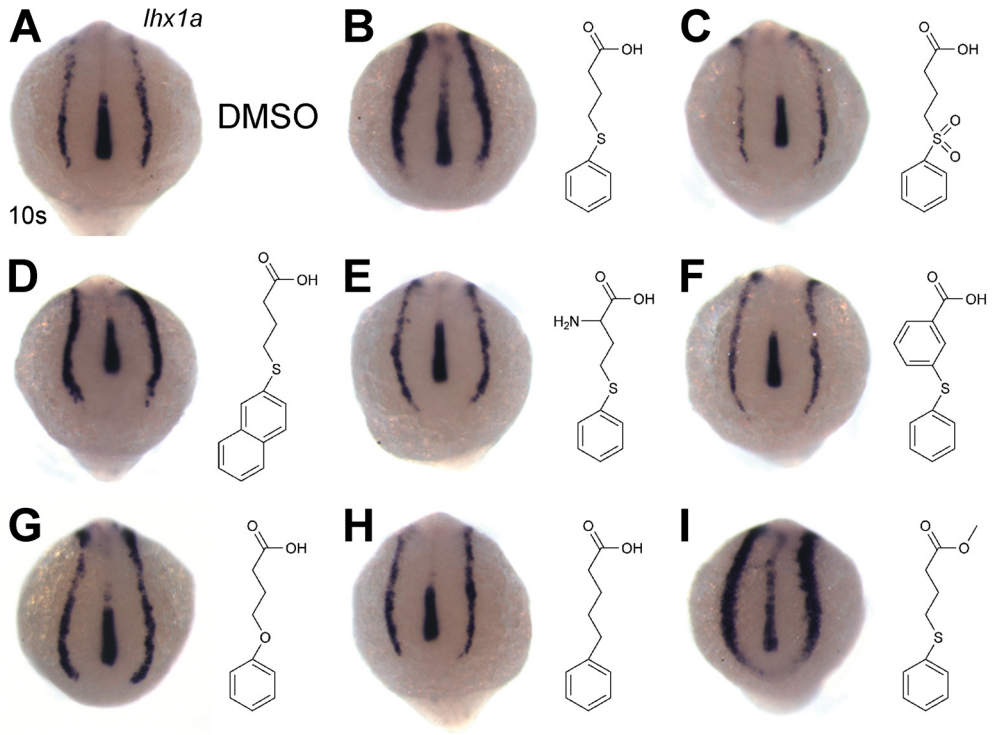

Figure 14. Structure-activity relationship studies reveal essential moieties for PTBA efficacy. (A through I) *In situ* hybridization for *lhx1a* expression in 10-somite embryos treated with 0.5% DMSO (A) or 3 μM of the following compounds: PTBA (B), 4-(phenylsulfonyl)butanoic acid (PSOBA) (C), 4-(naphthalen-2-ylthio)butanoic acid (D), 2-amino-PTBA (E), 3-(phenylthio)benzoic acid (F), 4-phenoxybutanoic acid (G), 5-phenylpentanoic acid (H), and methyl-4-(phenylthio)butanoate (I).

3.2.2 HDACis mimic the effects of PTBA

Subsequent structural analysis revealed that PTBA is a close analog of 4-phenylbutanoic acid (PBA), a known HDACi (**Figure 15, A and B**), and that both compounds exhibit some similarity to the HDACi trichostatin A (TSA) (**Figure 15C**). Indeed, all three structures contain the elements of the HDACi pharmacophore, a general representation of the functional domains within this class of compounds (**Figure 15D**). These include an aliphatic or aromatic cap, connecting unit, hydrophobic linker, and zinc-binding group.

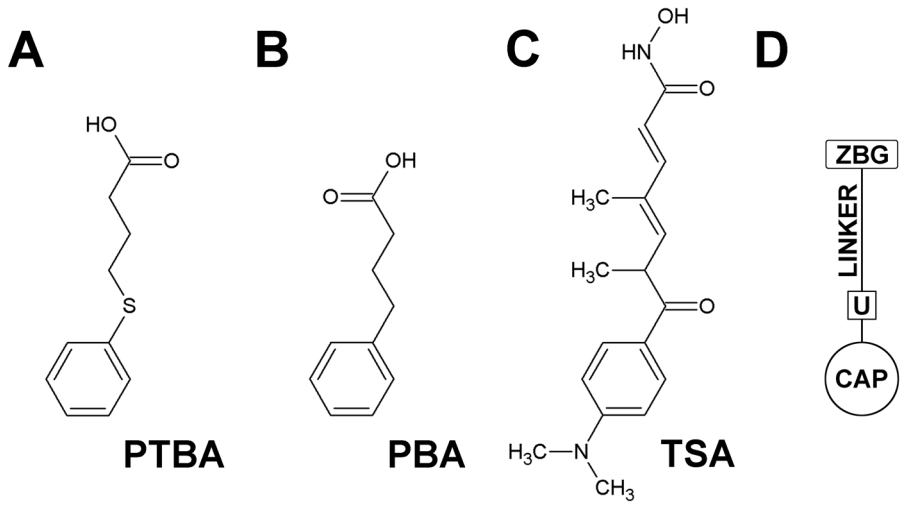

Figure 15. PTBA exhibits structural similarity to HDACis. (A through D) Structures of PTBA (A), PBA (B), TSA (C), and the general HDACi pharmacophore (D) containing a cap (CAP), connecting unit (U), hydrophobic linker (LINKER), and zinc-binding group (ZBG).

Because PBA and TSA are structurally analogous to PTBA, I determined if they shared the same ability to expand renal progenitor cells. Concentration-response experiments were performed to determine the concentrations of PBA or TSA necessary to elicit *lhx1a* expansion, if any (**Figures 16 and 17**).

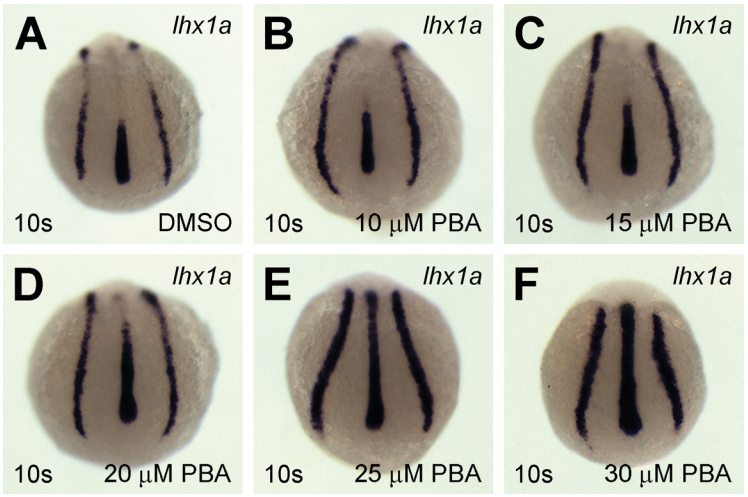

Figure 16. Treatment with the HDACi PBA expands the kidney field. (A through F) *In situ* hybridization for *lhx1a* in 10-somite embryos treated from 2 hpf with: 0.5% DMSO (A, *n* = 59), 10 μM PBA (B, *n* = 58), 15 μM PBA (C, *n* = 60), 20 μM PBA (D, *n* = 59), 25 μM PBA (E, *n* = 58), or 30 μM PBA (F, *n* = 53).

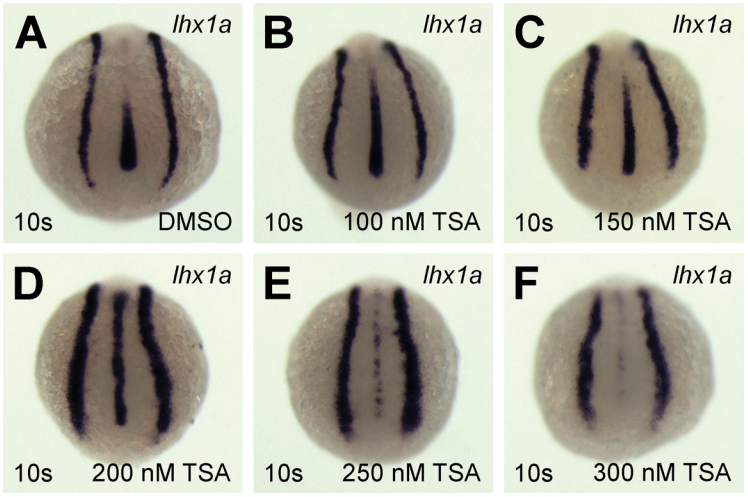

Figure 17. Treatment with the HDACi TSA expands the kidney field. (A through F) *In situ* hybridization for *lhx1a* in 10-somite embryos treated from 2 hpf with: 0.5% DMSO (A, *n* = 60), 100 nM TSA (B, *n* = 57), 150 nM TSA (C, *n* = 57), 200 nM TSA (D, *n* = 52), 250 nM TSA (E, *n* = 42), or 300 nM TSA (F, *n* = 40).

I determined that treatment with 25 μM PBA or 200 nM TSA produced an expansion of *lhx1a* expression consistent with that elicited by 3 μM PTBA (**Figures 16E and 17D compared with Figure 5B)**. Therefore, at least two known HDACis mimic the effects of PTBA, supporting the idea that PTBA likewise functions as an HDACi.

3.2.3 PBA and TSA exhibit greater toxicity than PTBA

I next tested how trunk mesoderm juxtaposed to the kidney field is affected by PBA and TSA treatments. I previously determined that PTBA treatment does not significantly affect the expression of somitic or vascular markers (**Figure 11, A through D**) Furthermore, although PTBA increased *ntla* expression, the general structure of the notochord remained relatively unchanged (**Figure 11, E and F**). However, TSA is a broad-spectrum HDACi that causes disruption of multiple tissues in zebrafish and demonstrates renal toxicity in cell culture.[146-148] Therefore, I treated embryos with 25 μM PBA or 200 nM TSA and compared the expression of *myod1*, *fli1a*, and *ntla* with that of control embryos. Expression of *myod1* was decreased in 57% of PBA-treated embryos (n = 53) and 100% of TSA-treated embryos, as compared to controls (n = 54) (**Figure 18, A through C**). Furthermore, TSA treatment caused an almost complete loss of the somitic blocks (**Figure 18C**). As compared with controls (n = 54), *fli1a* expression decreased in 78% of PBA-treated embryos (n = 54) and 95% of TSA-treated embryos (n = 55) (**Figure 18, D through F**). PBA increased *ntla* expression in 87% of treated embryos (n = 52), as compared to controls (n = 55) (**Figure 18, G and H**). This effect appears similar to the expanded *ntla* expression I observed following PTBA treatment (**Figure 11F**). In contrast, TSA disrupted normal *ntla* expression in 86% of treated embryos (n = 56), as compared with controls (**Figure 18, G and I**). This resulted in breaks in the *ntla* expression pattern (**Figure 18I, arrowheads**).

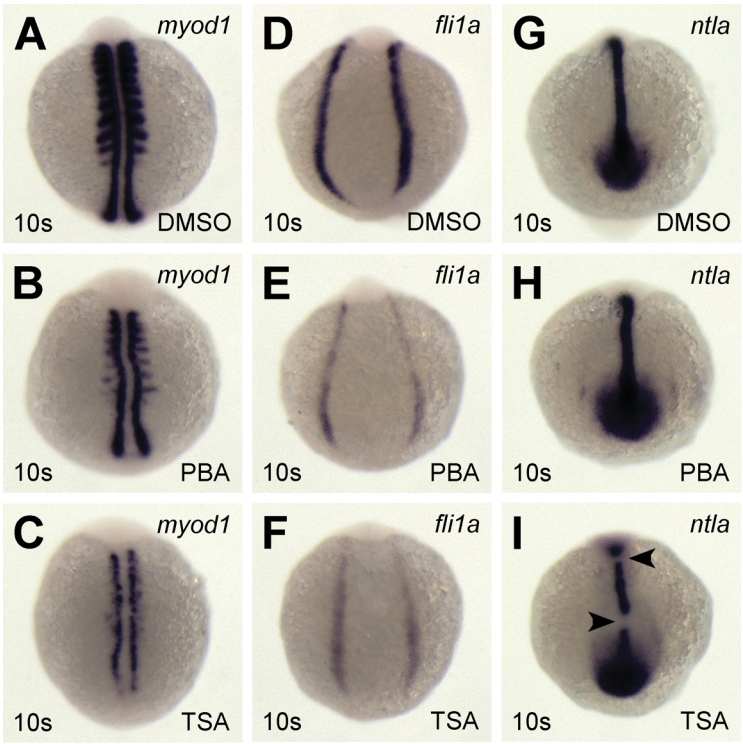

Figure 18. Treatment with PBA or TSA affects nearby tissues**.** (A through I) *In situ* hybridization for *myod1* (A through C), *fli1a* (D through F), or *ntla* (G through I) in 10-somite embryos treated with 0.5% DMSO (A, D, and G), 25 μM PBA (B, E, and H), or 200 nM TSA (C, F, and I). Arrowheads indicate breaks in *ntla* expression.

To determine the toxicity of PBA and TSA relative to PTBA, I again performed phenotypic concentration-response experiments. I assessed 72 hpf larvae for the development of edemic phenotypes over the same concentration range used to test for expansion of the kidney field. Pericardial edema was evident in 23% of larvae treated with 25 μM PBA (n = 83) and 100% of larvae treated with 200 nM TSA (n = 35) (**Figures 19 and 20**). In addition, 25 μM PBA caused minimal, but significant death (8%, n = 90), while treatment with 200 nM TSA resulted in high lethality (61%, n = 90) (**Figures 19 and 20**).

3.2.4 PTBA functions as an HDACi *in vitro*

Because PBA and TSA mimic the ability of PTBA to expand renal progenitor cells, I determined whether PTBA functions as an HDACi. To evaluate this *in vitro*, I measured the deacetylation of a fluorescent peptide substrate in the presence of human HDACs. HDAC activity increased in direct proportion to the amount of HeLa cell nuclear extract added to the assay (**Figure 21, black triangle**). Addition of TSA completely blocked activity at all input levels of nuclear extract (**Figure 21, gray triangle**). Previous work showed that 5 mM PBA decreased HDAC activity in DSI9 mouse erythroleukemia cells to 19% of the control value.[149] To determine whether PTBA inhibited HDACs to a similar extent as PBA, I evaluated both compounds at 5 mM. PTBA and PBA showed similar potency, reducing the HDAC activity elicited by 10 μg HeLa extract to 30% of the control value (**Figure 21, red diamond and blue circle, respectively**). Previously, I observed that the PTBA analog, 4-(phenylsulfonyl)butanoic acid (PSOBA), demonstrated no ability to expand renal progenitor cells (**Figure 14C**). Therefore, I hypothesized that it would function poorly *in vitro* as an HDACi. As expected, 5 mM PSOBA decreased the HDAC activity elicited by 10 μg HeLa extract to only 70% of the control value (**Figure 21, green square**).

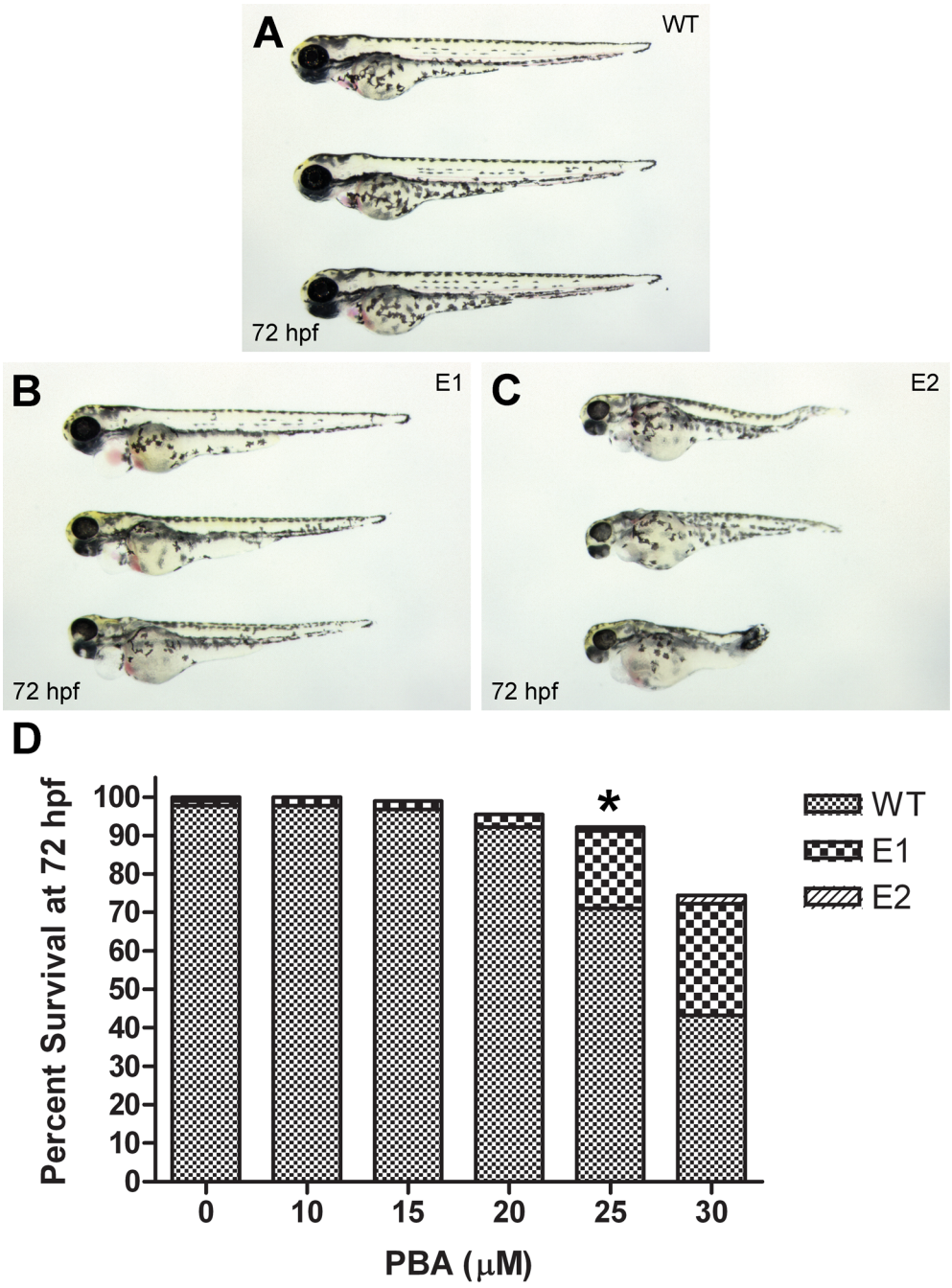

Figure 19. PBA elicits concentration-dependent effects on larval edema and survival. (A through D) Embryos were treated with 0 to 30 μM PBA from 2 hpf, and larvae were scored at 72 hpf using a phenotype-based classification system (see Chapter 2 Methods). (A) Wild-type (WT). (B) Edemic 1 (E1). (C) Edemic 2 (E2). (D) Graph of phenotypes after treatment with 0 to 30 μM PBA (n = 90 per concentration). Asterisk denotes lowest PBA concentration that exhibits a significant effect ($p < 0.05$) on survival.

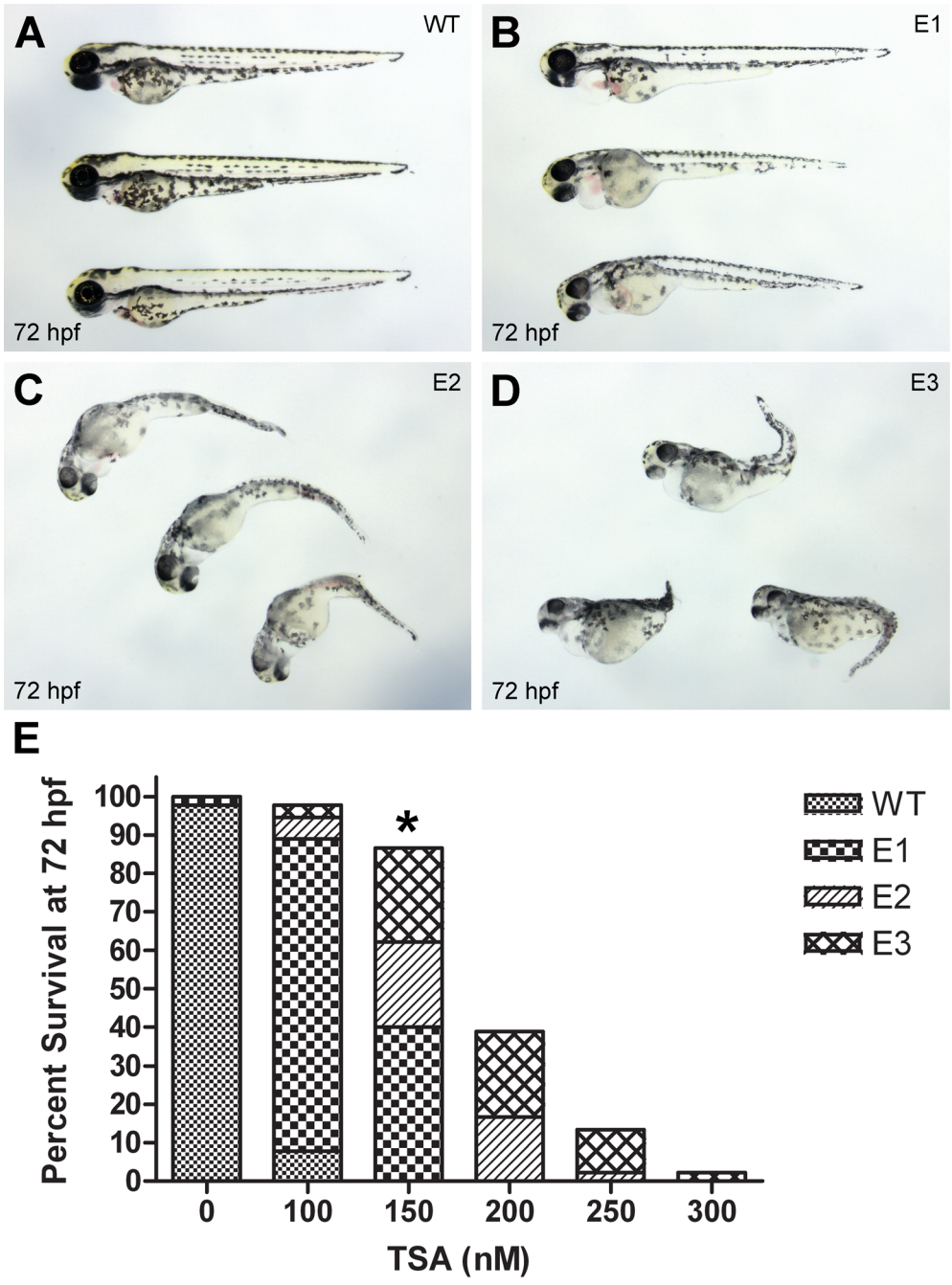

Figure 20. TSA elicits concentration-dependent effects on larval edema and survival. (A through D) Embryos were treated with 0 to 300 nM TSA from 2 hpf, and larvae were scored at 72 hpf using a phenotype-based classification system (see Chapter 2 Methods). (A) Wild-type (WT). (B) Edemic 1 (E1). (C) Edemic 2 (E2). (D) Edemic 3 (E3). (E) Graph of phenotypes after treatment with 0 to 300 nM PBA (n = 90 per concentration). Asterisk denotes lowest TSA concentration that exhibits a significant effect ($p < 0.05$) on survival.

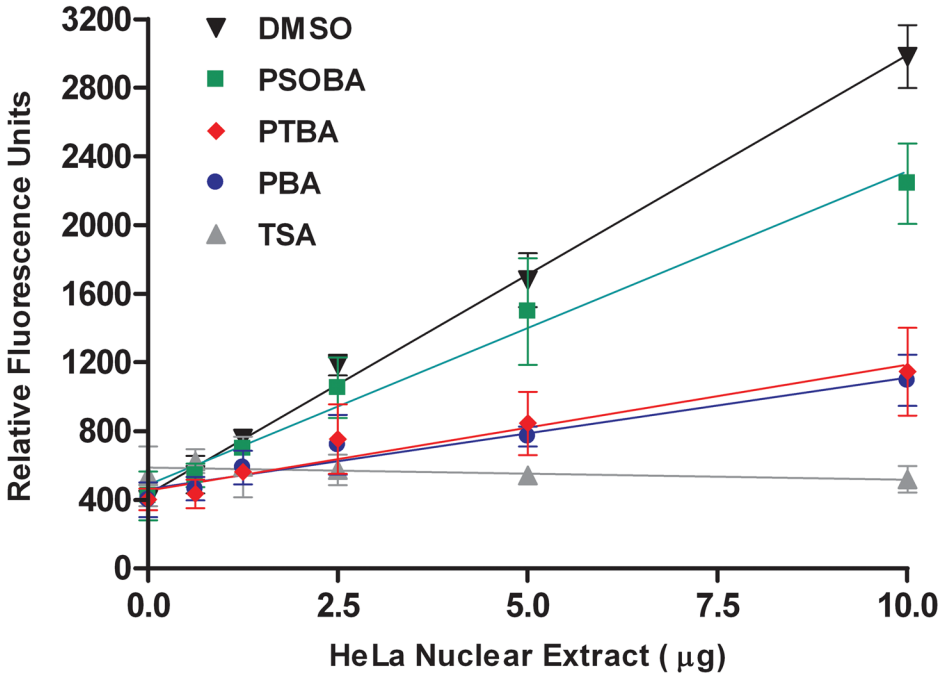

Figure 21. PTBA functions as an HDACi *in vitro*. Fluorescence histone deacetylation assay performed in the presence of 5 mM PTBA, 5 mM PBA, 5 mM PSOBA, 1 μM TSA, or 5% DMSO. At a given amount of nuclear extract, less fluorescence indicates less HDAC activity. Error bars represent the 95% confidence intervals for each data point.

3.2.5 PTBA functions as an HDACi *in vivo*

I next sought to determine whether the HDACi function of PTBA was quantifiable *in vivo*. I treated 24 hpf embryos with 3 μM PTBA, 25 μM PBA, or 200 nM TSA for 6 hours. Protein extracts were prepared and immunoblotted with an anti-hyperacetylated histone H4 antibody. Histone H4 hyperacetylation was observed following treatment with all three compounds at their tested concentrations, as compared with the control (**Figure 22**). Furthermore, increasing the compound concentration caused a corresponding increase in hyperacetylation (**Figure 22**). Therefore, both *in vitro* and *in vivo* results confirm that PTBA functions as an HDACi.

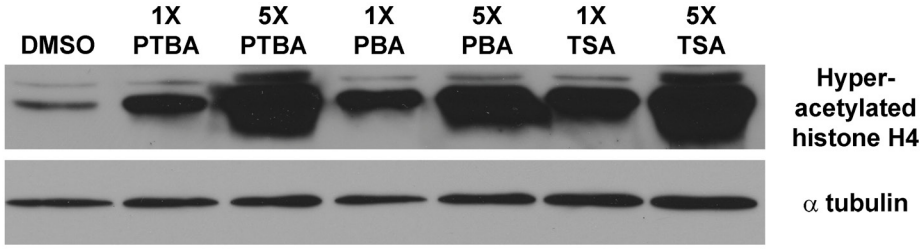

Figure 22. PTBA functions as an HDACi *in vivo*. Western blot examining the acetylation state of histone H4 isolated from embryos at 30 hpf that had been treated for 6 hours with 0.5% DMSO, 3 μM (1X) or 15 μM (5X) PTBA, 25 μM (1X) or 125 μM (5X) PBA, and 200 nM (1X) or 1 μM (5X) TSA. Western blot for α-tubulin demonstrates equal loading.

3.2.6 PTBA affects retinoic acid signaling

HDACis are believed to lower the threshold of RA necessary to activate transcription.[62] If PTBA treatment facilitates activation of the RA pathway, then expression of genes responsive to RA signaling should change. Consequently, I focused on two genes: *cyp26a1*, which is directly

activated by RA signaling,[150] and the cardiac gene *cmlc2*, whose expression in the heart field size is reduced by RA treatments.[151] In the previous study, *cmlc2* expression was assessed for RA-dependent effects in 18-somite embryos,[151] therefore embryos were collected at the 18-somite stage for continuity. As compared to controls (n = 58), expression of *cyp26a1* was increased in 100% of PTBA-treated embryos (n = 57) (**Figure 23, A and B**). In agreement with this result, *cmlc2* expression was decreased in 100% of PTBA-treated embryos (n = 58), as compared to controls (n = 57) (**Figure 23, C and D**).

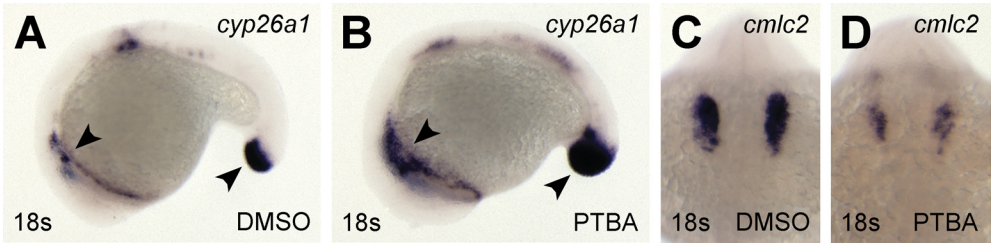

Figure 23. PTBA affects the expression of RA-responsive genes. (A through D) *In situ* hybridization for *cyp26a1* (A and B) and *cmlc2* (C and D) in 18-somite embryos treated with 0.5% DMSO (A and C) or 3 μM PTBA (B and D). Arrowheads highlight *cyp26a1* expression domains.

To provide a stronger link between PTBA treatment and RA signaling, mRNA encoding a dominant-negative RARα construct (DN-RARα), which is known to block RA signaling,[152] was injected prior to PTBA treatment. I performed *in situ* hybridization to determine the maximum amount of DN-RARα mRNA that could be injected at the one-cell stage without affecting *lhx1a* expression. In the tested range of 0 to 400 ng, embryos injected with 200 ng DN-RARα mRNA or less showed normal *lhx1a* expression, while higher doses caused aberrant or decreased expression (data not shown). Therefore, I chose to inject 200 ng DN-RARα mRNA to

assess the relationship between PTBA and the RA pathway. As compared with controls (*n* = 80), I observed an expansion of *lhx1a* expression in 90% of the mock-injected PTBA-treated embryos at the 10-somite stage (*n* = 78) (**Figure 24, A and B**). Expression of *lhx1a* appeared normal in 92% of embryos injected with 200 pg DN-RARα mRNA (*n* = 125) (**Figure 24C**). However, only 19% of the embryos injected with 200 pg DN-RARα mRNA and subsequently treated with PTBA showed expanded *lhx1a* expression (*n* = 125) (**Figure 24D**). Therefore, these data suggest that PTBA-mediated expansion of renal progenitor cells is dependent on the retinoic acid pathway.

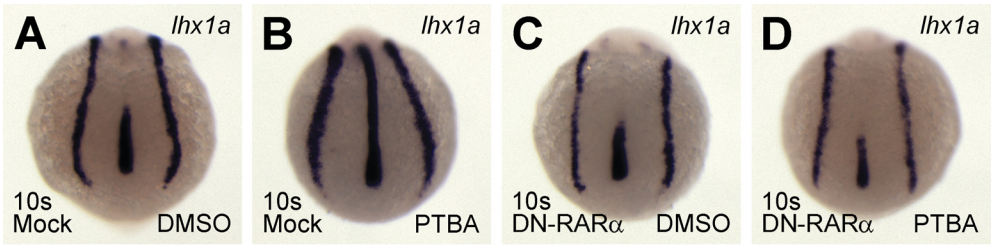

Figure 24. RA signaling mediates PTBA efficacy. (A through D) *In situ* hybridization in 10-somite embryos mock-injected with 1% fluorescein dextran (A and B) or injected with 200 pg of DN-RARα mRNA and 1% fluorescein dextran (C and D). At 5 hpf, embryos were treated with 0.5% DMSO (A and C) or 3 μM PTBA (B and D).

3.3 METHODS

3.3.1 Zebrafish husbandry

Zebrafish husbandry was performed as described in Chapter 2.

3.3.2 Compound sources and treatments

PTBA and methyl-4-(phenylthio)butanoate were synthesized as described in Chapter 2. 4-(Naphthalen-2-ylthio)butanoic acid (NSC2733), 3-(phenylthio)benzoic acid (NSC113994), and 2-amino-PTBA (NSC140113) were obtained from the NCI/DTP Open Repository. PBA, TSA, 4-phenoxybutanoic acid, and 5-phenylpentanoic acid were obtained from Sigma-Aldrich. PSOBA was obtained from Matrix Scientific. Treatments were performed as described in Chapter 2, except for the *in vivo* hyperacetylation assays and DN-RARα experiments (see below).

3.3.3 *In situ* hybridization

In situ hybridization was performed as described in Chapter 2.

3.3.4 Histone hyperacetylation assays

SDS-PAGE and Western blotting were performed as described previously with some modifications.[148] Proteins were separated on 18% SDS-PAGE gels. Membranes were incubated

at 4 ^{o}C overnight with 1:1000 anti-hyperacetylated histone H4 antibody (06-946, Millipore) or 1:1000 anti-α-tubulin antibody (Sigma-Aldrich) in PBT containing 5% nonfat milk.

3.3.5 Fluorescence HDAC assays

In vitro HDAC activity assays were performed using a fluorescence HDAC assay kit (Active Motif) according to the manufacturer's instructions. For maintaining compound solubility at 5 mM, the final DMSO concentration in all assay wells was increased to 5%. Fluorescence was detected using an M5 Plate Reader (Molecular Dynamics)

3.3.6 mRNA synthesis and microinjections

Synthetic mRNA was generated from the XRARα1^{405}/pCD61 construct[152] (NotI digested) using a T7 mMessage mMachine kit (Ambion). Zebrafish embryos were injected at the one-cell stage either with 200 pg of synthetic mRNA and 1% fluorescein dextran (Sigma-Aldrich) or with 1% fluorescein dextran alone (mock) and allowed to develop in E3 culture medium at 28.5 ^{o}C. At the 256-cell stage, only fluorescein-dextran positive embryos were selected for PTBA treatment, which occurred at 5 hpf.

4.0 DEVELOPMENT OF PTBA ANALOGS

4.1 HYPOTHESIS

My previous work determined that treating zebrafish embryos with PTBA, a novel HDACi, increased the number of renal progenitor cells. Significantly, this led to a corresponding increase in pronephric size, suggesting that these cells are capable of contributing to nephrogenesis. As early as 1989, Bacallo and Fine proposed that kidney regeneration follows the same pattern of differentiation events that lead to nephrogenesis.[153] Both processes begin with the proliferation of renal progenitor cells to provide the raw material necessary for subsequent differentiation into kidney tissue.[153] Since PTBA stimulates renal progenitor cell proliferation during pronephric development, it may function similarly during kidney regeneration. However, developing PTBA into a potential therapeutic requires the consideration of both its efficacy and toxicity. Furthermore, expanding the structure-activity relationship study to a wider selection of small molecules may yield better candidates for future *in vivo* studies. Therefore, I chose to evaluate a panel of structural and functional analogs of PTBA to identify compounds exhibiting nanomolar efficacy and low toxicity in kidney cell culture. I hypothesized that modifying the key structural elements that determine the HDACi activity of PTBA would improve its ability to expand renal progenitor cells.

4.2 RESULTS

4.2.1 Phenotypic screening of PTBA analogs

As I have previously shown, treating zebrafish embryos with 3 μM PTBA generates pericardial edema by 72 hpf (**Figure 4**). This PTBA concentration also stimulates the proliferation of renal progenitor cells during pronephric development (**Figures 6 and 12**). Furthermore, by 48 hpf, embryos treated with 3 μM PTBA exhibit wider pronephric tubules and a failure of *wt1a* convergence at the dorsal midline (**Figures 8, 9, and 10**) Therefore, it is reasonable to hypothesize that the edemic phenotype reflects aberrant kidney morphogenesis resulting from an overabundance of renal progenitor cells. Consequently, I performed a phenotypic screen on a panel of PTBA analogs at 3 μM to identify potentially effective compounds.

Each of the compounds chosen for analysis represents either a structural or functional analog of the lead compound, PTBA. The structural analogs contain functional group additions or substitutions in one of four elements of the PTBA structure. These modify the key determinants of HDACi activity as predicted by the general pharmacophore: the aliphatic cap, connecting unit, hydrophobic linker, and zinc-binding group (**Table 1**). The structural analogs selected for the panel each contain one or more of these modifications (**Table 1**). Several functional group choices were based on previous structure-activity relationship studies of PTBA. For example, methylating the zinc-binding group of PTBA generated a compound equally capable of expanding *lhx1a* expression in treated embryos (**Figure 14I**). Therefore, the efficacy of several alkylated analogs was assessed.

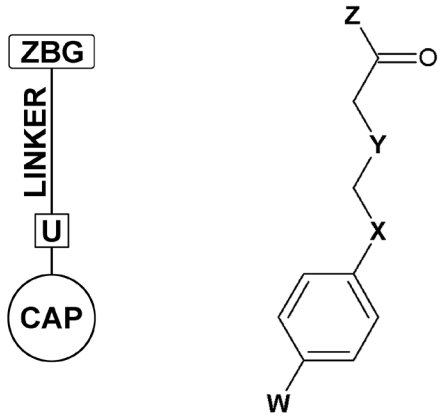

Compound Name	Aliphatic Cap (W)	Connecting Unit (X)	Fatty Acid Linker (Y)	Zinc-Binding Group (Z)
4-(phenylthio)butanoic acid (PTBA)	H	S	CH_2	OH
4-(naphthalen-2-ylthio)butanoic acid	C_6H_6	S	CH_2	OH
4-(phenylsulfonyl)butanoic acid	H	SO_2	CH_2	OH
4-phenoxybutanoic acid	H	O	CH_2	OH
4-(phenylamino)butanoic acid	H	NH	CH_2	OH
5-phenylpentanoic acid	H	CH_2	CH_2	OH
3-(phenylthio)benzoic acid	H	S	C_6H_6	OH
methyl 4-(phenylthio)butanoate	H	S	CH_2	OCH_3
propyl 4-(phenylthio)butanoate	H	S	CH_2	$O(CH_2)_2CH_3$
butan-2-yl 4-(phenylthio)butanoate	H	S	CH_2	$OCH(CH_3)CH_2CH_3$
tert-butyl 4-(phenylthio)butanoate	H	S	CH_2	$OC(CH_3)_3$
N-hydroxy-4-(phenylthio)butanamide	H	S	CH_2	NHOH
methyl 4-[(4-methylphenyl)thio]butanoate	CH_3	S	CH_2	OCH_3
methyl 4-[(4-methoxyphenyl)thio]butanoate	OCH_3	S	CH_2	OCH_3
methyl 4-[(4-fluorophenyl)thio]butanoate	F	S	CH_2	OCH_3
methyl 4-[(4-chlorophenyl)thio]butanoate	Cl	S	CH_2	OCH_3
methyl 4-[(4-bromophenyl)thio]butanoate	Br	S	CH_2	OCH_3
N-hydroxy-4-[(4-methylphenyl)thio]butanamide	CH_3	S	CH_2	NHOH
N-hydroxy-4-[(4-methoxyphenyl)thio]butanamide	OCH_3	S	CH_2	NHOH
4-[(4-fluorophenyl)thio]-*N*-hydroxybutanamide	F	S	CH_2	NHOH
4-[(4-chlorophenyl)thio]-*N*-hydroxybutanamide	Cl	S	CH_2	NHOH
4-[(4-bromophenyl)thio]-*N*-hydroxybutanamide	Br	S	CH_2	NHOH

Table 1. Structural analogs of PTBA. (Top left) General structure of the HDACi pharmacophore containing an aliphatic or aromatic cap (CAP), connecting unit (U), hydrophobic linker (LINKER), and zinc-binding group (ZBG). (Top right) General structure of a PTBA analog containing functional group substitutions as described in the table below.

In addition, I observed that the hydroxamic acid HDACi, trichostatin A (TSA), exhibited high efficacy, increasing *lhx1a* expression at 200 nM. (**Figure 17D**). Hydroxamic acids, which form two coordinate bonds with the active site zinc, are generally stronger than carboxylic acids, including PTBA, which form only one.[154] Thus, several of the analogs tested contained hydroxamate moieties on the zinc-binding group.

Ten functional analogs were also chosen to represent a subset of known HDACis of several different classes (**Figure 25**). These include inhibitors derived from carboxylic acids, hydroxamic acids, benzamides, and natural products.[155] With the exception of butanoic acid, all of the chosen compounds have predicted octanol-water partition coefficients (LogPs) greater than 1 (**Appendix A**). LogP indicates the hydrophobicity of a given molecule, with lipophilic compounds exhibiting higher values.[156,157] Previous work determined that zebrafish embryos absorb compounds with logP values between 1 and 12 from embryo medium.[116,158]

The 32 compounds and a DMSO control were examined for their ability to generate pericardial edema in zebrafish larvae by 72 hpf (**Table 2**). Treatment with 12 compounds did not cause a statistically-significant decrease in the number of wild-type larval phenotypes, as compared with controls. This group included the four compounds containing connecting unit substitutions, seven of the known HDACis, and one alkylated analog, *tert*-butyl 4-(phenylthio)butanoate. Treatment with each of the remaining analogs generated edemic and/or lethal phenotypes that were scored using the phenotype-based classification system from Chapter 2. Three of these compounds, TSA, valproic acid, and apicidin, are known HDAC inhibitors. The lethality of 3 μM TSA was expected, since I previously demonstrated that 300 nM TSA killed greater than 90% of treated 72 hpf larvae (**Figure 20**).

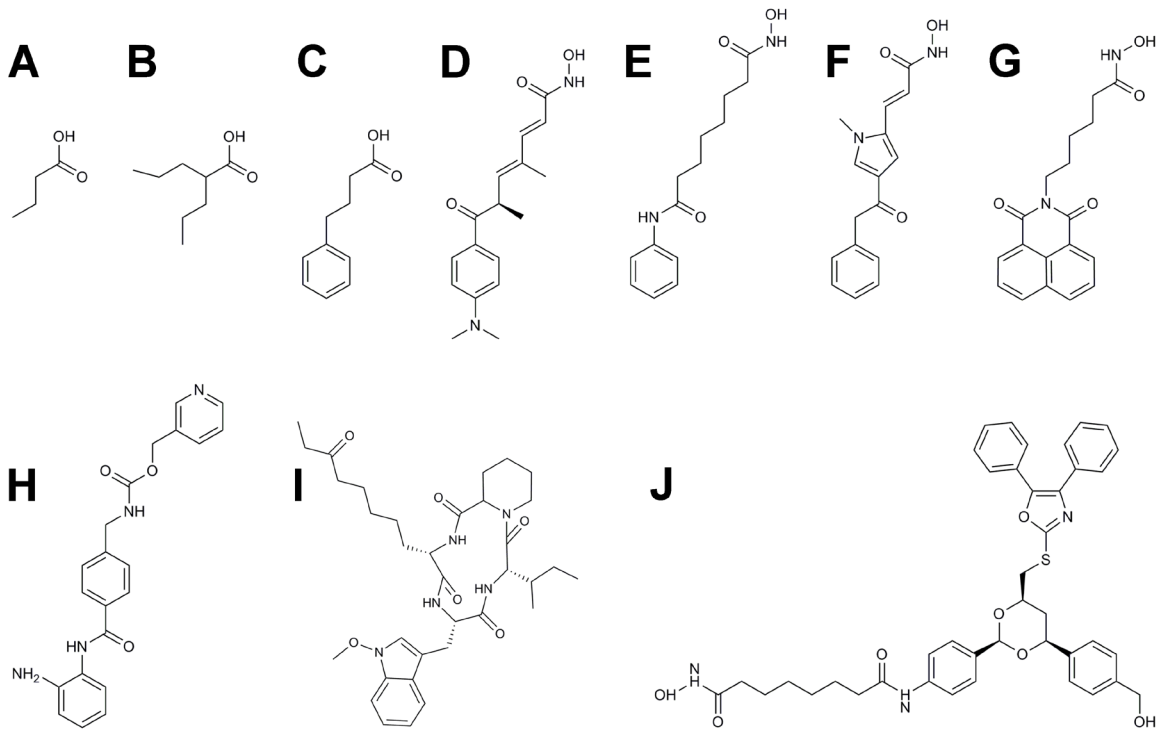

Figure 25. Functional analogs of PTBA. (A through J) Structures of the HDACis butanoic acid (A), valproic acid (B), 4-phenylbutanoic acid (PBA, C), trichostatin A (TSA, D), SAHA (E), APHA compound 8 (F), Scriptaid (G), MS-275 (H), apicidin (I), and tubacin (J).

Compound Name	Wild-type (WT)	Edemic 1 (E1)	Edemic 2 (E2)	Edemic 3 (E3)	Dead
0.5% DMSO	36	0	0	0	0
4-phenoxybutanoic acid	36	0	0	0	0
4-(phenylsulfonyl)butanoic acid	36	0	0	0	0
5-phenylpentanoic acid	36	0	0	0	0
APHA compound 8	36	0	0	0	0
MS-275	36	0	0	0	0
PBA	36	0	0	0	0
SAHA	36	0	0	0	0
tubacin	36	0	0	0	0
4-(phenylamino)butanoic acid	35	1	0	0	0
Scriptaid	35	1	0	0	0
butanoic acid	35	0	0	0	1
tert -butyl 4-(phenylthio)butanoate	33	3	0	0	0
The compounds below this line cause significant decreases in wild-type larval phenotypes at 3 μM ($p < 0.05$)					
valproic acid	25	11	0	0	0
4-(naphthalen-2-ylthio)butanoic acid	25	9	0	0	2
N -hydroxy-4-[(4-methoxyphenyl)thio]butanamide	16	20	0	0	0
methyl 4-[(4-bromophenyl)thio]butanoate	8	27	1	0	0
3-(phenylthio)benzoic acid	2	34	0	0	0
4-[(4-bromophenyl)thio]-*N* -hydroxybutanamide	1	23	12	0	0
butan-2-yl 4-(phenylthio)butanoate	2	19	12	2	1
PTBA	0	13	17	5	1
methyl 4-[(4-chlorophenyl)thio]butanoate	0	10	6	19	1
methyl 4-[(4-methoxyphenyl)thio]butanoate	0	2	24	9	1
N -hydroxy-4-(phenylthio)butanamide	0	3	20	13	0
propyl 4-(phenylthio)butanoate	0	7	8	15	6
methyl 4-(phenylthio)butanoate	0	0	2	26	8
methyl 4-[(4-methylphenyl)thio]butanoate	0	0	2	23	11
4-[(4-chlorophenyl)thio]-*N* -hydroxybutanamide	0	0	0	22	14
N -hydroxy-4-[(4-methylphenyl)thio]butanamide	0	0	0	14	22
4-[(4-fluorophenyl)thio]-*N* -hydroxybutanamide	0	0	0	8	28
methyl 4-[(4-fluorophenyl)thio]butanoate	0	0	0	0	36
apicidin	0	0	0	0	36
TSA	0	0	0	0	36

Table 2. Phenotypes observed in larvae treated with PTBA analogs. Embryos were treated with each compound at 3 μM from 2 hpf, and larvae were scored at 72 hpf using a phenotype-based classification system (Chapter 2). Compounds below the indicated line exhibit a significant decrease ($p < 0.05$) in the occurrence of wild-type phenotypes as determined by Fisher's exact test.

Furthermore, with the exception of apicidin, all of the compounds that cause more severe phenotypes than PTBA contain either hydroxamic or alkylated zinc-binding groups. Taken together, these results suggest that modifications of PTBA anticipated to alter its underlying HDACi function may affect compound efficacy during pronephric development. However, pericardial edema can develop as a result of organ dysfunction unrelated to the kidney.[159-161] Therefore, I determined the effect of each of these compounds, if any, on renal progenitor cells.

To accomplish this, I examined *lhx1a* expression in treated embryos at the 10-somite stage. I performed *in situ* hybridizations on embryos treated with decreasing concentrations of compound, beginning at 3 μM (**Table 3,** raw data in **Appendix B**). The results were categorized relative to the efficacy of PTBA at a given concentration and are detailed below.

4.2.2 PTBA analog efficacy in renal progenitor cells at 3 μM

Of the 12 compounds that exhibited no significant effect on larval phenotype, 10 compounds did not expand *lhx1a* expression as compared with controls (no expansion, $n = 36$) (**Tables 2 and 3**). This group includes HDACis, such as SAHA and tubacin, which exhibit similar potency to TSA *in vitro*.[162] However, treatment with 3 μM Scriptaid or *tert*-butyl 4-(phenylthio)butanoate increased *lhx1a* expression in 39% and 25% of the tested embryos ($n = 36$ each), respectively, as compared with controls (no expansion, $n = 36$) (**Figure 26, A, C, and E**). Therefore, the failure to develop pericardial edema following treatment is a predictive, but not absolute, indicator of an ineffective analog.

Compound Name	3 μM	1.5 μM	800 nM	400 nM	200 nM	100 nM
0.5% DMSO	−	−	−	−	−	−
4-phenoxybutanoic acid	−	ND	ND	ND	ND	ND
4-(phenylsulfonyl)butanoic acid	−	ND	ND	ND	ND	ND
5-phenylpentanoic acid	−	ND	ND	ND	ND	ND
APHA compound 8	−	ND	ND	ND	ND	ND
MS-275	−	ND	ND	ND	ND	ND
PBA	−	ND	ND	ND	ND	ND
SAHA	−	ND	ND	ND	ND	ND
tubacin	−	ND	ND	ND	ND	ND
4-(phenylamino)butanoic acid	−	ND	ND	ND	ND	ND
Scriptaid	+/−	ND	ND	ND	ND	ND
butanoic acid	−	ND	ND	ND	ND	ND
tert -butyl 4-(phenylthio)butanoate	+/−	ND	ND	ND	ND	ND
valproic acid	+/−	ND	ND	ND	ND	ND
4-(naphthalen-2-ylthio)butanoic acid	−	ND	ND	ND	ND	ND
N -hydroxy-4-[(4-methoxyphenyl)thio]butanamide	+/−	ND	ND	ND	ND	ND
methyl 4-[(4-bromophenyl)thio]butanoate	+/−	ND	ND	ND	ND	ND
3-(phenylthio)benzoic acid	−	ND	ND	ND	ND	ND
4-[(4-bromophenyl)thio]-*N* -hydroxybutanamide	+	+/−	ND	ND	ND	ND
butan-2-yl 4-(phenylthio)butanoate	+	+	+/−	ND	ND	ND
PTBA	+	+	+/−	ND	ND	ND
methyl 4-[(4-chlorophenyl)thio]butanoate	+	+/−	ND	ND	ND	ND
methyl 4-[(4-methoxyphenyl)thio]butanoate	+	+	+	+/−	−	ND
N -hydroxy-4-(phenylthio)butanamide	+	+	+/−	ND	ND	ND
propyl 4-(phenylthio)butanoate	+	+	+/−	ND	ND	ND
methyl 4-(phenylthio)butanoate	+	+	+/−	ND	ND	ND
methyl 4-[(4-methylphenyl)thio]butanoate	+	+	+	−	−	ND
4-[(4-chlorophenyl)thio]-*N* -hydroxybutanamide	+	+	+/−	ND	ND	ND
N -hydroxy-4-[(4-methylphenyl)thio]butanamide	+	+	+	−	−	ND
4-[(4-fluorophenyl)thio]-*N* -hydroxybutanamide	+	+	+	+/−	−	ND
methyl 4-[(4-fluorophenyl)thio]butanoate	XX	+	+	+/−	+/−	ND
apicidin	XX	XX	XX[1]	+/−	−	ND
TSA	XX	XX	XX	XX	+	+

Table 3. *Lhx1a* expansion caused by analog treatment. *In situ* hybridization for *lhx1a* expression in 10-somite embryos treated from 2 hpf with each compound at the listed concentration. Analogs were classified according to their ability to increase *lhx1a* expression as effective (+), partially effective (+/−), or ineffective (−). Analogs that killed all embryos at a given concentration before reaching 10 somites are listed as XX. If the efficacy of a compound was not determined at a given concentration it is listed as ND. Note[1]: embryos surviving treatment with 800 nM apicidin (31%, n = 36) displayed general toxicity precluding efficacy scoring. Raw data are listed in Appendix B.

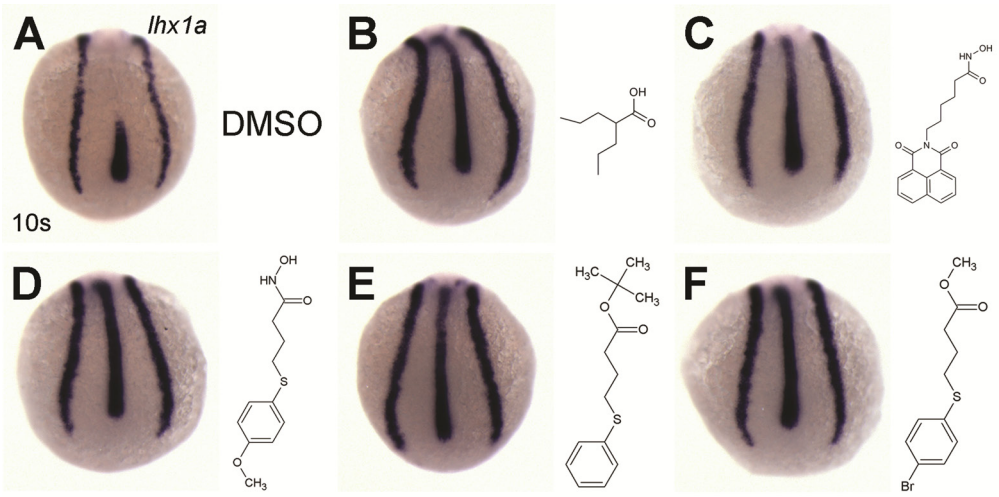

Figure 26. PTBA analogs exhibiting partial efficacy at 3 μM. (A through F) *In situ* hybridization for *lhx1a* expression in 10-somite embryos treated from 2 hpf with 0.5% DMSO (A) or 3 μM of the following compounds: valproic acid (20% expansion) (B), Scriptaid (25% expansion) (C), *N*-hydroxy-4-[(4-methoxyphenyl)thio]butanamide (31% expansion) (D), *tert*-butyl 4-(phenylthio)butanoate (39% expansion) (E), and methyl 4-[(bromophenyl)thio]butanoate (74% expansion) (F).

Lhx1a expression analysis separated the 20 compounds, including PTBA, which caused edemic or lethal phenotypes into four groups. The first group, consisting of 4-(napthalen-2-ylthio)butanoic acid and 3-(phenylthio) benzoic acid, caused no expansion of *lhx1a* in the treated embryos (**Table 3**). Therefore, their edemic phenotypes probably result from non-kidney related effects during embryonic development.

The second group, consisting of three compounds, expanded *lhx1a* expression in less than 75% of the treated embryos in comparison to controls (**Figure 26A**). This group included valproic acid, a known HDACi, (20% expansion, $n = 35$), *N*-hydroxy-4-[(4-methoxyphenyl)thio] butanamide (31% expansion, $n = 35$), and methyl 4-[(bromophenyl)thio]butanoate (74% expansion, $n = 35$) (**Figure 26, B, D, and F**).

The third group consisted of 12 effective compounds, including PTBA, that expanded *lhx1a* expression in greater than 90% of the treated embryos as compared with controls (**Table 3**). The eleven PTBA analogs all contained either hydroxamic or alkylated zinc-binding groups. Compounds with these structural motifs also caused the most edema and lethality in the phenotypic screen (**Table 2**). Furthermore, all compounds showing greater than 90% efficacy by *in situ* hybridization demonstrate phenotypic effects similar to or more severe than those caused by PTBA (**Tables 2 and 3**). Therefore, the severity of edemic phenotypes does appear to correlate with the ability of a given PTBA analog to expand renal progenitor cells with some exceptions as previously noted. These compounds were subsequently tested to determine their efficacies at sequentially lower concentrations.

The final group, consisting of methyl 4-[(4-fluorophenyl)thio)]butanoate, apicidin, and trichostatin A, killed all treated embryos before they reached the 10-somite stage (**Table 3**). Toxicity of these compounds at 3 μM does not preclude them from expanding renal progenitor

cells at lower concentrations. Indeed, I previously observed that treating embryos with 200 nM TSA expands *lhx1a* expression in a manner similar to 3 μM PTBA (**Figure 17D compared with Figure 5B**). Therefore, the efficacy of these compounds at concentrations below 3 μM was assessed along with the previous group.

4.2.3 PTBA analog efficacy in renal progenitor cells at 1.5 μM

Two compounds, apicidin and TSA, were lethal at 1.5 μM, while 13 others demonstrated some ability to expand *lhx1a* expression in 10-somite embryos. Two of these were partially effective, expanding less than 75% of the treated embryos when compared with controls (no expansion, n = 36) (**Figure 27A**). These were 4-[(bromophenyl)thio]-*N*-hydroxybutanamide (47% expansion, n = 36) and methyl 4-[(4-chlorophenyl)thio]butanoate (72% expansion, n = 36) (**Figure 27, B and C**). Because they lacked the efficacy of the remaining analogs, these compounds were not evaluated further.

Eleven compounds, including PTBA (83% expansion, n = 35) (**Figure 27D**), showed efficacy in greater than 80% of the treated embryos. Four contained hydroxamic zinc-binding groups, with three of these also carrying a substituted aliphatic cap: *N*-hydroxy-4-(phenylthio)butanamide (92% expansion, n = 36), *N*-hydroxy-4-[(4-methylphenyl)thio] butanamide (97% expansion, n = 33), 4-[(4-chlorophenyl)thio]-*N*-hydroxybutanamide (97% expansion, n = 36), and 4-[(4-fluorophenyl)thio]-*N*-hydroxybutanamide (100% expansion, n = 36) (**Figure 27, E through H**).

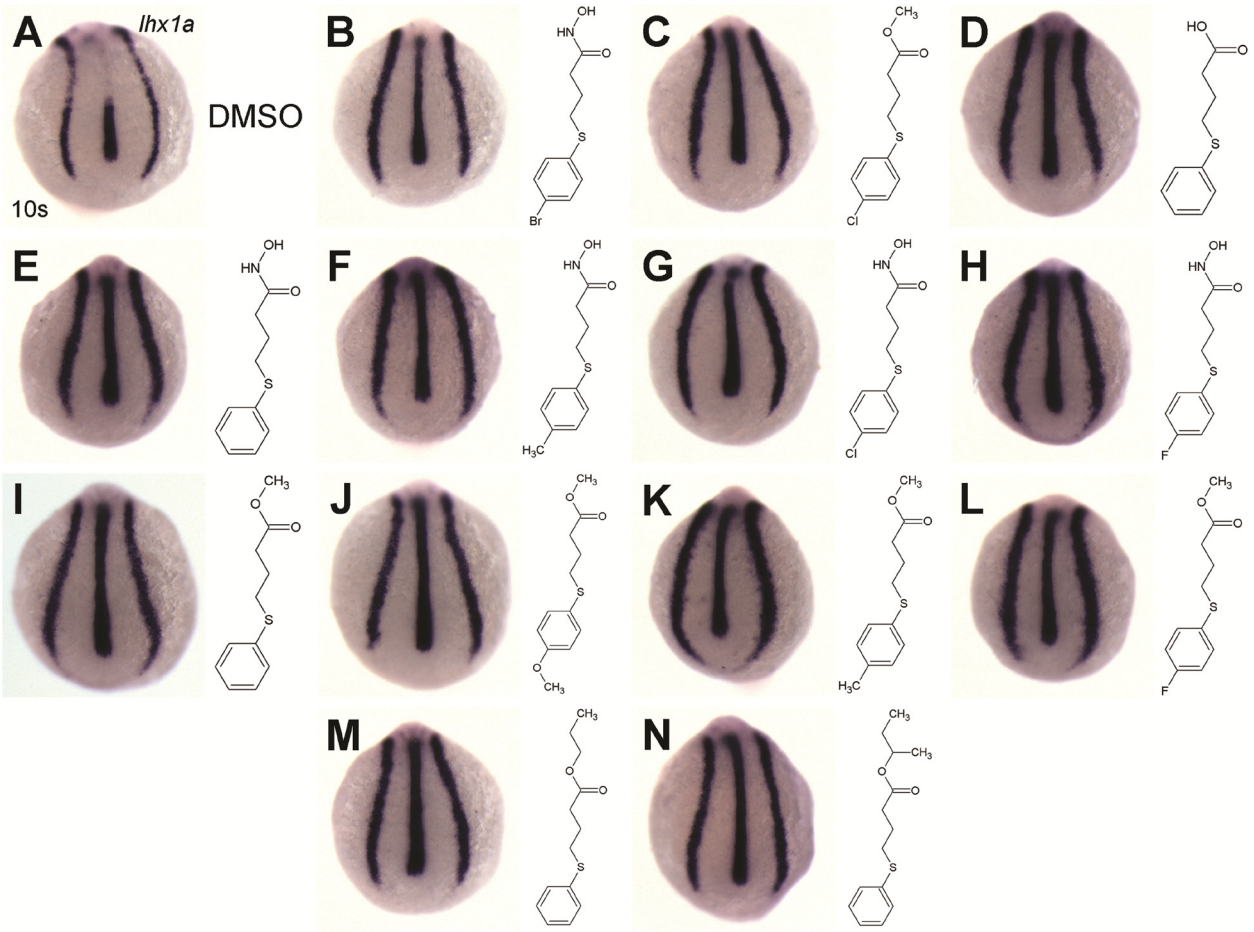

Figure 27. PTBA analogs exhibiting efficacy at 1.5 μM. (A through N) *In situ* hybridization for *lhx1a* expression in 10-somite embryos treated from 2 hpf with 0.5% DMSO (A) or 1.5 μM of the following compounds: 4-[(bromophenyl)thio]-*N*-hydroxybutanamide (47% expansion) (B), 4-[(4-chlorophenyl)thio]butanoate (72% expansion) (C), PTBA (83% expansion) (D), *N*-hydroxy-4-(phenylthio)butanamide (92% expansion) (E) , *N*-hydroxy-4-[(4-methylphenyl)thio]butanamide (97% expansion) (F), 4-[(4-chlorophenyl)thio]-*N*-hydroxybutanamide (97% expansion) (G), 4-[(4-fluorophenyl)thio]-*N*-hydroxybutanamide (100% expansion, n = 36) (H), methyl-4-(phenylthio)butanoate (89% expansion) (I), methyl 4-[(4-methoxyphenyl)thio]butanoate (91% expansion) (J), methyl 4-[(4-methylphenyl)thio] butanoate (100% expansion) (K), methyl 4-[(4-fluorophenyl)thio]butanoate (100% expansion) (L), propyl 4-(phenylthio)butanoate (89% expansion) (M), and butan-2-yl 4-(phenylthio)butanoate (89% expansion) (N).

Four analogs had methylated zinc-binding groups, with three of these also including aliphatic cap substitutions: methyl-4-(phenylthio)butanoate (89% expansion, *n* = 36), methyl 4-[(4-methoxyphenyl)thio]butanoate (91% expansion, *n* = 35), methyl 4-[(4-methylphenyl)thio] butanoate (100% expansion, *n* = 36), and methyl 4-[(4-fluorophenyl)thio]butanoate (100% expansion, *n* = 30) (**Figure 27, I through L**). The remaining two analogs demonstrating over 80% efficacy carried propyl- and *sec*-butyl substitutions, respectively, on their zinc-binding groups: propyl 4-(phenylthio)butanoate (89% expansion, *n* = 36) and butan-2-yl 4-(phenylthio)butanoate (89% expansion, *n* = 35) (**Figure 27, M and N**). Because each of these 10 PTBA analogs exhibited efficacy above that of PTBA, these data support the approach of targeting motifs important in HDACi activity.

4.2.4 PTBA analog efficacy on renal progenitor cells at 800 nM

Treatments at 800 nM revealed two distinct groups of analogs based on efficacy. The partially effective compounds, consisting of PTBA and five analogs, expanded *lhx1a* expression in less than 25% of treated 10-somite embryos as compared with controls (**Table 3**). With the exception of 4-[(4-chlorophenyl)thio]-N-hydroxybutanamide, none of these compounds carried a substituted aliphatic cap. Because of their already limited efficacy at 800 nM, these compounds were not tested at lower concentrations. The five members of the more effective second group increased *lhx1a* expression in greater than 45% of treated embryos as compared with controls (no expansion, *n* = 36) (**Figure 28A**). This group of analogs included methyl 4-[(methylphenyl)thio]butanoate (49% expansion, *n* = 35), methyl 4-[(methoxyphenyl)thio] butanoate (57% expansion, *n* = 35), 4-[(4-fluorophenyl)thio]-*N*-hydroxybutanamide (60% expansion, *n* = 35), *N*-hydroxy-4[(methylphenyl)thio]butanamide (61% expansion, *n* = 36) and

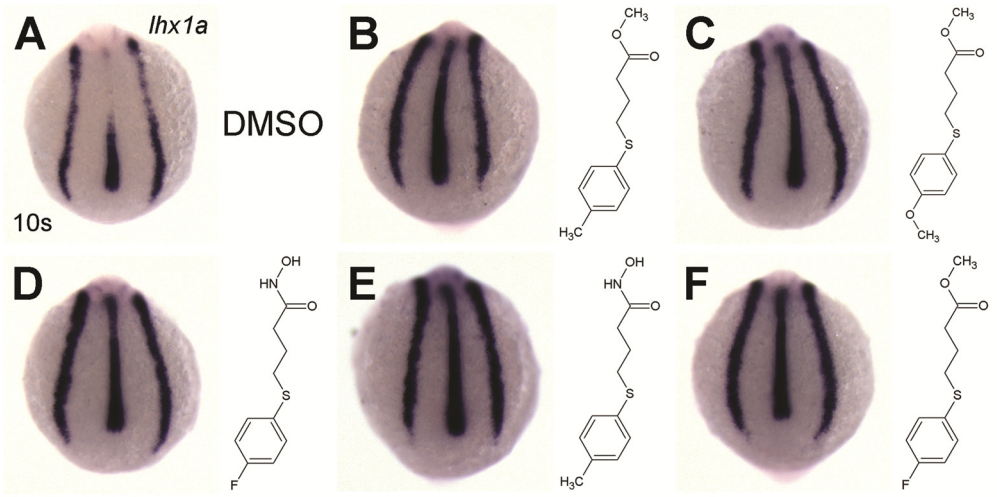

Figure 28. PTBA analogs exhibiting efficacy at 800 nM. (A through F) *In situ* hybridization for *lhx1a* expression in 10-somite embryos treated from 2 hpf with 0.5% DMSO (A) or 800 nM of the following compounds: methyl 4-[(methylphenyl)thio]butanoate (49% expansion) (B), methyl 4-[(methoxyphenyl)thio]butanoate (57% expansion) (C), 4-[(4-fluorophenyl)thio]-*N*-hydroxybutanamide (60% expansion) (D), N-hydroxy-4[(methylphenyl)thio]butanamide (61% expansion) (E), and methyl 4-[(4-fluorophenyl)thio] butanoate (64% expansion, $n = 36$) (F).

methyl 4-[(4-fluorophenyl)thio]butanoate (64% expansion, *n* = 36) (**Figure 28, B through F**). Each of these compounds contained substitutions in both the zinc-binding group and aliphatic cap. These substitutions represented only a limited selection of functional groups. The zinc-binding groups contained either hydroxamic acids or methylated carboxylic acids, while the aliphatic caps carried either methyl-, methoxy-, or fluoro- substitutions. These results suggest that certain structural motifs impart improved efficacy to the PTBA backbone.

Treatment with 800 nM apicidin killed 69% of the treated embryos (*n* = 36) (**Table 3**). Surviving embryos exhibited general toxicity that precluded the scoring of *lhx1a* expansion (data not shown). TSA treatment at 800 nM was lethal (**Table 3**). The five analogs exhibiting greater than 45% efficacy, apicidin, and TSA were retested at 400 nM.

4.2.5 PTBA analog efficacy on renal progenitor cells at 400 nM or below

Three of the five remaining structural analogs of PTBA and apicidin exhibited a partial ability to expand *lhx1a* expression at 400 nM in comparison to controls (*n* = 35) (**Figure 29A**). Of these, 400 nM 4-[(4-fluorophenyl)thio]-*N*-hydroxybutanamide expanded 35% of treated embryos (*n* = 34), the highest percentage of any tested PTBA structural analog at this concentration (**Figure 29B**). Two others, methyl 4-[(methoxyphenyl)thio]butanoate (29% expansion, *n* = 35) (**Figure 29C**) and methyl 4-[(4-fluorophenyl)thio]butanoate (26% expansion, *n* = 35), increased *lhx1a* expression in over 25% of treated embryos. Furthermore, methyl 4-[(4-fluorophenyl)thio]butanoate also caused partial *lhx1a* expansion at 200 nM (22% expansion, *n* = 32) (**Figure 29D**), while the other two structural analogs were ineffective (**Table 3**). This represents the lowest observed concentration of a structural PTBA analog capable of expanding renal progenitor cells.

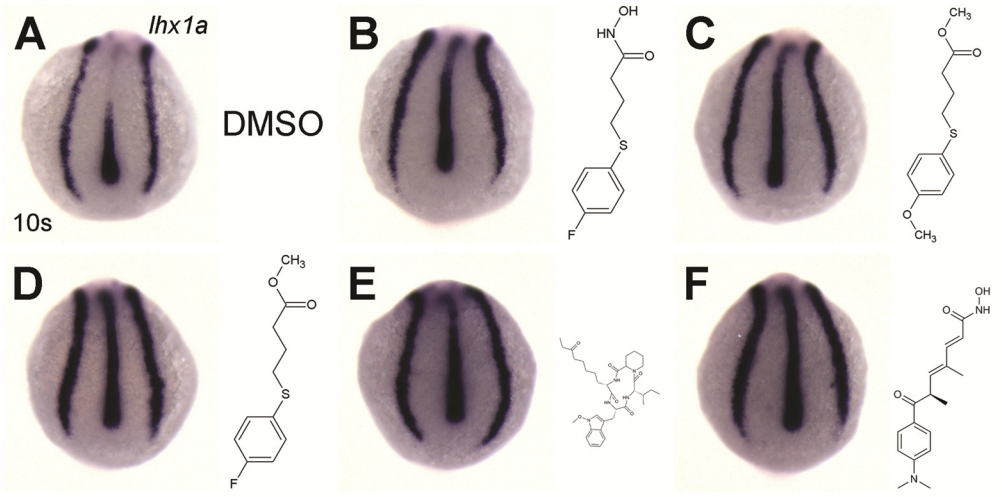

Figure 29. PTBA analogs exhibiting efficacy at or below 400 nM. (A through F) *In situ* hybridization for *lhx1a* expression in 10-somite embryos treated from 2 hpf with 0.5% DMSO (A) or concentrations of the following compounds as indicated: 400 nM 4-[(4-fluorophenyl)thio]-*N*-hydroxybutanamide (35% expansion) (B), 400 nM methyl 4-[(methoxyphenyl)thio]butanoate (29% expansion) (C), 200 nM methyl 4-[(4-fluorophenyl) thio]butanoate (26% expansion) (D), 400 nM apicidin (22% expansion) (E), and 100 nM TSA (97% expansion) (F).

Treatment with 400 nM apicidin expanded 22% of treated embryos (n = 36) (**Figure 29E**), but was ineffective at 200 nM. All embryos treated with 400 nM trichostatin A died before reaching 10 somites (**Table 3**). However, treatment with 200 nM TSA caused *lhx1a* expansion in 100% of treated embryos as compared with controls (n = 29) (**Table 3**). This observation is in agreement with my previous results (**Figure 17D**). Treatment with 100 nM TSA was also effective (97% expansion, n = 35), marking the lowest tested concentration of any PTBA analog, structural or functional, affecting renal progenitor cells (**Figure 29F**).

4.2.6 Toxicity assays

The cytotoxicity of the 15 compounds exhibiting efficacy or lethality at 3 μM was tested by collaborators, Drs. Lori Emert-Sedlak and Tom Smithgall of the Department of Microbiology and Molecular Genetics, in a conditionally-immortalized mouse podocyte cell line. Podocytes are polarized epithelial cells located on the glomerular basement membrane that contribute to the integrity of the filtration barrier.[5] For the purposes of these experiments, they function as an indicator of renal toxicity. Following 72 hours of treatment with each compound concentrations ranging from 30 μM to 3 nM, podocyte viability was assessed by measuring residual metabolic activity (**Figure 30,** raw data in **Appendix C**). From these data, Dr. Emert-Sedlak calculated the concentration where 50% of the exposed podocytes remained viable (E_{50}). Of the 15 analogs tested, only two, TSA and apicidin, caused sufficient cytotoxicity to allow the calculation of an E_{50} value. Over the course of three experiments, TSA exhibited a mean E_{50} of 96 nM (s = 51 nM), while the mean E_{50} for apicidin was 152 nM (s = 54 nM). Treatment with PTBA or each of 12 structural analogs never decreased podocyte viability below the 50% threshold, even when tested at 30 μM (**Figure 30**). In fact, over three experiments, podocyte viability never dropped

below 80% following treatment with any of these compounds. Therefore, PTBA analogs carrying cap and/or zinc-binding group modifications, do not increase the toxicity of the compound relative to PTBA. These results suggest that the efficacy of PTBA can be improved through analog development without causing a corresponding increase in compound toxicity.

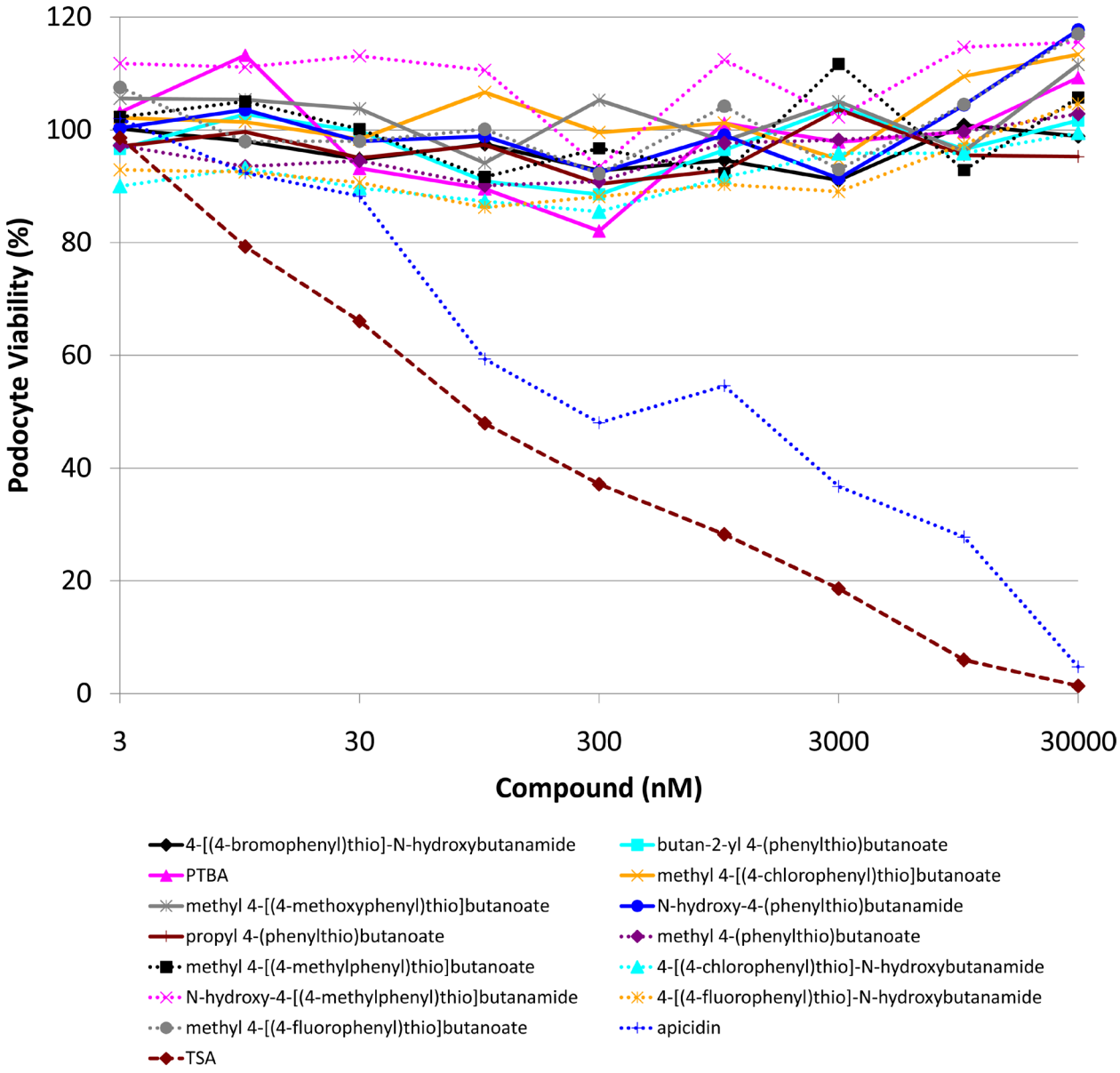

Figure 30. Structural PTBA analogs exhibit low toxicity in cultured podocytes. Podocytes were treated for 72 hours with 30 μM, 10 μM, 1 μM, 300 nM, 100 nM, 30 nM, 10 nM, or 3 nM of each compound or a DMSO control. Viability was assessed using Cell Titer-Blue. Viability was calculated as a percentage of the DMSO control, which was considered 100% viability. Data represent the average results of three independent experiments using duplicate wells for each condition.

4.3 METHODS

4.3.1 Zebrafish husbandry

Zebrafish husbandry was performed as described in Chapter 2

4.3.2 Compound sources and treatments

PTBA and methyl-4-(phenylthio)butanoate were synthesized as described in Chapter 2. 4-(Naphthalen-2-ylthio)butanoic acid (NSC2733) and 3-(phenylthio)benzoic acid (NSC113994), were obtained from the NCI/DTP Open Repository. APHA compound 8, Apicidin, butanoic acid, PBA, 4-phenoxybutanoic acid, 5-phenylpentanoic acid, Scriptaid, TSA, and valproic acid were obtained from Sigma-Aldrich. MS-275 and SAHA were obtained from Cayman Chemical Co. 4-(phenylsulfonyl)butanoic acid was obtained from Matrix Scientific. Tubacin was a gift of Dr. Ralph Mazitschek of the Broad Institute (Cambridge, MA). The remaining PTBA analogs were synthesized by Dr. Vasiliy Korotchenko of the Department of Pharmaceutical Sciences. Three independent groups of 12 chorionated 2 hpf embryos were arrayed in individual wells of 24-well plates. E3 medium was removed with a glass pipette and replaced with 800 µl treatment solutions containing 0.5% DMSO in E3 with or without compound at the reported concentrations.

4.3.3 *In situ* hybridization

In situ hybridization for *lhx1a* was performed as described in Chapter 2. Embryos were considered expanded if they exhibited *lhx1a* expression consistent with that resulting from treatment with 3 μM PTBA. Compounds were classified as effective, partially-effective, or ineffective based on comparison to the effects of PTBA at a given concentration.

4.3.4 Phenotypic screening

Phenotypic screening of PTBA analogs was performed identically to the concentration-response experiments detailed in Chapter 2. Embryos were treated with each PTBA analog from 2 to 72 hpf as described above.

4.3.5 Podocyte cytotoxicity assays

The conditionally-immortalized mouse podocyte cell line was a gift of Dr. Leslie Bruggeman of Case Western Reserve University (Cleveland, OH). The isolation and characterization of these cells have been previously described.[163,164] Mouse podocytes were plated at a density of 6,000 cells per 200 μl in 96-well plates to elicit log-phase growth. The indicated PTBA analogs were added at 30 μM, 10 μM, 1 μM, 300 nM, 100 nM, 30 nM, or 3 nM and incubated at 33 ^{o}C for 72 hours. The final DMSO concentration was maintained at 0.2% in all treatments except 30 μM (0.6%). After incubation, cytotoxicity was analyzed using the Cell Titer-Blue Cell Viability Assay (Promega) per manufacturer's instructions. Reagent (20 μl) was added to 100 μl of cells and plates were incubated for 2 hours at 37 ^{o}C. Fluorescence was read at

$560_{Ex}/590_{Em}$ on a Gemini SpectramaxXS (Molecular Devices) plate reader. Viability was calculated as a percentage of the DMSO control, which was considered 100% viability. Data represent the results of three independent experiments using duplicate wells for each condition. E50 values were determined from the transformed and normalized data by non-linear regression.

5.0 DISCUSSION

5.1 LESSONS FROM SMALL MOLECULE SCREENING

From a screen of almost 2000 small molecules, we identified a compound, PTBA, that had not been previously reported as a "hit" in 136 previous chemical library screens[165]. The success of our screen validates the use of an edemic phenotype as an indicator of aberrant kidney development. Furthermore, it emphasizes the importance of sound experimental design in determining the desired outcome. Many factors should be considered before beginning to interrogate libraries containing thousands of small molecules. Indeed, depending on the predetermined goals and parameters of the screen, investigators can generate completely different data sets using the same compound library.

To illustrate this point, consider the results of the chemical screens performed by my own lab and those of the neighboring Tsang lab.[166,167] Both groups tested zebrafish embryos at 10 μM using NCI/DTP Diversity Set compounds drawn from daughter plates derived from the same DMSO stocks. Furthermore, each lab identified a compound, PTBA or BCI, that expanded progenitor cells, leading to increased kidney or heart size, respectively. However, the differing experimental approaches utilized by our groups masked the effects of the other small molecule. The Tsang lab identified BCI by treating transgenic embryos carrying a fluorescent FGF-signaling reporter from 24 to 32 hpf. Since PTBA loses efficacy at about 15 hpf and edema

typically does not develop until at least 48 hpf, PTBA-treated embryos would appear wild-type. Therefore, even if they had recorded interesting secondary phenotypes beyond those involved in FGF signaling, PTBA would have been missed using this approach. Likewise, BCI-treated 72 hpf larvae were scored as wild-type in our phenotypic screen, even though they almost certainly contained enlarged hearts. Although both screens were ultimately successful, their unique observations depended on the selection of treatment windows and phenotypes appropriate for the research. Without these considerations, the effects of interesting small molecules can be easily overlooked.

Another important factor contributing to the discovery of PTBA was the concentration chosen for the screen. In this, we were very fortunate. All compounds were ostensibly tested at 10 μM in embryo medium. Had this truly been the case, then my data suggests that PTBA treatment would have killed all the embryos before reaching 72 hpf. Since we performed no further characterization on compounds found to be lethal at the screening concentration, PTBA might never have been characterized. Luckily, compound concentrations in DMSO stocks can vary several fold from the reported value in small molecule libraries.[131] Thus, the concentration in the PTBA-containing well was probably much closer to 3-5 μM, allowing edema formation and generating a positive hit. Furthermore, had we decided to screen at a lower concentration, the larvae may have appeared wild-type, again precluding any further testing. This exposes a flaw in the way many small molecule screens are performed: very few involve screening at multiple concentrations. It could be argued that repeated screening of a library is a waste of time and effort, especially if hits have been identified. However, small molecule libraries generally already represent a significant investment of resources, and follow-up screens at different

concentrations merit consideration. At the very least, compounds observed to be lethal in the initial screen could be retested at lower concentrations in search of relevant phenotypes.

5.2 MODELING HOW PTBA ENGAGES THE RA PATHWAY

Treating zebrafish embryos with PTBA stimulates RA signaling, as evidenced by its effects on the RA-responsive genes *cyp26a1* and *cmlc2*. Consequently, blocking RA signaling at the receptor level with dominant-negative RARα greatly reduced PTBA efficacy. Therefore, PTBA likely interacts with some elements of the RA signaling pathway in order to stimulate renal progenitor cell proliferation during pronephric development. The characterization of PTBA as a novel HDACi suggests that the targets are most likely the HDACs controlling the repression of RA-responsive genes.

In the absence of RA, an RAR/RXR dimer binds the RARE in regulated promoters and recruits complexes of corepressor proteins, including an HDAC (**Figure 31A**). The HDAC deacetylates nearby nucleosomes, causing chromatin condensation which inhibits gene transcription. When RA binds the RAR/RXR dimer, it elicits a conformational change that removes the HDAC from close proximity to the nucleosomes (**Figure 31B**). This facilitates the activity of coactivators, such as histone acetyltransferases, which decondense the chromatin and allow transcription to occur. By inhibiting the corepressor HDAC, HDACis have been hypothesized to lower the RA concentration necessary to activate the RAR/RXR dimer (**Figure 31C**).[62] In this way, PTBA could stimulate RA signaling at the receptor level without affecting the endogenous RA concentration.

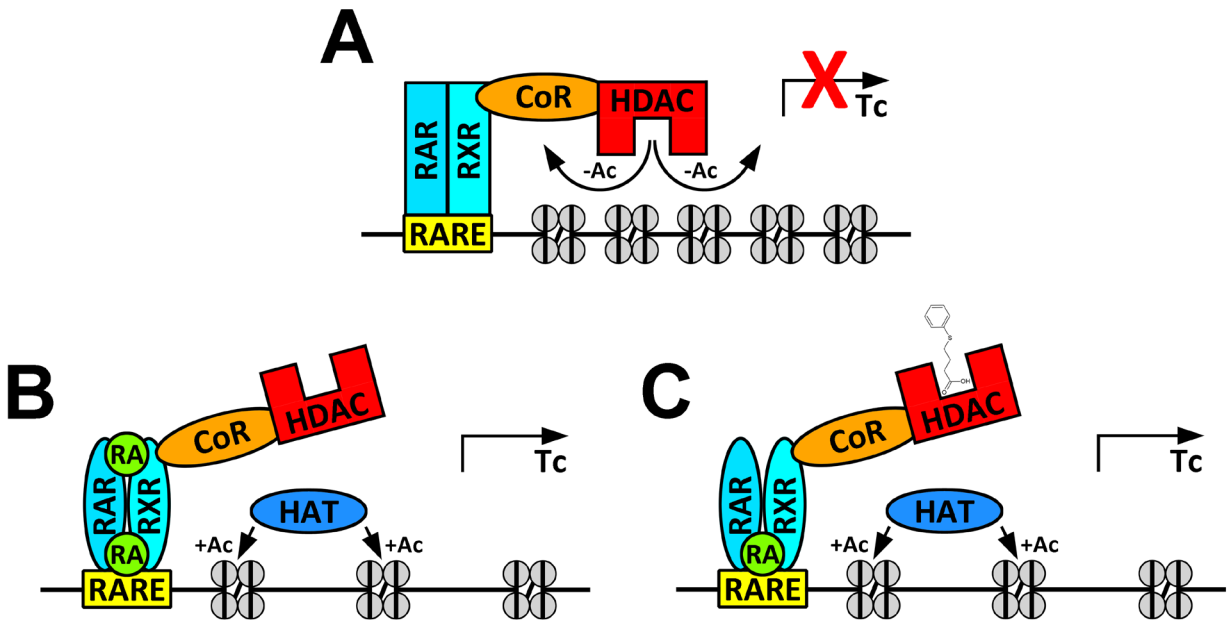

Figure 31. HDACis enhance RA signaling. (A) In the absence of RA, RAR/RXR dimers recruit a corepressor complex (CoR) containing an HDAC. The HDAC deacetylates nucleosomes, causing chromatin condensation and preventing transcription. (B) In the presence of RA, the RAR/RXR dimer undergoes a conformational change, removing the HDAC from close association with nucleosomes. This allows coactivators such as a histone acetyltransferase (HAT) to acetylate the nucleosomes, which decondenses the chromatin and permits transcription. (C) HDAC inhibitors, such as PTBA, have been hypothesized to decrease the required concentration of RA necessary to trigger the RAR/RXR conformational switch. Figure adapted from Menegola and coworkers.[62]

The downstream target of RA-signaling that mediates the effects of PTBA on renal progenitor cells remains unknown. Since my results argue that PTBA treatment stimulates renal progenitor cell proliferation without significantly transforming juxtaposed tissues, the effect is probably local. Therefore, PTBA may enhance RA signaling directly within renal progenitor cells, leading to increased proliferation. Because attenuation does not require the synthesis of protein intermediates, this hypothesis is compatible with the previous work of Cartry and coworkers.[63] They observed that treating *Xenopus* embryos with RA caused *lhx1a* expansion even in the presence of the protein synthesis inhibitor, cycloheximide.[63] Furthermore, treating kidney epithelial cell lines with RA increased both thymidine uptake and the proportion of cells in S-phase.[168,169] Therefore, it is possible that the proliferative machinery in renal progenitor cells may respond to RA-signaling in a similar manner.

5.3 THERAPEUTIC POTENTIAL OF PTBA

5.3.1 Proliferation: the intersection of development and regeneration

In many respects, the process of kidney regeneration mimics that of nephrogenesis.[153] In both cases, a multipotent cell first proliferates to provide the necessary raw material and then differentiates into the required tissue type. Several hypotheses have been proposed to explain the source of the multipotent cells involved in regeneration. The first, and most generally accepted, suggests that these cells arise from tissue dedifferentiation near the site of damage.[170] Other groups argue that the multipotent cells are actually stem cells of intrarenal or extrarenal origin.[171,172] In any case, it is reasonable to assume that these cells share elements in common

with renal progenitor cells. Therefore, I hypothesize that they may also exhibit similar proliferation in response to PTBA treatment.

This hypothesis may explain the observations made by other groups regarding the relationship between HDAC inhibition and renal regeneration. In one study, Imai and coworkers demonstrated that treating mice with daily injections of TSA attenuated renal damage following injury.[173] Since PTBA and TSA both function as HDACis and expand renal progenitor cells, they may also act similarly in facilitating renal regeneration. In another study, Marumo and coworkers demonstrated that the expression of Hdac5 was significantly decreased following acute ischemic damage in mouse kidneys.[174] This suggests that the reduction of HDAC activity may serve as an important part of the regeneration process. Therefore, at least some evidence supports the idea that PTBA may function as a useful therapeutic following acute kidney injury.

5.3.2 Analog efficacy in a mouse model of acute kidney injury

To test this hypothesis, we have been collaborating with Drs. Raymond Harris and Mark de Caestecker at Vanderbilt University. Dr. Harris' lab has developed a transgenic mouse model of acute kidney injury using diphtheria toxin (DT) as a nephrotoxic agent. Unlike humans, mice are normally resistant to DT exposure. This resistance arises from several amino acid differences in the protein acting as the DT receptor, heparin-binding EGF-like growth factor (Hbegf).[175] Transgenic mice (PTC-DTR) express human HBEGF in their proximal tubules, creating the conditions for an acute and specific damage event.

Since blood is a buffered solution, testing PTBA would have been a poor choice. At neutral pH, the zinc-binding group would be deprotonated and the resulting polar charge would greatly decrease its absorption through cell membranes. Instead we tested an effective structural

analog carrying a methylated zinc-binding group, methyl 4-(phenylthio)butanoate (MPTB). PTC-DTR mice were injected with DT and damage was allowed to accrue for one day. At this time, mice were given daily injections of MPTB or a DMSO control for the next six days. Preliminary data from a single group of mice suggest that MPTB treatment significantly increases the rate of renal recovery by approximately 30% (**Figure 32**). Therefore, PTBA analogs demonstrate some promise as renal therapeutics following acute kidney injury.

5.3.3 Factors governing the toxicity of PTBA analogs

Toxicity is also an important consideration during the development of any drug. At its effective concentration, I observed that PTBA exhibits much milder effects on juxtaposed mesodermal tissues in comparison to TSA. Furthermore, structural PTBA analogs, even when administered at 30 μM, demonstrated little effect on podocyte cell viability in cell culture assays. However, my data suggest that treating podocytes with 100 nM TSA would be expected to kill at least 50% of the cells within 72 hours. There are at least two possible explanations for this difference in toxicity, each reflecting different considerations of HDAC-HDACi binding.

Crystallography studies have revealed how several HDACis block substrate access by interacting with the Zn^{2+} in the catalytic site of an HDAC. Therefore, most HDACis, including carboxylic and hydroxamic acids, function as competitive inhibitors of HDACs, although noncompetitive HDACis, such as Trapoxin A, have been characterized.[176-179] In this example, taken from the Protein Data Bank, TSA occupies the binding site of human HDAC7 by coordinating its hydroxamic acid motif with the catalytic Zn^{2+} (**Figure 33**). In general, hydroxamic HDACis bind HDACs much more strongly than HDACis containing carboxylic acid

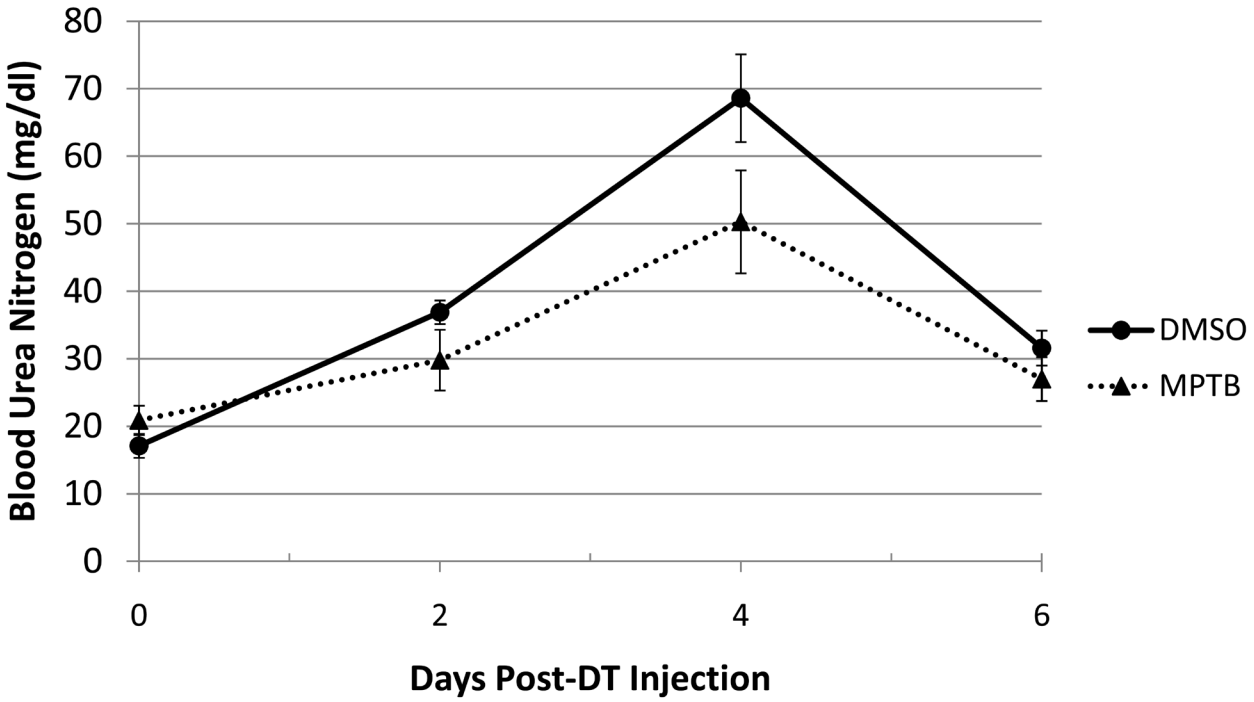

Figure 32. Treatment with MPTB increases the rate of renal recovery in mice following acute kidney injury. Female PTC-DTR mice were injected with 0.1 μg/kg DT on day 0. Beginning on day 1, mice were treated with daily injections of 1% DMSO or 3.4 mg/kg MPTB (n = 5 per group). Blood urea nitrogen (BUN), a biomarker of nitrogenous wastes, was determined every two days following DT injection. Error bars are the standard error of the mean. Asterisk represents a significant difference in BUN concentration ($p < 0.002$) as determined by t-test. Data generated by Mark de Caestecker.

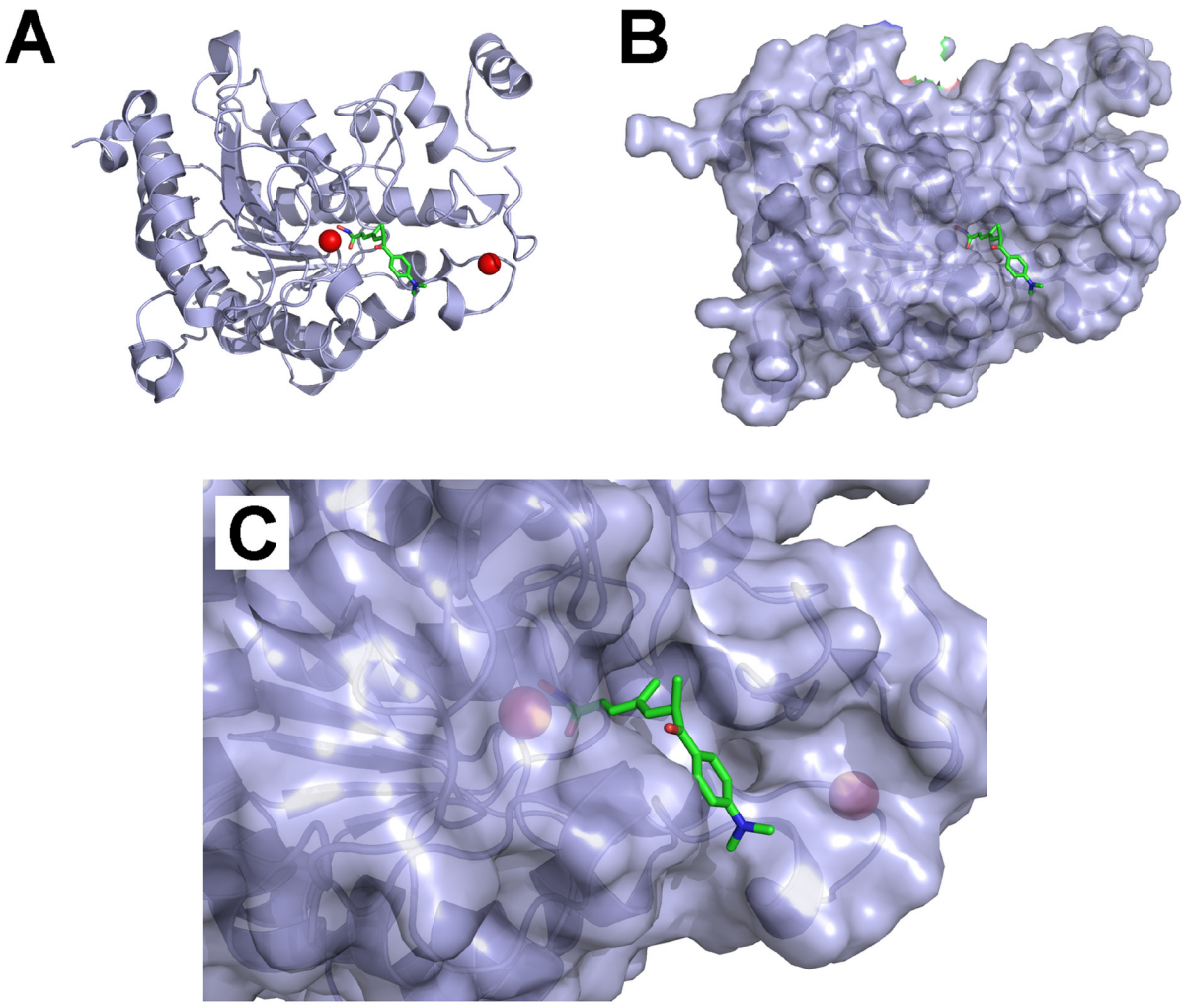

Figure 33. Binding of TSA to human HDAC7 as determined by X-ray crystallography. (A) TSA co-crystallized with HDAC7 (ribbon model). (B) TSA co-crystallized with HDAC7 (space-filling model). (C) Magnification of (B), showing coordination of the hydroxamic motif of TSA with the catalytic site Zn^{2+}. Panels generated by Tom Smithgall from Protein Data Bank entry 3C10.

zinc-binding groups, such as PTBA.[154] This is because PTBA should form only one coordinate bond with the active site zinc, an arrangement known as monodentate binding.[154] In contrast, the hydroxamic acid of TSA binds in a bidentate fashion, forming two coordinate bonds with the active site zinc.[154] This difference is reflected in the results of my *in vitro* HDAC analysis. I observed that TSA inhibited all HDAC activity at micromolar concentrations, while PTBA reduced HDAC activity by only 70% at millimolar concentrations. However, this large efficacy difference is not evident *in vivo*. PTBA and TSA were found to generate similar increases in histone hyperacetylation at concentrations within about one log of each other. These data suggest that additional factors may be involved in determining compound efficacy in the context of a whole organism.

The difference in HDAC isoform specificity between carboxylic and hydroxamic acids may provide a possible explanation for these observations. HDAC isoforms are separated into four classes based on their size, homology, cellular localization, and catalytic activity (**Figure 34**).[180] For example, Class I isoforms generally exhibit nuclear localization, while Class II HDACs are primarily cytoplasmic.[181] Carboxylic acid HDACis are considered to be specific inhibitors of Class I and IIa HDACs, while hydroxamic acids target Class I, II, and IV isoforms (**Figure 34**).[180,182-184] Meanwhile, the Class III HDACs (sirtuins), utilize an NAD^+-dependent catalysis mechanism that remains unaffected by carboxylic or hydroxamic HDACis (**Figure 34**).[185,186] Although the class specificity of PTBA has not yet been confirmed, it can be hypothesized to function as a Class I/IIa-specific inhibitor like other carboxylic acids.

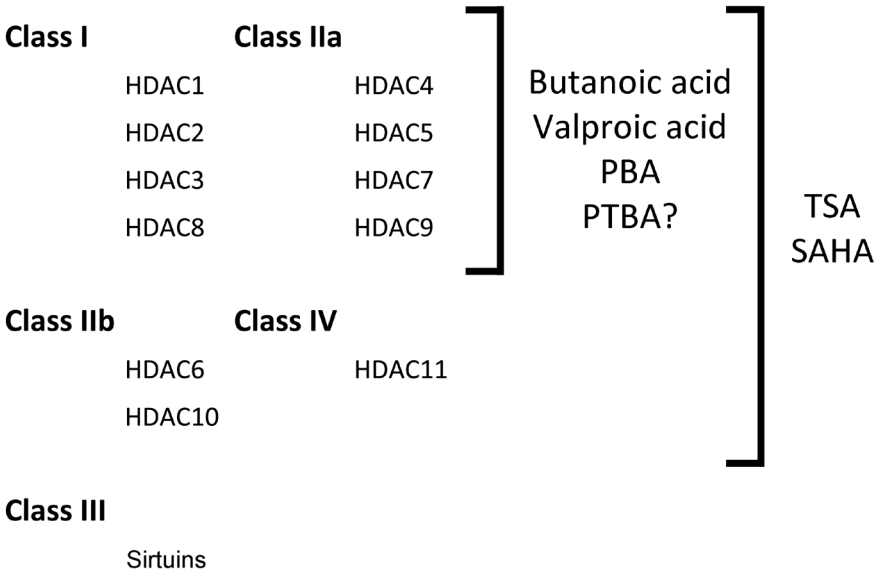

Figure 34. HDAC classes inhibited by carboxylic and hydroxamic acid HDACis. Carboxylic acid HDACis: butanoic acid, valproic acid, PBA, and TSA. Hydroxamic acid HDACis: TSA and SAHA. Class I, II, and IV HDACs utilize Zn^{2+}-dependent catalysis, while the Class III sirtuins employ an NAD+-dependent mechanism.

Several inferences can be made from these isoform specificities. First, if PTBA efficacy in zebrafish embryos does indeed require the inhibition of one or more HDAC isoforms, then hdacs 6, 10, and 11 are probably not targeted. Therefore, it is possible that the increased toxicity observed in TSA-treated embryos may result from its effect on these hdacs. Of particular interest is HDAC6, which functions as a microtubule-associated deacetylase.[187] Affecting the post-translational modifications of the microtubule network causes broad effects on cell signaling and the maintenance of homeostasis.[187] However, embryos treated with tubacin, an HDAC6-specific HDACi,[188] appeared wild-type in my phenotypic screens. It is possible that tubacin's LogP of 6.34, the highest of any tested PTBA analog (**Appendix A**), may prevent efficient compound absorption and could account for the lack of phenotype.

Furthermore, the broad specificity of hydroxamic HDACis suggested that hydroxamic PTBA analogs would demonstrate greater efficacy at the expense of increased toxicity. Indeed, several hydroxamic analogs increased *lhx1a* expression in treated embryos at concentrations equal to or less than PTBA. However, my data from zebrafish embryos and podocyte culture suggest that this modification has little to no effect on compound toxicity. This may imply that the hydroxamic analogs remain weak inhibitors despite the improved strength of the zinc-binding group. Accordingly, their HDACi activity should be determined empirically in future *in vitro* assays. Alternatively, the products generated from the metabolism of TSA may cause the deleterious effects observed in treated embryos. Indeed, some evidence suggests that the *N*-demethylated byproducts of TSA remain pharmacologically active and persist in the circulation for at least an hour following administration.[189] However, it is currently unknown if these metabolic waste products affect normal cellular processes.

5.3.4 HDACis are clinically relevant

Previous clinical studies with known HDACis suggest that structural analogs of PTBA may function as viable therapeutics. Indeed, both trichostatin A (Vorinostat) and valproic acid have received U.S. Food and Drug Administration (FDA) approval for oral administration to treat T-cell lymphoma and epilepsy, respectively.[190] Importantly, the sodium salt of PBA (Buphenyl), one of the closest structural analogs of PTBA, also received FDA approval in 1996 for the treatment of urea cycle disorders.[191] To date, Buphenyl remains the only FDA-approved treatment for chronic management of the excess blood ammonia (hyperammonemia) generated by enzymatic deficiencies in urea metabolism.[192] Prescribed daily doses of Buphenyl as an oral medication often reach gram quantities, with some patients taking as much as 20 g/day.[193] Thus, it may be possible to safely administer other PTBA analogs at similarly high doses. In addition, Buphenyl exhibits good bioavailability of about 80% when taken orally.[194] Unfortunately, Buphenyl has a short half-life ($t_{1/2}$ ~ 1 hr) following administration, as it is rapidly converted to phenylacetic acid.[194] However, this limitation can be easily overcome by prescribing multiple daily dosings.[194] Therefore, the favorable pharmacological properties of sodium PBA support the future development of other PTBA analogs for clinical use.

5.4 IMPORTANT CONSIDERATIONS AND OPEN QUESTIONS

Despite these encouraging results, several critiques must be considered to make a fair assessment of the contributions and future impact of this work. Although, the zebrafish pronephros serves as an excellent model of individual metanephric nephrons, metanephroi are complex organs

consisting of millions of nephrons. It is unknown how accurately simple pronephric models reflect conditions within the broader context of general metanephric kidney function. Future experiments with PTBA analogs in mouse models of kidney injury may help to address this concern. Furthermore, while my data suggest that PTBA treatment affects normal pronephric function, thus causing the edemic phenotype, this was not determined empirically. Although the pronephros is almost certainly nonfunctional at 48 hpf because the glomerulus has not yet formed, fluorescent dextran injections could provide further confirmation. Indeed, it would be interesting to determine if PTBA-treated embryos manage to form functional pronephroi later in development.

My research provided some insight into the mechanism of PTBA efficacy, revealing the involvement of the RA signaling pathway and HDAC inhibition. However, the specific target of PTBA activity remains unknown. Ostensibly, this should be an HDAC isoform or isoforms, perhaps representing a specific HDAC class. However, it is important to note that HDACis modify many non-histone proteins in their capacity as lysine deacetylases.[195] These targets include hormone receptors, signal transducers, transcriptions factors, structural proteins, and chaperones.[195] Therefore, target identification may not be a straightforward prospect. However, I believe that an investigation of possible HDAC targets still represents the best place to start. My preliminary results suggest that the expression patterns of individual hdac isoforms remain relatively ubiquitous in 24 hpf zebrafish embryos (data not shown). It may be helpful to determine if any of these become compartmentalized in the pronephric region later in development. These isoforms would be good candidates as potential PTBA effectors. Furthermore, like other carboxylic acid HDACis, PTBA would be expected to exhibit some Class I/IIa specificity. If this characteristic is confirmed in future investigations, then isoforms of

these classes should also merit some interest. Morpholino knockdown of these candidates in an effort to recapitulate *lhx1a* expansion in the IM would provide an excellent approach for target validation.

When developing potential human therapeutics using zebrafish, consideration should be given to the variation in HDAC orthologs across species. Although zebrafish hdacs, such as hdac1, share a large degree of amino acid identity with the HDACs of other vertebrates, discrepancies remain (**Figure 35**). These differences could alter the efficacy of PTBA or its analogs when applied in other model systems or in humans. Encouragingly, PTBA demonstrated the ability to function *in vitro* as an HDACi using human HDAC isoforms derived from HeLa cell extracts. However, this result does not eliminate the possibility of differing efficacies when assessing individual HDAC orthologs.

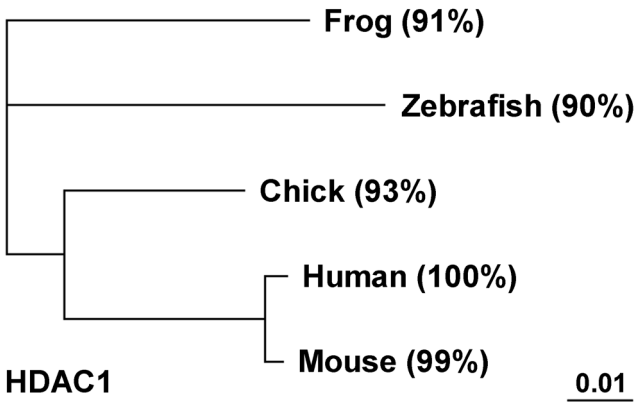

Figure 35. Evolutionary relationship between HDAC1 orthologs in selected vertebrates. Cladogram generated using TreeView software (ver. 1.6.6) and HDAC1 RefSeq protein sequences for each species. Percentage denotes percent sequence identity with the human isoform. Scale bar represents nucleotide substitutions per site.

In addition to the points raised above, several other open questions remain unanswered. Potent HDACis, such as SAHA and MS-275, showed no effect on zebrafish embryos when they were treated at 3 μM. This was an unexpected result which could reflect poor absorption of the compounds into the embryos, short half-lives, or a zebrafish-specific effect. Hyperacetylation assays could be performed to determine if the compounds are indeed able to exert a physiological effect on embryos, despite the lack of edemic phenotype. Furthermore, exploring the downstream effects of HDAC inhibition, such as the stimulation of coactivators, would provide further confirmation of the mechanism of PTBA efficacy. For example, pharmacologically inhibiting the activity of histone acetyltransferases (HATs) would be expected to block PTBA efficacy by interfering with its signaling. One final point of interest is better understanding the differences in PTBA efficacy when compared to TSA in my *in vitro* and *in vivo* assays. *In vitro*, TSA is thousands of times more effective than PTBA in inhibiting HDAC activity, while *in vivo* the difference is greatly reduced. Of course, the varying HDAC class specificities of the two compounds may play a role in this effect. However, I suspect that the structural elements of PTBA, particularly the thiol group, may provide the compound with unique *in vivo* pharmacokinetics.

5.5 NEXT GENERATION PTBA ANALOGS

My results demonstrate that several PTBA analogs exhibit improved efficacy with little to no increase in toxicity. These second generation compounds are excellent candidates to improve renal recovery in future animal studies. However, I believe that my work marks only the first steps in the development of this family of compounds. Using only simple functional group

substitutions, I was able to identify PTBA structural analogs that were only several times less effective than TSA. However, these same analogs exhibit several hundred times less toxicity than TSA in podocyte cell culture. This represents the key benefit offered by this class of "weak" inhibitors. It is true that almost all of the effective PTBA analogs cause some degree of edemic and/or lethal phenotypes during zebrafish development. However, these teratogenic effects should not be an issue when treating an adult, whose tissues primarily consist of differentiated cells. Indeed, according to our collaborators, the PTC-DTR mice treated with MPTB exhibit no overt signs of toxicity (data not shown).

Because the second generation PTBA analogs exhibit little toxicity, I believe that there is still ample room for further efficacy improvements. The results of my research offer some guidelines for this process. In general, substitutions of the aliphatic cap region increased compound efficacy. Adding functional groups to the phenyl ring represents a simple way to increase the LogP value of the base compound, which may aid absorption through biological membranes. Alternatively, the cap substitutions may interact with amino acids in the binding pocket of the HDAC, improving the affinity of the compound. Interestingly, even halogenated groups, which are often metabolized into toxic byproducts,[196] appear to be tolerable.

The sulfur atom forming the connecting unit of PTBA also appears to be a critical activity determinant. In comparison to its substituted analogs, I observed that only PTBA exhibited significant efficacy. Since the LogP values of PTBA and the analogs carrying connecting unit substitutions are similar, I doubt that improved absorption plays a role. More likely, the sulfur atom forms unique interactions within the HDAC binding pocket. This may include serving as a hydrogen bond acceptor due to the presence of an unbound electron pair.

Unfortunately, only one analog carrying a linker group was available for testing. Adding a bulky ring structure to the linker decreased the analog's efficacy relative to PTBA. The increased rigidity of the normally flexible hydrophobic chain may explain this effect. I believe that increasing the length of the linker region remains an untapped opportunity to generate a better analog. Indeed, the linkers of the more potent HDACis, including TSA and SAHA, contain seven and eight carbons respectively.

Finally, I also observed that analogs carrying methylated or hydroxamic zinc-binding groups exhibit improved efficacy. Adding alkyl groups to the zinc-binding group might be expected to interfere with the formation of coordinate bonds with the active site zinc. However, it is likely that the ubiquitous esterases found in target cells hydrolyze and remove the alkyl groups upon absorption. Furthermore, since alkylation prevents deprotonization of the carboxylic acid, these analogs would be expected to be more effective in buffered solutions. The hydroxamic analogs of PTBA also demonstrated improved efficacy, although perhaps not as much as I had expected. Although they possess stronger zinc-binding groups, they suffer from increased polarity as evidenced by lower LogP values. Therefore, the expected increase in binding affinity may be counterbalanced by decreased absorption. Importantly, the hydroxamic PTBA analogs demonstrate none of the toxicity of TSA in cell culture experiments. Further modifications of these structures, perhaps incorporating some elements of the TSA structure, may yield a family of highly potent compounds.

It is my sincere hope that this research forms the foundation for new therapeutic approaches to improve outcome following renal damage. Preliminary results show promise, and further investigations with subsequent generations of PTBA analogs are certainly warranted. Furthermore, my research suggests that we should not be so quick to dismiss compounds others

may consider weak or uninteresting. In 1979, PTBA and several analogs were first discussed as compounds with "expected biological activity."[197] It required over thirty years and one graduate student's career to confirm this prediction.

APPENDIX A

PARTITION COEFFICIENTS OF PTBA ANALOGS

Compound Name	XLogP
butanoic acid	0.79
4-(phenylsulfonyl)butanoic acid	1.01
4-(phenylamino)butanoic acid	1.41
N -hydroxy-4-[(4-methoxyphenyl)thio]butanamide	1.52
APHA compound 8	1.52
N -hydroxy-4-(phenylthio)butanamide	1.55
4-[(4-fluorophenyl)thio]-*N* -hydroxybutanamide	1.65
SAHA	1.86
N -hydroxy-4-[(4-methylphenyl)thio]butanamide	1.91
MS-275	2.02
4-phenoxybutanoic acid	2.14
4-[(4-chlorophenyl)thio]-*N* -hydroxybutanamide	2.18
Scriptaid	2.18
4-[(4-bromophenyl)thio]-*N* -hydroxybutanamide	2.24
4-(phenylthio)butanoic acid (PTBA)	2.29
4-phenylbutanoic acid (PBA)	2.42

Compound Name	XLogP
methyl 4-[(4-methoxyphenyl)thio]butanoate	2.59
methyl 4-(phenylthio)butanoate	2.61
5-phenylpentanoic acid	2.70
methyl 4-[(4-fluorophenyl)thio]butanoate	2.71
valproic acid	2.75
trichostatin A (TSA)	2.75
methyl 4-[(4-methylphenyl)thio]butanoate	2.98
methyl 4-[(4-chlorophenyl)thio]butanoate	3.24
methyl 4-[(4-bromophenyl)thio]butanoate	3.31
propyl 4-(phenylthio)butanoate	3.51
4-(naphthalen-2-ylthio)butanoic acid	3.54
tert -butyl 4-(phenylthio)butanoate	3.60
butan-2-yl 4-(phenylthio)butanoate	3.94
apicidin	4.41
3-(phenylthio)benzoic acid	4.45
tubacin	6.34

Table 4. Predicted octanol-water partition coefficients (XLogPs) of the PTBA analogs. XLogP values were calculated from the chemical structures using XLOGP3 (ver. 3.2.2), a web-based application available at http://www.sioc-ccbg.ac.cn/software/xlogp3/.

APPENDIX B

PHENOTYPIC SCREENING OF PTBA ANALOGS

Compound Name	3 μM	1.5 μM	800 nM	400 nM	200 nM	100 nM
0.5% DMSO	0/36 (0%)	0/36 (0%)	0/36 (0%)	0/35 (0%)	0/35 (0%)	0/35 (0%)
4-phenoxybutanoic acid	0/35 (0%)	ND	ND	ND	ND	ND
4-(phenylsulfonyl)butanoic acid	0/35 (0%)	ND	ND	ND	ND	ND
5-phenylpentanoic acid	0/36 (0%)	ND	ND	ND	ND	ND
APHA compound 8	0/36 (0%)	ND	ND	ND	ND	ND
MS-275	0/36 (0%)	ND	ND	ND	ND	ND
PBA	0/36 (0%)	ND	ND	ND	ND	ND
SAHA	0/36 (0%)	ND	ND	ND	ND	ND
tubacin	0/36 (0%)	ND	ND	ND	ND	ND
4-(phenylamino)butanoic acid	0/35 (0%)	ND	ND	ND	ND	ND
Scriptaid	9/36 (25%)	ND	ND	ND	ND	ND
butanoic acid	0/36 (0%)	ND	ND	ND	ND	ND
tert -butyl 4-(phenylthio)butanoate	14/36 (39%)	ND	ND	ND	ND	ND
valproic acid	7/35 (20%)	ND	ND	ND	ND	ND
4-(naphthalen-2-ylthio)butanoic acid	0/35 (0%)	ND	ND	ND	ND	ND
N -hydroxy-4-[(4-methoxyphenyl)thio]butanamide	11/35 (0%)	ND	ND	ND	ND	ND
methyl 4-[(4-bromophenyl)thio]butanoate	26/35 (74%)	ND	ND	ND	ND	ND
3-(phenylthio)benzoic acid	0/36 (0%)	ND	ND	ND	ND	ND
4-[(4-bromophenyl)thio]-*N* -hydroxybutanamide	33/35 (94%)	17/36 (47%)	ND	ND	ND	ND
butan-2-yl 4-(phenylthio)butanoate	35/35 (100%)	31/35 (89%)	5/36 (14%)	ND	ND	ND
PTBA	33/36 (92%)	29/35 (83%)	2/36 (6%)	ND	ND	ND
methyl 4-[(4-chlorophenyl)thio]butanoate	34/35 (97%)	26/36 (72%)	ND	ND	ND	ND
methyl 4-[(4-methoxyphenyl)thio]butanoate	35/35 (100%)	32/35 (91%)	20/35 (57%)	10/35 (29%)	1/36 (3%)	ND
N -hydroxy-4-(phenylthio)butanamide	36/36 (100%)	33/36 (92%)	2/33 (6%)	ND	ND	ND
propyl 4-(phenylthio)butanoate	31/33 (94%)	32/36 (89%)	7/36 (19%)	ND	ND	ND
methyl 4-(phenylthio)butanoate	30/31 (97%)	32/36 (89%)	7/34 (21%)	ND	ND	ND
methyl 4-[(4-methylphenyl)thio]butanoate	35/35 (100%)	36/36 (100%)	17/35 (49%)	5/36 (14%)	1/36 (3%)	ND
4-[(4-chlorophenyl)thio]-*N* -hydroxybutanamide	34/36 (94%)	35/36 (97%)	6/36 (17%)	ND	ND	ND
N -hydroxy-4-[(4-methylphenyl)thio]butanamide	28/28 (100%)	32/33 (97%)	22/36 (61%)	3/35 (9%)	1/36 (3%)	ND
4-[(4-fluorophenyl)thio]-*N* -hydroxybutanamide	27/27 (100%)	36/36 (100%)	23/36 (64%)	12/34 (35%)	2/36 (6%)	ND
methyl 4-[(4-fluorophenyl)thio]butanoate	XX	30/30 (100%)	21/35 (60%)	9/35 (26%)	7/32 (22%)	ND
apicidin	XX	XX	XX[1]	8/36 (22%)	2/36 (6%)	ND
TSA	XX	XX	XX	XX	29/29 (100%)	34/35 (100%)

Table 5. Raw data for Table 3. Data are *lhx1a* expanded/total embryos for each condition.

APPENDIX C

PODOCYTE TOXICITY DATA

Compound Name	0 nM	3 nM	10 nM	30 nM	100 nM	300 nM	1 μM	3 μM	10 μM	30 μM
4-[(4-bromophenyl)thio]-N-hydroxybutanamide	96.84	97.23	98.78	99.76	92.83	92.51	92.31	92.58	97.25	100.91
butan-2-yl 4-(phenylthio)butanoate	103.80	89.23	94.02	95.82	78.55	78.83	77.39	94.94	85.45	84.42
PTBA	101.87	102.61	99.52	96.34	100.50	98.50	103.48	105.20	118.24	108.66
methyl 4-[(4-chlorophenyl)thio]butanoate	100.37	99.47	98.77	97.99	97.29	98.01	96.36	96.57	94.85	96.87
methyl 4-[(4-methoxyphenyl)thio]butanoate	96.62	100.57	98.58	99.10	96.92	97.80	96.20	103.70	94.54	100.89
N-hydroxy-4-(phenylthio)butanamide	99.57	100.64	100.49	98.24	97.84	96.18	92.99	94.87	96.38	102.32
propyl 4-(phenylthio)butanoate	97.33	96.55	97.15	92.20	112.43	89.93	91.31	107.62	91.10	93.37
methyl 4-(phenylthio)butanoate	97.76	94.47	95.18	98.52	99.30	97.06	94.38	95.80	95.67	99.30
methyl 4-[(4-methylphenyl)thio]butanoate	101.23	97.84	101.27	101.52	97.29	97.77	96.96	117.37	92.07	93.00
4-[(4-chlorophenyl)thio]-N-hydroxybutanamide	98.68	100.24	94.97	97.12	95.12	92.37	95.63	94.58	97.04	105.03
N-hydroxy-4-[(4-methylphenyl)thio]butanamide	99.50	98.79	97.34	98.78	98.09	93.64	96.15	97.79	100.31	104.01
4-[(4-fluorophenyl)thio]-N-hydroxybutanamide	102.87	99.42	99.24	97.59	95.87	96.68	96.14	101.60	103.91	111.27
methyl 4-[(4-fluorophenyl)thio]butanoate	100.19	98.19	98.92	98.21	98.01	95.39	91.74	94.92	91.60	99.42
apicidin	96.63	97.69	96.24	92.14	60.10	47.51	34.37	21.05	13.18	4.23
TSA	99.77	96.44	71.38	59.45	40.75	24.72	15.37	13.02	7.68	2.74

Table 6. Toxicity of PTBA analogs in cultured podocytes (first replicate). Toxicity was assayed by CellTiter-Blue Cell Viability Assay. Values represent percentage of viable podocytes following 72 hours of treatment with each analog at the listed concentration (see **Chapter 4**, **Methods**). These data were used to generate **Figure 30**.

Compound Name	0 nM	3 nM	10 nM	30 nM	100 nM	300 nM	1 μM	3 μM	10 μM	30 μM
4-[(4-bromophenyl)thio]-N-hydroxybutanamide	102.71	95.93	96.27	93.77	100.33	94.36	97.71	104.78	106.38	108.81
butan-2-yl 4-(phenylthio)butanoate	98.48	93.42	102.76	100.72	95.19	97.17	98.30	103.13	107.58	96.94
PTBA	108.92	107.92	106.80	87.50	73.09	48.38	86.15	85.65	82.07	103.27
methyl 4-[(4-chlorophenyl)thio]butanoate	98.98	112.49	100.78	99.85	103.78	99.44	100.31	99.37	106.16	100.47
methyl 4-[(4-methoxyphenyl)thio]butanoate	99.72	107.52	101.62	101.96	82.91	107.86	94.09	98.80	97.33	124.86
N-hydroxy-4-(phenylthio)butanamide	101.41	100.37	99.95	98.21	98.93	94.60	98.27	93.69	102.96	104.16
propyl 4-(phenylthio)butanoate	102.51	98.73	98.54	101.02	95.51	97.63	95.98	98.65	105.95	87.81
methyl 4-(phenylthio)butanoate	95.35	98.49	87.01	83.25	68.79	67.00	94.22	90.70	88.62	99.76
methyl 4-[(4-methylphenyl)thio]butanoate	99.55	102.14	102.24	101.01	92.89	96.77	101.59	101.32	105.77	105.21
4-[(4-chlorophenyl)thio]-N-hydroxybutanamide	102.53	89.65	102.23	93.87	96.23	99.37	98.33	98.97	102.83	100.24
N-hydroxy-4-[(4-methylphenyl)thio]butanamide	98.71	96.79	98.39	99.69	99.22	88.31	94.15	96.20	99.23	107.99
4-[(4-fluorophenyl)thio]-N-hydroxybutanamide	99.26	90.60	98.59	94.16	95.64	95.64	95.55	92.93	99.23	106.66
methyl 4-[(4-fluorophenyl)thio]butanoate	103.92	101.29	98.95	94.82	93.84	89.31	85.72	88.84	96.93	103.53
apicidin	100.41	104.71	76.48	84.06	47.56	36.11	51.66	39.18	27.16	0.05
TSA	93.91	95.52	80.15	76.57	48.22	39.64	40.07	23.39	5.57	-0.68

Table 7. Toxicity of PTBA analogs in cultured podocytes (second replicate). Toxicity was assayed by CellTiter-Blue Cell Viability Assay. Values represent percentage of viable podocytes following 72 hours of treatment with each analog at the listed concentration (see **Chapter 4**, **Methods**). These data were used to generate **Figure 30**.

Compound Name	0 nM	3 nM	10 nM	30 nM	100 nM	300 nM	1 μM	3 μM	10 μM	30 μM
4-[(4-bromophenyl)thio]-N-hydroxybutanamide	106.04	107.34	98.92	90.71	99.20	91.38	93.86	75.86	98.85	86.81
butan-2-yl 4-(phenylthio)butanoate	114.81	107.20	111.57	102.79	98.87	89.60	113.55	113.92	96.66	123.60
PTBA	101.87	98.82	133.43	95.71	95.04	99.29	113.84	102.72	98.71	115.85
methyl 4-[(4-chlorophenyl)thio]butanoate	94.19	94.49	104.62	97.19	118.90	101.24	106.98	88.29	127.49	142.80
methyl 4-[(4-methoxyphenyl)thio]butanoate	113.14	108.64	115.86	110.15	102.48	110.09	103.80	112.49	96.70	109.02
N-hydroxy-4-(phenylthio)butanamide	100.47	99.91	110.22	97.53	99.75	86.46	105.92	85.65	113.89	146.66
propyl 4-(phenylthio)butanoate	81.64	95.87	103.17	91.81	84.11	83.73	91.22	104.56	89.36	104.54
methyl 4-(phenylthio)butanoate	97.76	98.77	98.37	101.82	102.35	108.40	104.39	108.18	114.82	109.44
methyl 4-[(4-methylphenyl)thio]butanoate	100.49	106.83	111.52	97.81	84.72	95.66	78.23	116.44	80.78	119.01
4-[(4-chlorophenyl)thio]-N-hydroxybutanamide	91.33	80.15	82.52	78.02	70.64	64.66	80.82	93.95	87.69	93.10
N-hydroxy-4-[(4-methylphenyl)thio]butanamide	124.65	139.74	137.60	140.89	134.40	98.16	146.90	112.85	144.52	134.57
4-[(4-fluorophenyl)thio]-N-hydroxybutanamide	99.41	88.72	79.80	80.20	67.21	72.07	79.30	72.61	89.41	95.87
methyl 4-[(4-fluorophenyl)thio]butanoate	99.97	123.08	95.89	100.93	108.43	91.91	135.11	95.14	124.96	148.21
apicidin	96.63	103.57	104.36	88.48	70.37	60.48	77.77	49.93	42.98	9.96
TSA	99.77	103.85	86.37	62.19	54.89	47.05	29.26	19.36	4.63	1.97

Table 8. Toxicity of PTBA analogs in cultured podocytes (third replicate). Toxicity was assayed by CellTiter-Blue Cell Viability Assay. Values represent percentage of viable podocytes following 72 hours of treatment with each analog at the listed concentration (see **Chapter 4**, **Methods**). These data were used to generate **Figure 30**.

BIBLIOGRAPHY

1 Smith, H. W. *From fish to philosopher: the story of our internal environment*. Ciba edition, revised and enlarged edn, (Ciba Pharmaceutical Products, Inc., Summit, NJ, 1959).

2 Rennke, H. G. & Denker, B. M. *Renal pathophysiology: the essentials*. 3rd edn, (Lippincott Williams & Wilkins, Philadelphia, PA, 2010).

3 Eaton, D. C. & Pooler, J. P. *Vander's renal physiology*. 7th edn, (McGraw-Hill Medical, New York, NY, 2009).

4 Brenner, B. M., ed. *Brenner & Rector's the kidney*. 8th edn, (Saunders Elsevier, Philadelphia, PA, 2008).

5 Vize, P. D., Woolf, A. S. & Bard, J. B. L., eds. *The kidney: from normal development to congenital disease*. (Academic Press, San Diego, CA, 2003).

6 Brenner, B. M., Hostetter, T. H. & Humes, H. D. Glomerular permselectivity: barrier function based on discrimination of molecular size and charge. *Am J Physiol* **234**, F455-460, (1978).

7 Sherwood, L. *Fundamentals of physiology: a human perspective*. 3rd edn, (Thomson Brooks/Cole, Belmont, CA, 2006).

8 Hoy, W. E. *et al.* Nephron number, glomerular volume, renal disease and hypertension. *Curr Opin Nephrol Hypertens* **17**, 258-265, (2008).

9 Zhou, W., Boucher, R. C., Bollig, F., Englert, C. & Hildebrandt, F. Characterization of mesonephric development and regeneration using transgenic zebrafish. *Am J Physiol Renal Physiol*, (2010).

10 Saxen, L. *Organogenesis of the kidney*. (Cambridge University Press, Cambridge, UK, 1987).

11 Jones, E. A. Xenopus: a prince among models for pronephric kidney development. *J Am Soc Nephrol* **16**, 313-321, (2005).

12 Drummond, I. A. The zebrafish pronephros: a genetic system for studies of kidney development. *Pediatr Nephrol* **14**, 428-435, (2000).

13 Mobjerg, N., Larsen, E. H. & Jespersen, A. Morphology of the kidney in larvae of Bufo viridis (Amphibia, Anura, Bufonidae). *J Morphol* **245**, 177-195, (2000).

14 Davidson, A. J. Mouse kidney development in *StemBook* (Harvard Stem Cell Institute. Available online at http://www.stembook.org, Cambridge, MA, 2009)

15 Dressler, G. R. Advances in early kidney specification, development and patterning. *Development* **136**, 3863-3874, (2009).

16 Mauch, T. J., Yang, G., Wright, M., Smith, D. & Schoenwolf, G. C. Signals from trunk paraxial mesoderm induce pronephros formation in chick intermediate mesoderm. *Dev Biol* **220**, 62-75, (2000).

17 Bellairs, R. & Osmond, M. *The atlas of chick development*. 2nd edn, (Elsevier Academic Press, San Diego, CA, 2005).

18 Nieuwkoop, P. D. & Faber, J., eds. *Normal table of Xenopus laevis (Daudin)*. (Garland Publishing, Inc., New York, NY, 1994).

19 Chan, T. C. & Asashima, M. Development of the embryonic kidney. *Clin Exp Nephrol* **4**, 1-10, (2000).

20 Dressler, G. R., Deutsch, U., Chowdhury, K., Nornes, H. O. & Gruss, P. Pax2, a new murine paired-box-containing gene and its expression in the developing excretory system. *Development* **109**, 787-795, (1990).

21 Kreidberg, J. A. *et al.* WT-1 is required for early kidney development. *Cell* **74**, 679-691, (1993).

22 Sainio, K. *et al.* Glial-cell-line-derived neurotrophic factor is required for bud initiation from ureteric epithelium. *Development* **124**, 4077-4087, (1997).

23 Nigam, S. K. & Shah, M. M. How does the ureteric bud branch? *J Am Soc Nephrol* **20**, 1465-1469, (2009).

24 Heffner, L. J. & Schust, D. J. *The reproductive system at a glance*. 3rd edn, (Wiley-Blackwell, Oxford, UK, 2010).

25 Reimschuessel, R. A fish model of renal regeneration and development. *ILAR J* **42**, 285-291, (2001).

26 Chen, N., Aleksa, K., Woodland, C., Rieder, M. & Koren, G. Ontogeny of drug elimination by the human kidney. *Pediatr Nephrol* **21**, 160-168, (2006).

27 James, R. G. & Schultheiss, T. M. Patterning of the avian intermediate mesoderm by lateral plate and axial tissues. *Dev Biol* **253**, 109-124, (2003).

28 Slack, J. M. W. *From egg to embryo: regional specification in early development*. (Cambridge University Press, Cambridge, UK, 1991).

29 Bouchard, M., Souabni, A., Mandler, M., Neubuser, A. & Busslinger, M. Nephric lineage specification by Pax2 and Pax8. *Genes Dev* **16**, 2958-2970, (2002).

30 James, R. G. & Schultheiss, T. M. Bmp signaling promotes intermediate mesoderm gene expression in a dose-dependent, cell-autonomous and translation-dependent manner. *Dev Biol* **288**, 113-125, (2005).

31 Tsang, T. E. *et al.* Lim1 activity is required for intermediate mesoderm differentiation in the mouse embryo. *Dev Biol* **223**, 77-90, (2000).

32 Barak, H., Rosenfelder, L., Schultheiss, T. M. & Reshef, R. Cell fate specification along the anterior-posterior axis of the intermediate mesoderm. *Dev Dyn* **232**, 901-914, (2005).

33 Carroll, T., Wallingford, J., Seufert, D. & Vize, P. D. Molecular regulation of pronephric development. *Curr Top Dev Biol* **44**, 67-100, (1999).

34 Dressler, G. R. The cellular basis of kidney development. *Annu Rev Cell Dev Biol* **22**, 509-529, (2006).

35 Lang, D., Powell, S. K., Plummer, R. S., Young, K. P. & Ruggeri, B. A. PAX genes: roles in development, pathophysiology, and cancer. *Biochem Pharmacol* **73**, 1-14, (2007).

36 Balczarek, K. A., Lai, Z. C. & Kumar, S. Evolution of functional diversification of the paired box (Pax) DNA-binding domains. *Mol Biol Evol* **14**, 829-842, (1997).

37 Plachov, D. *et al.* Pax8, a murine paired box gene expressed in the developing excretory system and thyroid gland. *Development* **110**, 643-651, (1990).

38 Asano, M. & Gruss, P. Pax-5 is expressed at the midbrain-hindbrain boundary during mouse development. *Mech Dev* **39**, 29-39, (1992).

39 Torres, M., Gomez-Pardo, E., Dressler, G. R. & Gruss, P. Pax-2 controls multiple steps of urogenital development. *Development* **121**, 4057-4065, (1995).

40 Mansouri, A., Chowdhury, K. & Gruss, P. Follicular cells of the thyroid gland require Pax8 gene function. *Nat Genet* **19**, 87-90, (1998).

41 Carroll, T. J. & Vize, P. D. Synergism between Pax-8 and lim-1 in embryonic kidney development. *Dev Biol* **214**, 46-59, (1999).

42 Bouchard, M., Pfeffer, P. & Busslinger, M. Functional equivalence of the transcription factors Pax2 and Pax5 in mouse development. *Development* **127**, 3703-3713, (2000).

43 Brand, M. *et al.* Mutations in zebrafish genes affecting the formation of the boundary between midbrain and hindbrain. *Development* **123**, 179-190, (1996).

44 Lun, K. & Brand, M. A series of no isthmus (noi) alleles of the zebrafish pax2.1 gene reveals multiple signaling events in development of the midbrain-hindbrain boundary. *Development* **125**, 3049-3062, (1998).

45 Majumdar, A., Lun, K., Brand, M. & Drummond, I. A. Zebrafish no isthmus reveals a role for pax2.1 in tubule differentiation and patterning events in the pronephric primordia. *Development* **127**, 2089-2098, (2000).

46 Serluca, F. C. & Fishman, M. C. Pre-pattern in the pronephric kidney field of zebrafish. *Development* **128**, 2233-2241, (2001).

47 Pfeffer, P. L., Gerster, T., Lun, K., Brand, M. & Busslinger, M. Characterization of three novel members of the zebrafish Pax2/5/8 family: dependency of Pax5 and Pax8 expression on the Pax2.1 (noi) function. *Development* **125**, 3063-3074, (1998).

48 Zheng, Q. & Zhao, Y. The diverse biofunctions of LIM domain proteins: determined by subcellular localization and protein-protein interaction. *Biol Cell* **99**, 489-502, (2007).

49 Hobert, O. & Westphal, H. Functions of LIM-homeobox genes. *Trends Genet* **16**, 75-83, (2000).

50 Barnes, J. D., Crosby, J. L., Jones, C. M., Wright, C. V. & Hogan, B. L. Embryonic expression of Lim-1, the mouse homolog of Xenopus Xlim-1, suggests a role in lateral mesoderm differentiation and neurogenesis. *Dev Biol* **161**, 168-178, (1994).

51 Fujii, T. *et al.* Expression patterns of the murine LIM class homeobox gene lim1 in the developing brain and excretory system. *Dev Dyn* **199**, 73-83, (1994).

52 Taira, M., Jamrich, M., Good, P. J. & Dawid, I. B. The LIM domain-containing homeo box gene Xlim-1 is expressed specifically in the organizer region of Xenopus gastrula embryos. *Genes Dev* **6**, 356-366, (1992).

53 Shawlot, W. & Behringer, R. R. Requirement for Lim1 in head-organizer function. *Nature* **374**, 425-430, (1995).

54 Ariizumi, T. & Asashima, M. In vitro induction systems for analyses of amphibian organogenesis and body patterning. *Int J Dev Biol* **45**, 273-279, (2001).

55 Chan, T. C., Takahashi, S. & Asashima, M. A role for Xlim-1 in pronephros development in Xenopus laevis. *Dev Biol* **228**, 256-269, (2000).

56 Potter, S. S., Hartman, H. A., Kwan, K. M., Behringer, R. R. & Patterson, L. T. Laser capture-microarray analysis of Lim1 mutant kidney development. *Genesis* **45**, 432-439, (2007).

57 Mukhopadhyay, M. *et al.* Dickkopf1 is required for embryonic head induction and limb morphogenesis in the mouse. *Dev Cell* **1**, 423-434, (2001).

58 Lieven, O., Knobloch, J. & Ruther, U. The regulation of Dkk1 expression during embryonic development. *Dev Biol* **340**, 256-268, (2010).

59 Lyons, J. P. *et al.* Requirement of Wnt/beta-catenin signaling in pronephric kidney development. *Mech Dev* **126**, 142-159, (2009).

60 Campo-Paysaa, F., Marletaz, F., Laudet, V. & Schubert, M. Retinoic acid signaling in development: tissue-specific functions and evolutionary origins. *Genesis* **46**, 640-656, (2008).

61 Blomhoff, R. & Blomhoff, H. K. Overview of retinoid metabolism and function. *J Neurobiol* **66**, 606-630, (2006).

62 Menegola, E., Di Renzo, F., Broccia, M. L. & Giavini, E. Inhibition of histone deacetylase as a new mechanism of teratogenesis. *Birth Defects Res C Embryo Today* **78**, 345-353, (2006).

63 Cartry, J. *et al.* Retinoic acid signalling is required for specification of pronephric cell fate. *Dev Biol* **299**, 35-51, (2006).

64 Preger-Ben Noon, E., Barak, H., Guttmann-Raviv, N. & Reshef, R. Interplay between activin and Hox genes determines the formation of the kidney morphogenetic field. *Development* **136**, 1995-2004, (2009).

65 Wingert, R. A. *et al.* The cdx genes and retinoic acid control the positioning and segmentation of the zebrafish pronephros. *PLoS Genet* **3**, 1922-1938, (2007).

66 Bollig, F. *et al.* A highly conserved retinoic acid responsive element controls wt1a expression in the zebrafish pronephros. *Development* **136**, 2883-2892, (2009).

67 Alarcon, P., Rodriguez-Seguel, E., Fernandez-Gonzalez, A., Rubio, R. & Gomez-Skarmeta, J. L. A dual requirement for Iroquois genes during Xenopus kidney development. *Development* **135**, 3197-3207, (2008).

68 Desbaillets, I., Ziegler, U., Groscurth, P. & Gassmann, M. Embryoid bodies: an in vitro model of mouse embryogenesis. *Exp Physiol* **85**, 645-651, (2000).

69 Kim, D. & Dressler, G. R. Nephrogenic factors promote differentiation of mouse embryonic stem cells into renal epithelia. *J Am Soc Nephrol* **16**, 3527-3534, (2005).

70 Mainguy, G. *et al.* A position-dependent organisation of retinoid response elements is conserved in the vertebrate Hox clusters. *Trends Genet* **19**, 476-479, (2003).

71 Taira, M., Otani, H., Jamrich, M. & Dawid, I. B. Expression of the LIM class homeobox gene Xlim-1 in pronephros and CNS cell lineages of Xenopus embryos is affected by retinoic acid and exogastrulation. *Development* **120**, 1525-1536, (1994).

72 Tsang, M. Zebrafish: A tool for chemical screens. *Birth Defects Res C Embryo Today* **90**, 185-192, (2010).

73 Battle, H. I. & Hisaoka, K. K. Effects of ethyl carbamate (urethan) on the early development of the teleost Brachydanio rerio. *Cancer Res* **12**, 334-340, (1952).

74 Hisaoka, K. K. The effects of 4-acetylaminofluorene on the embryonic development of the zebrafish. I. Morphological studies. *Cancer Res* **18**, 527-535, (1958).

75 Hisaoka, K. K. The effects of 2-acetylaminofluorene on the embryonic development of the zebrafish. II. Histochemical studies. *Cancer Res* **18**, 664-667, (1958).

76 Hisaoka, K. K. & Hopper, A. F. Some effects of barbituric and diethylbarbituric acid on the development of the zebra fish, Brachydanio rerio. *Anat Rec* **129**, 297-307, (1957).

77 Grunwald, D. J. & Eisen, J. S. Headwaters of the zebrafish -- emergence of a new model vertebrate. *Nat Rev Genet* **3**, 717-724, (2002).

78 Streisinger, G. Attainment of minimal biological variability and measurements of genotoxicity: production of homozygous diploid zebra fish. *Natl Cancer Inst Monogr* **65**, 53-58, (1984).

79 Hill, A. J., Teraoka, H., Heideman, W. & Peterson, R. E. Zebrafish as a model vertebrate for investigating chemical toxicity. *Toxicol Sci* **86**, 6-19, (2005).

80 Nüsslein-Volhard, C. & Dahm, R. *Zebrafish: a practical approach*. (Oxford University Press, Oxford, UK, 2002).

81 Kari, G., Rodeck, U. & Dicker, A. P. Zebrafish: an emerging model system for human disease and drug discovery. *Clin Pharmacol Ther* **82**, 70-80, (2007).

82 Stern, H. M. & Zon, L. I. Cancer genetics and drug discovery in the zebrafish. *Nat Rev Cancer* **3**, 533-539, (2003).

83 Zon, L. I. & Peterson, R. T. In vivo drug discovery in the zebrafish. *Nat Rev Drug Discov* **4**, 35-44, (2005).

84 Hirsch, N., Zimmerman, L. B. & Grainger, R. M. Xenopus, the next generation: X. tropicalis genetics and genomics. *Dev Dyn* **225**, 422-433, (2002).

85 Muda, M. & McKenna, S. Model organisms and target discovery. *Drug Discov Today Tech* **1**, 55-59, (2004).

86 Detrich, H. W., Westerfield, M. & Zon, L. I. *Essential zebrafish methods: genetics and genomics*. (Academic Press, San Diego, CA, 2009).

87 Bill, B. R., Petzold, A. M., Clark, K. J., Schimmenti, L. A. & Ekker, S. C. A primer for morpholino use in zebrafish. *Zebrafish* **6**, 69-77, (2009).

88 Doyon, Y. *et al.* Heritable targeted gene disruption in zebrafish using designed zinc-finger nucleases. *Nat Biotechnol* **26**, 702-708, (2008).

89 Meng, X., Noyes, M. B., Zhu, L. J., Lawson, N. D. & Wolfe, S. A. Targeted gene inactivation in zebrafish using engineered zinc-finger nucleases. *Nat Biotechnol* **26**, 695-701, (2008).

90 Bahary, N. *et al.* The Zon laboratory guide to positional cloning in zebrafish. *Methods Cell Biol* **77**, 305-329, (2004).

91 Guryev, V. *et al.* Genetic variation in the zebrafish. *Genome Res* **16**, 491-497, (2006).

92 Conn, M. P. *Sourcebook of models for biomedical research*. (Humana Press Inc., Totowa, NJ, 2008).

93 Postlethwait, J., Amores, A., Cresko, W., Singer, A. & Yan, Y. L. Subfunction partitioning, the teleost radiation and the annotation of the human genome. *Trends Genet* **20**, 481-490, (2004).

94 Hashiguchi, M., Shinya, M., Tokumoto, M. & Sakai, N. Nodal/Bozozok-independent induction of the dorsal organizer by zebrafish cell lines. *Dev Biol* **321**, 387-396, (2008).

95 He, S. *et al.* Genetic and transcriptome characterization of model zebrafish cell lines. *Zebrafish* **3**, 441-453, (2006).

96 National Library of Medicine (NLM) and National Institutes of Health (NIH). *PubMed [electronic resource]*. (NLM:NIH, Bethesda, MD). http://www.ncbi.nlm.nih.gov /pubmed/.

97 Brittijn, S. A. *et al.* Zebrafish development and regeneration: new tools for biomedical research. *Int J Dev Biol* **53**, 835-850, (2009).

98 Sullivan, C. & Kim, C. H. Zebrafish as a model for infectious disease and immune function. *Fish Shellfish Immunol* **25**, 341-350, (2008).

99 Knapik, E. W. ENU mutagenesis in zebrafish--from genes to complex diseases. *Mamm Genome* **11**, 511-519, (2000).

100 Lieschke, G. J. & Currie, P. D. Animal models of human disease: zebrafish swim into view. *Nat Rev Genet* **8**, 353-367, (2007).

101 Moens, C. B., Donn, T. M., Wolf-Saxon, E. R. & Ma, T. P. Reverse genetics in zebrafish by TILLING. *Brief Funct Genomic Proteomic* **7**, 454-459, (2008).

102 Vize, P. D., Seufert, D. W., Carroll, T. J. & Wallingford, J. B. Model systems for the study of kidney development: use of the pronephros in the analysis of organ induction and patterning. *Dev Biol* **188**, 189-204, (1997).

103 Pedersen, A., Skjong, C. & Shawlot, W. Lim 1 is required for nephric duct extension and ureteric bud morphogenesis. *Dev Biol* **288**, 571-581, (2005).

104 Drummond, I. Making a zebrafish kidney: a tale of two tubes. *Trends Cell Biol* **13**, 357-365, (2003).

105 Wingert, R. A. & Davidson, A. J. The zebrafish pronephros: a model to study nephron segmentation. *Kidney Int* **73**, 1120-1127, (2008).

106 Picker, A., Scholpp, S., Bohli, H., Takeda, H. & Brand, M. A novel positive transcriptional feedback loop in midbrain-hindbrain boundary development is revealed through analysis of the zebrafish pax2.1 promoter in transgenic lines. *Development* **129**, 3227-3239, (2002).

107 Swanhart, L. M. *et al.* Characterization of an lhx1a transgenic reporter in zebrafish. *Int J Dev Biol* **54**, 731-736, (2010).

108 Drummond, I. A. *et al.* Early development of the zebrafish pronephros and analysis of mutations affecting pronephric function. *Development* **125**, 4655-4667, (1998).

109 Kramer-Zucker, A. G., Wiessner, S., Jensen, A. M. & Drummond, I. A. Organization of the pronephric filtration apparatus in zebrafish requires Nephrin, Podocin and the FERM domain protein Mosaic eyes. *Dev Biol* **285**, 316-329, (2005).

110 Cianciolo Cosentino, C., Roman, B. L., Drummond, I. A. & Hukriede, N. A. Intravenous microinjections of zebrafish larvae to study acute kidney injury. *J Vis Exp*, (2010).

111 Hentschel, D. M. *et al.* Rapid screening of glomerular slit diaphragm integrity in larval zebrafish. *Am J Physiol Renal Physiol* **293**, F1746-1750, (2007).

112 Hentschel, D. M. *et al.* Acute renal failure in zebrafish: a novel system to study a complex disease. *Am J Physiol Renal Physiol* **288**, F923-929, (2005).

113 Murphey, R. D. & Zon, L. I. Small molecule screening in the zebrafish. *Methods* **39**, 255-261, (2006).

114 Wheeler, G. N. & Brandli, A. W. Simple vertebrate models for chemical genetics and drug discovery screens: lessons from zebrafish and Xenopus. *Dev Dyn* **238**, 1287-1308, (2009).

115 Peal, D. S., Peterson, R. T. & Milan, D. Small molecule screening in zebrafish. *J Cardiovasc Transl Res* **3**, 454-460, (2010).

116 Sachidanandan, C., Yeh, J. R., Peterson, Q. P. & Peterson, R. T. Identification of a novel retinoid by small molecule screening with zebrafish embryos. *PLoS One* **3**, e1947, (2008).

117 Chan, J. & Serluca, F. C. Chemical approaches to angiogenesis. *Methods Cell Biol* **76**, 475-487, (2004).

118 Kokel, D. *et al.* Rapid behavior-based identification of neuroactive small molecules in the zebrafish. *Nat Chem Biol* **6**, 231-237, (2010).

119 Rihel, J. *et al.* Zebrafish behavioral profiling links drugs to biological targets and rest/wake regulation. *Science* **327**, 348-351, (2010).

120 Burns, C. G. *et al.* High-throughput assay for small molecules that modulate zebrafish embryonic heart rate. *Nat Chem Biol* **1**, 263-264, (2005).

121 Vogt, A. *et al.* Automated image-based phenotypic analysis in zebrafish embryos. *Dev Dyn* **238**, 656-663, (2009).

122 Vogt, A., Codore, H., Day, B. W., Hukriede, N. A. & Tsang, M. Development of automated imaging and analysis for zebrafish chemical screens. *J Vis Exp*, (2010).

123 Paik, E. J., de Jong, J. L., Pugach, E., Opara, P. & Zon, L. I. A chemical genetic screen in zebrafish for pathways interacting with cdx4 in primitive hematopoiesis. *Zebrafish* **7**, 61-68, (2010).

124 Anderson, C. *et al.* Chemical genetics suggests a critical role for lysyl oxidase in zebrafish notochord morphogenesis. *Mol Biosyst* **3**, 51-59, (2007).

125 Peterson, R. T., Link, B. A., Dowling, J. E. & Schreiber, S. L. Small molecule developmental screens reveal the logic and timing of vertebrate development. *Proc Natl Acad Sci U S A* **97**, 12965-12969, (2000).

126 Yu, P. B. *et al.* Dorsomorphin inhibits BMP signals required for embryogenesis and iron metabolism. *Nat Chem Biol* **4**, 33-41, (2008).

127 Molina, G. A., Watkins, S. C. & Tsang, M. Generation of FGF reporter transgenic zebrafish and their utility in chemical screens. *BMC Dev Biol* **7**, 62, (2007).

128 North, T. E. *et al.* Prostaglandin E2 regulates vertebrate haematopoietic stem cell homeostasis. *Nature* **447**, 1007-1011, (2007).

129 Cao, Y. *et al.* Chemical modifier screen identifies HDAC inhibitors as suppressors of PKD models. *Proc Natl Acad Sci U S A* **106**, 21819-21824, (2009).

130 Drummond, I. A. Kidney development and disease in the zebrafish. *J Am Soc Nephrol* **16**, 299-304, (2005).

131 Popa-Burke, I. G. *et al.* Streamlined system for purifying and quantifying a diverse library of compounds and the effect of compound concentration measurements on the accurate interpretation of biological assay results. *Anal Chem* **76**, 7278-7287, (2004).

132 Sussman, C. R. *et al.* Cloning, localization, and functional expression of the electrogenic Na+ bicarbonate cotransporter (NBCe1) from zebrafish. *Am J Physiol Cell Physiol* **297**, C865-875, (2009).

133 Perner, B., Englert, C. & Bollig, F. The Wilms tumor genes wt1a and wt1b control different steps during formation of the zebrafish pronephros. *Dev Biol* **309**, 87-96, (2007).

134 Harris, W. A. & Hartenstein, V. Neuronal determination without cell division in Xenopus embryos. *Neuron* **6**, 499-515, (1991).

135 Westerfield, M. *The zebrafish book.* (University of Oregon Press, Eugene, OR, 1993).

136 Kimmel, C. B., Ballard, W. W., Kimmel, S. R., Ullmann, B. & Schilling, T. F. Stages of embryonic development of the zebrafish. *Dev Dyn* **203**, 253-310, (1995).

137 The NCI/DTP Open Chemical Repository. <http://dtp.cancer.gov>.

138 Zhang, L., Kendrick, C., Julich, D. & Holley, S. A. Cell cycle progression is required for zebrafish somite morphogenesis but not segmentation clock function. *Development* **135**, 2065-2070, (2008).

139 Minoru, U., Takao, N. & Kazuyuki, N. Substituted thiobutyric acid derivatives (assigned to Otsuka Pharmaceutical Co., Ltd., Japan). Jpn. Kokai Tokkyo Koho (1982), 9 pp. JP57058663(A) Publication date 1982-04-08 Showa.

140 Traynelis, V. J. & Love, R. F. Seven-membered heterocycles. I. Synthesis of benzo[*b*]thiepin 1,1-dioxide and 1-phenylsulfonyl-4-phenyl-1,3-butadiene. *J Org Chem* **26**, 2728-2733, (1961).

141 Kukalenko, S. S. Organic insectofungicides. I. Synthesis and some reactions of γ-arylthiobutyric acids. *Z Org Khim* **6**, 680-684, (1970).

142 Toyama, R., O'Connell, M. L., Wright, C. V., Kuehn, M. R. & Dawid, I. B. Nodal induces ectopic goosecoid and lim1 expression and axis duplication in zebrafish. *Development* **121**, 383-391, (1995).

143 Tang, R., Dodd, A., Lai, D., McNabb, W. C. & Love, D. R. Validation of zebrafish (Danio rerio) reference genes for quantitative real-time RT-PCR normalization. *Acta Biochim Biophys Sin (Shanghai)* **39**, 384-390, (2007).

144 Andersen, C. L., Jensen, J. L. & Orntoft, T. F. Normalization of real-time quantitative reverse transcription-PCR data: a model-based variance estimation approach to identify genes suited for normalization, applied to bladder and colon cancer data sets. *Cancer Res* **64**, 5245-5250, (2004).

145 Ruijter, J. M. *et al.* Amplification efficiency: linking baseline and bias in the analysis of quantitative PCR data. *Nucleic Acids Res* **37**, e45, (2009).

146 Dong, G. *et al.* Induction of apoptosis in renal tubular cells by histone deacetylase inhibitors, a family of anticancer agents. *J Pharmacol Exp Ther* **325**, 978-984, (2008).

147 Gurvich, N. *et al.* Association of valproate-induced teratogenesis with histone deacetylase inhibition in vivo. *FASEB J* **19**, 1166-1168, (2005).

148 Noel, E. S. *et al.* Organ-specific requirements for Hdac1 in liver and pancreas formation. *Dev Biol* **322**, 237-250, (2008).

149 Lea, M. A. & Tulsyan, N. Discordant effects of butyrate analogues on erythroleukemia cell proliferation, differentiation and histone deacetylase. *Anticancer Res* **15**, 879-883, (1995).

150 Hu, P. *et al.* Retinoid regulation of the zebrafish cyp26a1 promoter. *Dev Dyn* **237**, 3798-3808, (2008).

151 Keegan, B. R., Feldman, J. L., Begemann, G., Ingham, P. W. & Yelon, D. Retinoic acid signaling restricts the cardiac progenitor pool. *Science* **307**, 247-249, (2005).

152 Blumberg, B. *et al.* An essential role for retinoid signaling in anteroposterior neural patterning. *Development* **124**, 373-379, (1997).

153 Bacallao, R. & Fine, L. G. Molecular events in the organization of renal tubular epithelium: from nephrogenesis to regeneration. *Am J Physiol* **257**, F913-924, (1989).

154 Jacobsen, F. E., Lewis, J. A. & Cohen, S. M. The design of inhibitors for medicinally relevant metalloproteins. *ChemMedChem* **2**, 152-171, (2007).

155 Villar-Garea, A. & Esteller, M. Histone deacetylase inhibitors: understanding a new wave of anticancer agents. *Int J Cancer* **112**, 171-178, (2004).

156 Lipinski, C. A., Lombardo, F., Dominy, B. W. & Feeney, P. J. Experimental and computational approaches to estimate solubility and permeability in drug discovery and development settings. *Adv Drug Deliv Rev* **46**, 3-26, (2001).

157 Testa, B., Carrupt, P. A., Gaillard, P., Billois, F. & Weber, P. Lipophilicity in molecular modeling. *Pharm Res* **13**, 335-343, (1996).

158 Peterson, R. T. & Fishman, M. C. Discovery and use of small molecules for probing biological processes in zebrafish. *Methods Cell Biol* **76**, 569-591, (2004).

159 Alexander, J., Rothenberg, M., Henry, G. L. & Stainier, D. Y. casanova plays an early and essential role in endoderm formation in zebrafish. *Dev Biol* **215**, 343-357, (1999).

160 Hughes, I. *et al.* Otopetrin 1 is required for otolith formation in the zebrafish Danio rerio. *Dev Biol* **276**, 391-402, (2004).

161 Korzh, S. *et al.* Requirement of vasculogenesis and blood circulation in late stages of liver growth in zebrafish. *BMC Dev Biol* **8**, 84, (2008).

162 Bradner, J. E. *et al.* Chemical phylogenetics of histone deacetylases. *Nat Chem Biol* **6**, 238-243, (2010).

163 Mundel, P. *et al.* Rearrangements of the cytoskeleton and cell contacts induce process formation during differentiation of conditionally immortalized mouse podocyte cell lines. *Exp Cell Res* **236**, 248-258, (1997).

164 Schwartz, E. J. *et al.* Human immunodeficiency virus-1 induces loss of contact inhibition in podocytes. *J Am Soc Nephrol* **12**, 1677-1684, (2001).

165 National Center for Biotechnology Information (NCBI) and National Library of Medicine (NLM). *PubChem [electronic resource]*. (NCBI: NLM, Bethesda, MD). http://pubchem.ncbi.nlm.nih.gov/.

166 de Groh, E. D. *et al.* Inhibition of histone deacetylase expands the renal progenitor cell population. *J Am Soc Nephrol* **21**, 794-802, (2010).

167 Molina, G. *et al.* Zebrafish chemical screening reveals an inhibitor of Dusp6 that expands cardiac cell lineages. *Nat Chem Biol* **5**, 680-687, (2009).

168 Anderson, R. J., Ray, C. J. & Hattler, B. G. Retinoic acid regulation of renal tubular epithelial and vascular smooth muscle cell function. *J Am Soc Nephrol* **9**, 773-781, (1998).

169 Argiles, A., Kraft, N. E., Hutchinson, P., Senes-Ferrari, S. & Atkins, R. C. Retinoic acid affects the cell cycle and increases total protein content in epithelial cells. *Kidney Int* **36**, 954-959, (1989).

170 Bonventre, J. V. Dedifferentiation and proliferation of surviving epithelial cells in acute renal failure. *J Am Soc Nephrol* **14 Suppl 1**, S55-61, (2003).

171 Kwon, O. *et al.* Bone marrow-derived endothelial progenitor cells and endothelial cells may contribute to endothelial repair in the kidney immediately after ischemia-reperfusion. *J Histochem Cytochem* **58**, 687-694, (2010).

172 Oliver, J. A. *et al.* Proliferation and migration of label-retaining cells of the kidney papilla. *J Am Soc Nephrol* **20**, 2315-2327, (2009).

173 Imai, N. *et al.* Inhibition of histone deacetylase activates side population cells in kidney and partially reverses chronic renal injury. *Stem Cells* **25**, 2469-2475, (2007).

174 Marumo, T., Hishikawa, K., Yoshikawa, M. & Fujita, T. Epigenetic regulation of BMP7 in the regenerative response to ischemia. *J Am Soc Nephrol* **19**, 1311-1320, (2008).

175 Mitamura, T., Higashiyama, S., Taniguchi, N., Klagsbrun, M. & Mekada, E. Diphtheria toxin binds to the epidermal growth factor (EGF)-like domain of human heparin-binding EGF-like growth factor/diphtheria toxin receptor and inhibits specifically its mitogenic activity. *J Biol Chem* **270**, 1015-1019, (1995).

176 Bock, G. & Goode, J., eds. *Reversible protein acetylation*. (John Wiley & Sons Ltd, Chichester, UK, 2004).

177 Furumai, R. *et al.* Potent histone deacetylase inhibitors built from trichostatin A and cyclic tetrapeptide antibiotics including trapoxin. *Proc Natl Acad Sci U S A* **98**, 87-92, (2001).

178 Sekhavat, A., Sun, J. M. & Davie, J. R. Competitive inhibition of histone deacetylase activity by trichostatin A and butyrate. *Biochem Cell Biol* **85**, 751-758, (2007).

179 Su, H., Altucci, L. & You, Q. Competitive or noncompetitive, that's the question: research toward histone deacetylase inhibitors. *Mol Cancer Ther* **7**, 1007-1012, (2008).

180 Bieliauskas, A. V. & Pflum, M. K. Isoform-selective histone deacetylase inhibitors. *Chem Soc Rev* **37**, 1402-1413, (2008).

181 Balasubramanian, S., Verner, E. & Buggy, J. J. Isoform-specific histone deacetylase inhibitors: the next step? *Cancer Lett* **280**, 211-221, (2009).

182 Bolden, J. E., Peart, M. J. & Johnstone, R. W. Anticancer activities of histone deacetylase inhibitors. *Nat Rev Drug Discov* **5**, 769-784, (2006).

183 Butler, K. V. & Kozikowski, A. P. Chemical origins of isoform selectivity in histone deacetylase inhibitors. *Curr Pharm Des* **14**, 505-528, (2008).

184 Khan, N. *et al.* Determination of the class and isoform selectivity of small-molecule histone deacetylase inhibitors. *Biochem J* **409**, 581-589, (2008).

185 Richon, V. M. & O'Brien, J. P. Histone deacetylase inhibitors: a new class of potential therapeutic agents for cancer treatment. *Clin Cancer Res* **8**, 662-664, (2002).

186 Schemies, J., Uciechowska, U., Sippl, W. & Jung, M. NAD(+) -dependent histone deacetylases (sirtuins) as novel therapeutic targets. *Med Res Rev* **30**, 861-889, (2010).

187 Hubbert, C. *et al.* HDAC6 is a microtubule-associated deacetylase. *Nature* **417**, 455-458, (2002).

188 Haggarty, S. J., Koeller, K. M., Wong, J. C., Grozinger, C. M. & Schreiber, S. L. Domain-selective small-molecule inhibitor of histone deacetylase 6 (HDAC6)-mediated tubulin deacetylation. *Proc Natl Acad Sci U S A* **100**, 4389-4394, (2003).

189 Sanderson, L. *et al.* Plasma pharmacokinetics and metabolism of the histone deacetylase inhibitor trichostatin a after intraperitoneal administration to mice. *Drug Metab Dispos* **32**, 1132-1138, (2004).

190 U.S. Food and Drug Administration (FDA). *Drugs@FDA [electronic resource]*. (FDA, Silver Spring, MD). http://www.accessdata.fda.gov/scripts/cder/drugsatfda/.

191 Cederbaum, S., Lemons, C. & Batshaw, M. L. Alternative pathway or diversion therapy for urea cycle disorders now and in the future. *Mol Genet Metab* **100**, 219-220, (2010).

192 Ucyclyd Pharma Inc. *Buphenyl [electronic resource]*. (Ucyclyd Pharma Inc., Scottsdale, AZ). http://www.buphenyl.com/.

193 Lee, B. *et al.* Phase 2 comparison of a novel ammonia scavenging agent with sodium phenylbutyrate in patients with urea cycle disorders: safety, pharmacokinetics and ammonia control. *Mol Genet Metab* **100**, 221-228, (2010).

194 Gilbert, J. *et al.* A phase I dose escalation and bioavailability study of oral sodium phenylbutyrate in patients with refractory solid tumor malignancies. *Clin Cancer Res* **7**, 2292-2300, (2001).

195 Buchwald, M., Kramer, O. H. & Heinzel, T. HDACi--targets beyond chromatin. *Cancer Lett* **280**, 160-167, (2009).

196 Pohl, L. R. & Mico, B. A. Electrophilic halogens as potentially toxic metabolites of halogenated compounds. *Trends Pharmacol Sci* **5**, 61=64, (1984).

197 Hammam, A.-E. G. Some amides, anilides, and bis(hydrazides) of expected biological activity. *J Chem Eng Data* **24**, 379-380, (1979).